

**Immunity-Related GTPases in  
Cell-autonomous Resistance against *Toxoplasma gondii***

Inaugural-Dissertation  
zur  
Erlangung des Doktorgrades  
der Mathematisch-Naturwissenschaftlichen Fakultät  
der Universität zu Köln

vorgelegt von  
**Yang Zhao**  
aus Anqing, P.R. China

Köln 2008

Berichterstatter:

Prof. Dr. Jonathan C. Howard

Prof. Dr. Thomas Langer

Tag der mündlichen Prüfung:

15th, April 2008

献给我的父母和爱妻刘导



## TABLE OF CONTENTS

1. Introduction .....	1
1.1 Pathogens and immunity .....	1
1.2 Cytokines and interferons.....	3
1.3 Cell-autonomous immunity .....	5
1.4 GTP binding proteins .....	5
1.5 Interferon-inducible GTPases and dynamins .....	7
1.6 Immunity-related GTPases.....	8
1.6.1 IRG gene family .....	8
1.6.2 Induction and expression of the IRG proteins.....	9
1.6.3 Structure and biochemical properties of the IRG proteins .....	9
1.6.4 Subcellular localization of IRG proteins .....	11
1.6.5 Involvement of the IRGs in resistance against intracellular pathogens <i>in vivo</i> and <i>in vitro</i> .....	12
1.7 <i>Toxoplasma gondii</i> infection as a model to study the functions of IRG proteins .....	14
1.8 Aims of this study .....	17
2. Material and Methods.....	19
2.1 Reagents and Cells .....	19
2.1.1 Chemicals, Reagents and Accessories .....	19
2.1.2 Equipments.....	19
2.1.3 Materials.....	20
2.1.4 Enzymes and Proteins .....	20
2.1.5 Kits .....	20
2.1.6 Vectors and constructs used in the present study .....	20
2.1.7 Cell lines, bacterial and protozoan strains.....	21
2.1.8 Media.....	21
2.1.9 Serological reagents .....	22
2.1.10 Peptides .....	23
2.2 Molecular Biology.....	23
2.2.1 Agarose gel electrophoresis .....	23
2.2.2 Generation of the expression constructs.....	23
2.2.3 Cloning of PCR amplification products .....	25
2.2.4 Purification of DNA fragments from agarose gels.....	25
2.2.5 Ligation .....	25

2.2.6	Preparation of competent cells.....	26
2.2.7	Transformation of competent bacteria.....	26
2.2.8	Plasmid isolation.....	27
2.2.9	Determination of the concentration of DNA.....	27
2.2.10	Site directed mutagenesis.....	27
2.2.11	DNA Sequencing.....	28
2.3	Cell biology.....	28
2.3.1	Transfection.....	28
2.3.2	Transferrin uptaking experiments.....	28
2.3.3	Lysotracker loading experiments.....	29
2.3.4	Latex beads phagocytosis experiments.....	29
2.3.5	Immunocytochemistry.....	29
2.3.6	Peptide-streptavidin complex experiments.....	30
2.3.7	<i>In vitro</i> passage and infection of <i>Toxoplasma gondii</i> .....	30
2.3.8	Live cell imaging.....	31
2.3.9	Quantification of IRG signals on <i>T. gondii</i> parasitophorous vacuoles.....	31
2.3.10	Cell viability assay.....	32
2.3.11	Western blotting.....	32
3	Results-I.....	33
3.1	Irgm1 localizes to Golgi apparatus and late endocytic/lysosomal compartments.....	33
3.2	Both N and C terminal EGFP-tag lead to the mislocalization of Irgm1.....	36
3.3	Mislocalization of Irgm1 by EGFP tagging is nucleotide dependent.....	39
3.4	Phagosomal accumulation of Irgm1 is nucleotide dependent, but IFN- $\gamma$ independent. .....	40
3.5	Amphipathic helix near the C-terminus is responsible for both Golgi and lysosomal targeting of Irgm1.....	44
3.6	Artificial $\alpha$ K amphipathic peptide mimics the localization of endogenous Irgm1.....	50
3.7	Irgm1 is not recruited to <i>Toxoplasma gondii</i> ME49 strain vacuoles and is not absolutely necessary for IFN- $\gamma$ -dependent cell-autonomous resistance against <i>T. gondii</i> ME49 strain.....	52
4.	Results-II.....	56
4.1	Dynamics of the Irga6-loading onto the <i>T. gondii</i> ME49 strain parasitophorous vacuolar membrane.....	56

4.2 Disruption of the Irga6-positive <i>T. gondii</i> vacuoles is followed by parasite deterioration and host cell death.....	59
4.3 EGFP-LC3 associates with a proportion of <i>T. gondii</i> ME49 strain vacuoles independent of IFN- $\gamma$ .....	61
4.4 Intracellular <i>T. gondii</i> is killed after the disruption of parasitophorous vacuole.....	64
4.5 Host cell death is a mechanism of IFN- $\gamma$ -dependent cell-autonomous resistance against <i>T. gondii</i> avirulent strain.....	67
4.6 The property of host cell death induced by IFN- $\gamma$ and <i>T. gondii</i> avirulent strain infection is rather necrosis than apoptosis.....	70
4.7 Cathepsin B is not necessary for the IFN- $\gamma$ -dependent <i>T. gondii</i> avirulent strain elicited host cell necrosis.....	73
4.8 <i>T. gondii</i> avirulent strain induced IFN- $\gamma$ -dependent necrosis dominates over the virulent strain resistance mechanisms against IFN- $\gamma$ protection.....	74
5. Discussion.....	76
5.1 Irgm1 localizes mainly to the Golgi apparatus and lysosomes, and mislocalizes as a result of EGFP-tagging at the N or C terminus.....	76
5.2 Both Golgi and lysosomal localization of Irgm1 is dependent on a predicted amphipathic helix near the C-terminus.....	82
5.3 Irgm1 is not absolutely necessary for IFN- $\gamma$ -dependent cell-autonomous resistance against <i>T. gondii</i> .....	85
5.4 Loading of Irga6 onto the intracellular <i>T. gondii</i> vacuoles in real time.....	87
5.5 Intracellular <i>T. gondii</i> is killed after the disruption of the parasitophorous vacuole..	89
5.6 IFN- $\gamma$ -treated host cell undergoes necrotic-like death, which could serve as an IFN- $\gamma$ -mediated cell-autonomous resistance mechanism against <i>T. gondii</i> .....	90
5.7 Autophagy in cell-autonomous resistance against <i>T. gondii</i> infection.....	94
5.8 Virulent <i>vs</i> avirulent <i>T. gondii</i> strain infection.....	97
5.9 Manipulation of the host cell death: a common theme in the host-pathogen interaction.....	98
6. References.....	100
7. Summary.....	113
8. Zusammenfassung.....	114
9. Acknowledgement.....	116
10. Erklärung.....	117
11. Lebenslauf.....	118



# 1. Introduction

## 1.1 Pathogens and immunity

Our earth is now 4.6 billion years' old and the earliest life on our planet appeared approximately 4 billions years ago. Under the pressure of natural selection, life on earth evolved from single cell organisms (prokaryotes) to multicellular organisms (eukaryotes), as complicated as ourselves. During the evolution of life, some different organisms tend to live together to benefit each other (symbiosis). They either live in proximity or one lives inside of the other. One famous example is the adoption of cyanobacteria and proteobacteria by host cells which gave rise to chloroplasts and mitochondria, respectively (Margulis 1975; Sagan 1993). This co-adaptation can also been seen in our human beings that the beneficial bacteria flourish in the gastrointestinal tracts.

However, this is not always the case. Some microorganisms have evolved special mechanisms to invade, colonize and multiply in the host body at the expense of disturbing the normal physiology of the hosts. The disease-causing microorganisms are termed pathogens (from Greek *pathos* (suffering/emotion) and *gene* (to give birth to)). Traditionally, pathogens are divided into five main groups: viruses (including bacteriophages), bacteria, fungi, protozoa and worms. On the other hand, under the pressure of invading pathogens, the host organisms, especially the multicellular organisms such as vertebrates and plants, evolved sophisticated defense systems to resist the infection of pathogens. This defense mechanism in host organisms is therefore termed immunity (derived from Latin *immunis*, meaning exemption from public services).

The immune system protects the host organisms from being overrun by the invading pathogens with multiple layered defense mechanisms. Most simply, the physical barriers prevent the pathogens from entering the body. If a pathogen breaches these barriers, the innate immune system provides an immediate, but non-specific response. The innate system is thought to constitute an evolutionarily older defense strategy, and is the dominant immune system found in plants, fungi, insects, and primitive multicellular organisms (Janeway 2001). Even simple unicellular organisms such as bacteria possess enzyme systems to protect against

the viral infections. Other innate immune mechanisms include antimicrobial peptides called defensins, phagocytosis, and the complement system. However, if the pathogens successfully evade the innate immune responses, the vertebrates possess a third layer of protection, the adaptive immune system, which is activated by the innate immune responses. This improved response is then retained after the pathogens have been eliminated, in the form of an immunological memory, and allows the adaptive immune system to mount faster and stronger attacks each time this specific pathogen is encountered again (Janeway 2001).

Recognition of the infectious microorganism is the first and crucial step in immunity. Both innate and adaptive immunity depend on the ability of the immune system to distinguish between self and non-self molecules. When the pathogens invade the host, they are first recognized by the host innate immune system. In the innate immune system, the immune response is initiated by cells and molecules recognizing conserved features of microorganisms and activated immediately on encounter with them. These conserved features of pathogens are referred to as *pathogen-associated molecular patterns* (PAMPs), which include cell wall components (lipopolysaccharide, lipoprotein, peptidoglycan, flagellin, etc.), double-stranded RNA from viruses, or CpG-containing DNA. The recognition of PAMPs is accomplished by innate immune receptors termed *pattern recognition receptors* (PRRs). The list of PRRs is constantly expanding. Perhaps the most prominent PRRs include Toll-like receptors, the mannose receptor, Nod like receptors, and Plant R Proteins (Janeway 2002). For many host organisms, the innate immune system is enough to effectively eliminate most of the pathogens. For vertebrates, the innate immune system not only could directly eliminate the pathogens, but also could provide signals to further activate the adaptive immune system. The adaptive immune system, compared to innate immune system, is composed of highly specialized cells and molecules, which can recognize essentially unlimited numbers of different targets. This system is adaptive because it prepares itself for future challenges and it is highly adaptable because of irreversible genetic recombination and somatic hypermutation in the antigen receptor (TCRs and BCRs) gene segments (Janeway 2001).

## 1.2 Cytokines and interferons

Cytokines are a group of intercellular regulatory proteins and peptides with a mass of between 8 and 30 kDa, which are produced by a wide variety of cell types (both haemopoietic and non-haemopoietic) (DeFranco 2007). They play important roles in both innate and adaptive immunity, and some of them serve as bridges to transduce signals from innate immune system to activate the adaptive immune system. According to the structures, cytokines can be grouped into four families: the chemokines, the hematopoietins, the interferons (IFNs), and the tumor necrosis factor (TNF) family (Janeway 2001). The cytokines function in every aspects of immune response, including facilitating inflammation, activation of macrophages, T and B lymphocytes, chemotaxis, and also negative regulation of immune response (DeFranco 2007). Generally, cytokines are pleiotropic, multifunctional and sometimes redundant.

The interferons were originally discovered by their ability to induce resistance to viral infection in cells (Isaacs 1957). It was later appreciated that, in addition to regulating resistance to viral infection, interferons are widely functional in innate and adaptive immunity, including activation of macrophages and NK cells, enhancement of antigen presentation by induction of major histocompatibility complex (MHC) class I and II molecules, as well as modulation of normal and tumour cell survival and death (Boehm 1997; Schroder 2004; Borden 2007). They are nowadays extensively used in clinical practice for treatment of viral diseases, cancer, as well as autoimmune disease multiple sclerosis (MS) (Borden 2007).

According to sequence homology and molecular structures, as well as their receptor specificity, interferons are classified into three groups: Type I interferons, including IFN- $\alpha$  (14-20 members, depending on species) (van Pesch 2004), IFN- $\beta$  (Mogensen 1999), IFN- $\omega$  (Hauptmann 1985), IFN- $\kappa$  (LaFleur 2001), IFN- $\epsilon$  (Pestka 2004), IFN- $\delta$  (pigs) (Lefevre 1998) and IFN- $\tau$  (ruminants) (Bazer 1997); Type II interferon (IFN- $\gamma$  as sole member) (Bancroft 1993); Type III interferons, IFN- $\lambda$ s (3 members) (Kotenko 2003; Lasfar 2006). The type I interferons are synthesized and secreted by almost all nucleated cells when confronted with viral infection, while type II interferon (IFN- $\gamma$ ) is mainly secreted by activated T cells, NK cells and macrophages (Schroder 2004; Borden 2007). Each type of interferons is recognized by corresponding heterodimeric receptors, which signals mainly through JAK/STAT (Janus

kinase/Signal Transducers and Activators of Transcription) pathways (Figure 1.1). The activated STATs and other transcription factors (IRFs, interferon regulatory factors) are then translocated into the nucleus and drive the transcription and expression of interferon-stimulated genes (ISGs) promoted by IFN- $\gamma$ -activated site (GAS) elements and IFN-stimulated response elements (ISREs) (Schroder 2004; Borden 2007).

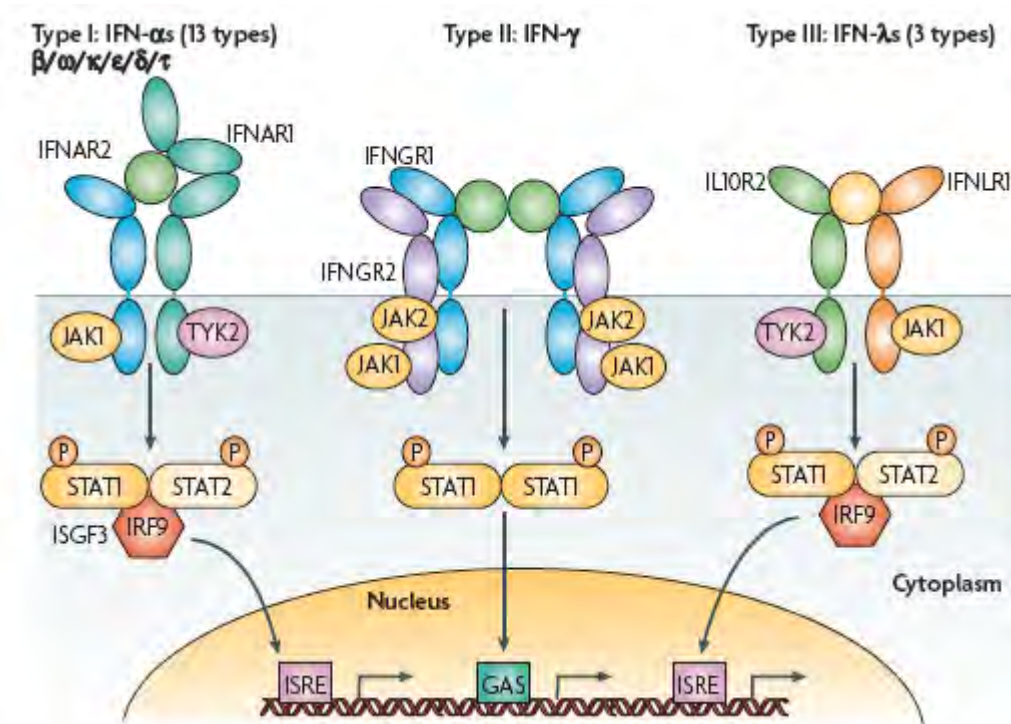


**Figure 1.1 Simplified scheme of interferon receptors and signaling pathways (from Borden 2007).**

Type I interferons (IFNs) ( $\alpha$ ,  $\beta$ ,  $\omega$ ,  $\kappa$ ,  $\epsilon$ ,  $\delta$  (pigs),  $\tau$  (ruminants)) interact with IFN ( $\alpha$ ,  $\beta$  and  $\omega$ ) receptor 1 (IFNAR1) and IFNAR2; type II IFN- $\gamma$  with IFN- $\gamma$  receptor 1 (IFNGR1) and IFNGR2; and type III IFN- $\lambda$ s with IFN- $\lambda$  receptor 1 (IFNLR1; also known as IL28RA) and interleukin 10 receptor 2 (IL10R2; also known as IL10RB). Type II IFN- $\gamma$  is an antiparallel homodimer exhibiting a two-fold axis of symmetry. It binds two IFNGR1 receptor chains, assembling a complex that is stabilized by two IFNGR2 chains. These receptors are associated with two kinases from the JAK family: JAK1 and TYK2 for type I and III IFNs; JAK1 and JAK2 for type II IFN. GAS, IFN- $\gamma$ -activated site; IRF9, IFN regulatory factor 9; ISGF3, IFN-stimulated gene factor 3, refers to the STAT1–STAT2–IRF9 complex; ISRE, IFN-stimulated response element; P, phosphate; STAT1/2, signal transducers and activators of transcription 1/2.

The pivotal functions of interferons in immunity can be documented in the phenotype of STAT1-deficient mice. STAT1 is essential in both type I and type II interferons signaling pathways. The mice lacking STAT1 showed no overt developmental defects, and normal numbers of T cells, B cells and macrophages in thymus and spleen. But these mice displayed a complete lack of responsiveness to either IFN- $\alpha$  or IFN- $\gamma$  and were highly sensitive to

infection by microbial pathogens and viruses (Durbin 1996; Meraz 1996). Similar phenotypes were also observed in IFN- $\gamma$  deficient and IFN- $\gamma$  receptor deficient mice (Huang 1993).

The pleiotropic functions of interferons are executed by interferon-stimulated genes. Examples of these are class I and II MHC molecules. Up-regulation of MHC molecules can enhance the antigen presentation and promote the delivery of the signals from innate immune system to the adaptive immune system (Boehm 1997). Other molecules induced by interferons include adhesion molecules (ICAM1, VCAM1, *et al*) and chemokines which can recruit leukocytes and promote inflammation (Boehm 1997; Schroder 2004). Indeed, by inducing as many as one thousand genes, IFN- $\gamma$  is extremely potent in activating the cytotoxic effector function among cells of innate and adaptive immunity including NK cells, dendritic cells, macrophages and T cells (Schroder 2004).

### **1.3 Cell-autonomous immunity**

Cells, including immune and non-immune cells, can resist pathogen infection without the participation of other cells (neutrophils, cytotoxic T cells, NK cells, macrophages, *et al*) and molecules (antibodies, complements, *et al*) from innate and adaptive immune systems. This is termed cell-autonomous immunity, even though, in most cases, it is acquired upon induction of cytokines. IFN- $\gamma$  is the most competent cytokine that can confer host cell autonomous resistance against viruses, pathogenic bacterium, and protozoa infection. Besides the IFN- $\gamma$ -induced genes introduced in chapter 1.2, the molecules responsible for cell-autonomous immunity include PKR, iNOS/NOS2, phox complex, NRAMP1, IDO, Mx, GBPs, and IRGs (Boehm 1997; Schroder 2004). In addition to the well-understood universal resistance mechanisms like ROS/NO production and tryptophan depletion, it is surprising, but also interesting, to notice that several of these abundantly induced proteins are GTP binding proteins (GTPases), whose functions are largely unknown (Martens 2006).

### **1.4 GTP binding proteins**

GTP binding proteins (GTPases) are a large family of hydrolase enzymes that can bind and hydrolyze GTP to GDP and/or GMP. These proteins participate in many cellular functions, such as translation (initiation, elongation, and release factors), signal transduction, cell

motility, intracellular transport, membrane trafficking, as well as cell-autonomous resistance against intracellular pathogens (Leipe 2002; Martens 2006).

GTPases function as molecular switches, cycling between active GTP-bound form and inactive GDP-bound form (Figure 1.2)(Bourne 1990; Bourne 1991). Only GTP-bound form proteins are able to interact with a variety of effector proteins, by which cellular responses are executed. During the GTPase cycle, other proteins such as GEF, GAP and GDI can regulate the activity of the GTPases. GEFs (guanine-nucleotide exchange factors) induce the dissociation of GDP from GTPases and facilitate GTP-binding, and therefore activate GTPases. In contrast, GAPs (GTPase-activating proteins) accelerate GTP hydrolysis by GTPases, and therefore drive GTPases to the inactive GDP-bound form. GDIs (guanine-nucleotide dissociation inhibitors) prevent the dissociation of GDP from GTPases and keep the enzymes in the inactive form (Vetter 2001). The GTP binding and hydrolysis takes place in the highly conserved nucleotide binding domain (G-domain) common to all GTPases. The G1-G5 motifs within the G-domain with more or less conserved sequences are the structural elements required for the nucleotide binding and hydrolysis (Leipe 2002).

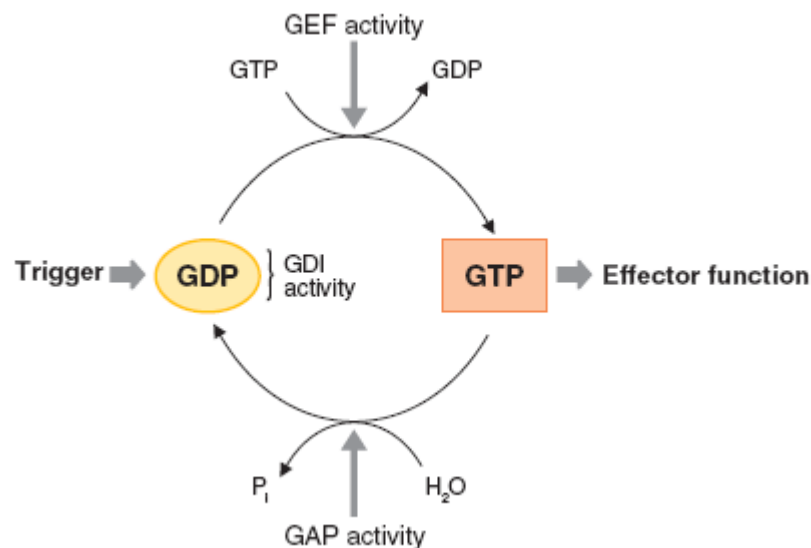


Figure 1.2 The GTPase cycle (from Martens 2006)

## 1.5 Interferon-inducible GTPases and dynamins

Four GTPase families were found to be strongly induced by interferons, including Mx GTPases, p65 guanylate-binding proteins (GBPs), very large inducible GTPases (VLIGs) and p47 immunity-related GTPases (IRGs). All these GTPases share biochemical characteristics with the dynamins, as these proteins show GTP-dependent self-oligomerization and accelerated GTP hydrolysis upon oligomerization (Martens 2006).

Dynamins are large GTPases with molecular weight of about 100 kDa. In addition to the conserved GTP-binding domain, classical dynamins have a pleckstrin homology (PH) domain involving phosphoinositide binding, a GTPase effector domain (GED) mediating self-oligomerization, a proline rich domain (PRD) interacting with SH3 domain-containing proteins, as well as a middle domain. The function of dynamins was originally discovered as proteins crucial in the scission process of clathrin-coated vesicles from plasma membrane. Later investigations showed that dynamins are important in many cellular processes involving membranes such as vesicles trafficking, division of organelles and cytokinesis (Hinshaw 2000; Praefcke 2004).

Among the interferon-inducible GTPases, the Mx family of dynamin homologs was the first to be found mediating cell-autonomous resistance against intracellular pathogens. The Mx1 gene was originally mapped in lab mouse A2G strain for its resistance against influenza virus infection (Lindenmann 1963; Lindenmann 1964). Isolated macrophages from A2G mice showed cell-autonomous resistance against viral infection (Lindenmann 1978). Mx genes are present in all vertebrates and two members are found in human (MxA and MxB) and mouse (Mx1 and Mx2), respectively (Staeheli 1985; Goetschy 1989; Simon 1991). The anti-viral function of Mx proteins is accomplished, at least in part, by binding to the viral nucleocapsids. This interferes with intracellular trafficking and activity of viral polymerases, thus inhibiting replication of many RNA viruses including influenza and measles viruses (Haller 2007). Mx proteins are exclusively induced by type I interferons (Simon 1991).

During the cellular responses to type II interferon (IFN- $\gamma$ ), p65 GBPs and p47 IRGs are the two dominant induced protein families (Boehm 1998). Type I interferons can also induce GBP and IRG proteins to a less extent (Nantais 1996; Bekpen 2005). The GBP family is conserved in vertebrates (Robertsen 2006). 10 members have been found in mice (mGBP1-

10)(Degrandi 2007) and 7 in human (hGBP1-7)(Cheng 1991; Olszewski 2006). Even though GBPs are massively induced by interferons, only a weak anti-virus effect was reported in cultured cells using an over-expression system (Anderson 1999; Carter 2005). Surprisingly, no genetic analysis using gene targeted mice has yet been reported to link the functions of GBPs to immunity against intracellular pathogens (viruses and microbes). In addition, roles of GBPs in regulation of vasculogenesis by proinflammatory cytokines and IFN-mediated cell growth were suggested (Guenzi 2001; Gorbacheva 2002; Guenzi 2003).

The third GTPase family induced by interferons is the VLIGs. These are the largest GTPases known so far, with molecular weight of about 280 kDa. The prototype of this family, VLIG-1, is massively induced by IFN- $\gamma$  and to a less extent by IFN- $\beta$  *in vitro*, and induced by *Listeria monocytogenes* infection *in vivo*. The G-domain of VLIGs is more closely related to IFN-inducible GTPases mediating cell-autonomous resistance, especially Mx and GBP families, than to other GTPase families. Therefore, it has been suggested that VLIGs are a new family of resistance GTPases although no direct test for this idea has been reported (Klamp 2003).

## **1.6 Immunity-related GTPases**

Unlike the poorly confirmed functions of GBP family in intracellular pathogen resistance, extensive experimental analyses have been reported describing the indispensable role of IRG family (p47 GTPases) in anti-microbial resistance in mice. A detailed introduction of the IRG family is therefore given here.

### **1.6.1 IRG gene family**

An extensive and detailed analysis of the IRG gene family has been reported (Bekpen 2005). Homologous genes of IRGs are present in zebrafish, dogs, rats, mice and humans. In C57Bl/6 mice strain, 21 genes have been found expressing 25 coding units. 4 genes are probably expressed as tandem proteins. Based on phylogenetic principles, IRG genes are further divided into *Irga*, *Irgb*, *Irgc*, *Irgd* and *Irgm* subfamilies. In the *Irgm* subfamily, the lysine in the canonical G1 nucleotide binding motif GX<sub>4</sub>GKS was replaced by methionine (GX<sub>4</sub>GMS). Most of the mouse genes have IRSE and/or GAS elements in their promoter regions. *Irga6*

has an additional liver specific promoter responsible for the expression of an alternative splicing form. The only exception in mice is *Irgc*, which lack both IRSE and GAS in its promoter. Instead a Sox-related element is present in the proximal promoter region. *Irga* subfamily is clustered on chromosome 18, whereas *Irgb*, *Irgd* and *Irgm* subfamilies are clustered on chromosome 11. *Irgc* is located alone in chromosome 7.

In humans, only two IRG gene homologs have been found. Human *IRGC* encodes a full-length IRG protein, which is highly homologous to mouse *Irgc*. They are more than 85% identical at nucleotide level and 90% at the amino acid level. The proximal promoter region of human *IRGC* is also largely conserved with that of mouse *Irgc*. Human *IRGM* encodes a considerably truncated protein that lacks the G5 motif in the classical nucleotide-binding domain, and is probably controlled by the LTR of an integrated ERV-9 repetitive element. *IRGC* and *IRGM* are located in human chromosome 19 and 5, respectively.

### **1.6.2 Induction and expression of the IRG proteins**

Consistent with the promoter situations of IRG genes, most mouse IRG proteins are only expressed upon induction by interferons. Type II interferon (IFN- $\gamma$ ) is the most potent inducer of IRGs. Some reports describing IRGs induction in other circumstances, e.g. LPS, may reflect the secondary production of IFNs (Zerrahn 2002; Lapaque 2006). In addition to the massively-inductivity of *Irga6* by IFNs, this member of IRGs has a high constitutive expression in the liver due to an alternative live specific promoter. The expression of *Irgc* and its human homologue *IRGC* are not IFN-regulatory and only constitutively expressed in the testis. Another member of IRGs in human, *IRGM*, was found to be expressed in cultured human cell lines Hela and GS293 and not subjected to interferons induction (Bekpen 2005; Rohde 2007).

### **1.6.3 Structure and biochemical properties of the IRG proteins**

*Irga6* is the only member of IRG proteins that has been successfully purified and whose biochemical properties have been systematically studied and crystal structure has been resolved to date. Recombinant *Irga6* purified from *E. coli* crystallized as a dimer in the nucleotide-free and GDP-bound form (Uthaiyah 2003). The *Irga6* molecule is built from a Ras-

like G-domain and a unique helical domain composed of N and C terminal helices. Based on sequence comparison and secondary structure prediction, Irga6 structure serves as a prototype for other IRG proteins (Figure 1.3)(Ghosh 2004). Recombinant Irga6 hydrolyzes GTP to GDP and form GTP-dependent oligomers. The hydrolysis activity is accelerated upon oligomerization with a maximum rate of 2 per minute per molecule of Irga6. Irga6 has a low nucleotide binding affinity ( $15\mu\text{M}$  for GTP and  $1\mu\text{M}$  for GDP) compared to Ras family GTPases. Considering the cellular concentration of GDP and GTP ( $120\mu\text{M}$  and  $330\mu\text{M}$ , respectively (Kleinecke 1979)), Irga6 is presumably in GDP-bound form in cells. The low affinities for nucleotide and cooperative hydrolysis upon oligomerization are properties shared also by GBPs, Mx proteins and dynamins, although GBPs and Mx proteins have similar affinities for GTP and GDP, while dynamins have a higher affinity for GTP (Uthaiiah 2003).

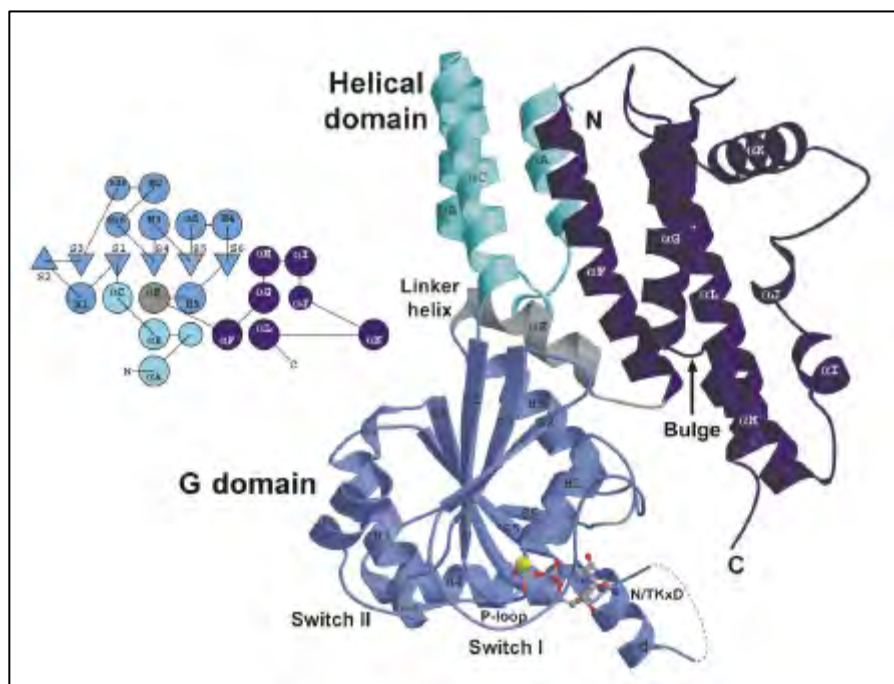


**Figure 1.3 Structure of Irga6 (from Ghosh 2004)**

Irga6 has an N-terminal myristoylation site MGxxxS and indeed, the myristoyl group contributes to the membrane association of Irga6 in cells (Martens 2004b). As a matter of fact, 11 members in IRG family carry the amino-terminal myristoylation signal (Bekpen 2005). Recent data showed that myristoylated Irga6 purified from insect Sf9 cells hydrolyses GTP to

GDP and GMP (Pavic 2007). This suggests that, *in vivo*, myristoylated IRG proteins may have strikingly different biochemical properties.

No exogenous proteins have been found as regulators (GEF, GAP and GDI) of IRG proteins. As a self-activating GTPase, Irga6 functions as GAP (GTPase-activating protein) for itself. Recent data suggested that IRGM proteins interact with Irga6 and Irgb6 to prevent inappropriate activation (Hunn 2007). In this sense, IRGM proteins function like GDI proteins for other members of IRGs. A microtubule-motor binding protein, Hook3, has been found to interact directly with Irga6, and is likely an effector protein of Irga6 rather than a regulator (Kaiser 2004).

Incomplete biochemical analyses of other IRG proteins were documented as well. Partially purified GST-Irgb6 and GST-Irgm3 fusion proteins have been shown to hydrolyze GTP to GDP (Taylor 1996; Carlow 1998). Weak GTPase activity was also reported for Irgm3 immunoprecipitates from IFN- $\gamma$  treated macrophages (Taylor 1996), and more than 90% of the bound nucleotide in precipitated Irgm3 was GTP, independent of IFN- $\gamma$  (Taylor 1997). This suggests that Irgm3 is mainly present in an active state in cells.

#### **1.6.4 Subcellular localization of IRG proteins**

IRG proteins associate with membranes to different degrees in IFN- $\gamma$  induced cells. Irgm1 and Irgm3 have been found almost exclusively in a membrane compartment, while more than 90% of Irgd is in the aqueous phase. Irgm2 has more membrane-bound form than cytosolic pool. Irga6 and Irgb6 partitioned roughly equally between membrane and cytosolic fractions (Martens 2004b). By immunofluorescence analyses, Irgm1 and Irgm2 localize to Golgi apparatus and Irgm3 is an ER-associated protein (Taylor 1997; Martens 2004a; Butcher 2005). Irga6 is targeted to ER, probably partially by a myristoyl group (Martens 2004b). IRGM proteins are organelle-targeted by a predicted  $\alpha$  helix near the C-terminus, which, in case of Irgm1, shows amphipathic property (Martens 2004b; Martens 2006). The resting localizations of IRG proteins are largely independent of GTPase activity as GTP-binding defective mutants show similar subcellular distributions, wherever tested (Taylor 1997; Martens 2004b).

Irga6 and Irgb6 forms GTP-dependent aggregates when expressed in the absence of IFN- $\gamma$ . Co-expression with IRGM proteins can restore the proper localization of Irga6 and Irgb6. Yeast 2-hybrid experiments also confirmed the direct interaction between different members of IRG family. Therefore, IRGM proteins can co-ordinate localization of other IRG protein family members (Martens 2006; Hunn 2007; Papis 2007).

In cells involving pathogen infections or phagocytosis, IRG proteins are relocalized from resting compartments to the active membrane systems. Irgm1 is rapidly relocalized to F-actin-rich plasma membrane ruffles associated with phagocytic cups in fibroblasts and macrophages (Martens 2004b). Irgm1 and Irgm3 have been found to associate with latex beads phagosomes rapidly after uptake (Butcher 2005). In addition, Irgm1 has been co-purified from mycobacterial phagosomes (MacMicking 2003). 5 members of IRGs have also been found on *Toxoplasma gondii* parasitophorous vacuole membrane shortly after the parasite invasion (Martens 2005). Compared to the nucleotide-binding independent of resting localization of IRG proteins, recruitment of IRGs to the *T. gondii* PVM requires the intact GTP binding motifs, suggesting a specific requirement for the nucleotide, presumably GTP, binding (Martens 2005; Hunn 2007).

Recent publications showed that Irgm1 colocalizes with MDC and LC3 positive compartments, suggesting an association between Irgm1 and autophagosome (Gutierrez 2004; Singh 2006). The authors accordingly suggested that Irgm1 has a pro-autophagic function as a mechanism for mycobacteria elimination. However, in those publications, EGFP tagged Irgm1 was used, even though the influence on proper localization of Irgm1 by EGFP tagging was not investigated. In the present studies, we try to answer this question by in depth analyses.

### **1.6.5 Involvement of the IRGs in resistance against intracellular pathogens *in vivo* and *in vitro***

Studies of IRG-deficient mice and isolated cells have shown that members of IRG family are indispensable, in most cases also non-redundant, resistance factors against a wide range of intracellular bacteria and protozoal pathogens (Martens 2006; Taylor 2007). The published results are summarized in table 1.1. Generally, Irgm1-deficient mice lose resistance to all

microbes tested so far; Irgm3-deficient mice show decreased resistance to a smaller group of protozoa and only one of several tested bacteria; and Irgd-deficient and Irga6-deficient mice only show weakly decreased or normal resistance to pathogens tested. The IRG-dependent resistances have also been documented on the cell-autonomous level: Irgm1 and Irgm3 are required for IFN- $\gamma$  induced control of *T. gondii* growth in macrophages (Butcher 2005); Irga6 and Irgm3 in control of *T. gondii* in astrocytes (Halonen 2001; Martens 2005); Irgm1 in control of *M. tuberculosis* and *T. cruzi* in macrophages (MacMicking 2003; Santiago 2005); Irgm1, Irgm3 and Irgb10 in control of *C. trachomatis* in fibroblasts (Bernstein-Hanley 2006; Miyairi 2007; Coers Manuscripts in preparation). In these cases, there is a strong correlation between loss of resistance in mice and loss of IFN- $\gamma$ -dependent control in cultured cells. This suggests that host cell-autonomous control of pathogens is a predominant function of IRG proteins. A recent report showed that a resistance/susceptibility polymorphism for *C. trachomatis* had been mapped to the region on mice chromosome 11 encoding Irgm3 and Irgb10. And the resistance/susceptibility was phenocopied at cellular levels as well (Bernstein-Hanley 2006; Miyairi 2007).

The localization of IRG proteins to the pathogen-containing vacuoles in host cells suggests that they may execute their function by controlling vacuole processing. The proposed mechanisms include (i) lysosome fusion and/or acidification of the vacuole (MacMicking 2003), (ii) vesiculation of the vacuolar membranes (Martens 2005; Ling 2006) and (iii) autophagy of the vacuolar contents (Gutierrez 2004; Ling 2006). Concerning the last hypothesis, most of studies so far have been performed *in vitro* and it remains to be confirmed whether autophagy can restrict intracellular pathogens *in vivo* by studying mice with targeted autophagy genes.

As mentioned above, Mx and GBP GTPase families have potential anti-virus functions. A limited number of reports have addressed whether IRG family are also anti-viral. Ebola virus and mouse cytomegalovirus are controlled normally in Irgm3-deficient mouse (Taylor 2000). In addition, Irgm1 and Irgd are not required for resistance against MCMV (Collazo 2001). *In vitro*, a slightly elevated resistance to RNA virus VSV, but not DNA virus HSV, was found in L cells stably expressing Irgb6 (Carlow 1998). An even weaker effect was documented for Coxsackie virus in HeLa cells expressing Irgm2 (Zhang 2003).

**Table 1.1 Summary of evidences supporting roles of IRG proteins in host resistance (modified from Taylor 2007)**

IRG proteins	Defined roles in host resistance		Possible mechanisms
	<i>In vivo</i>	In cultured cells	
Irgm1	<i>T. gondii</i> (Collazo 2001)	<i>T. gondii</i> (Butcher 2005)	-lysosomal fusion (MacMicking 2003; Deghmane 2007) -Haematopoiesis (Feng 2004; Santiago 2005) -Impaired macrophages adhesion and motility (Henry 2007) -Autophagy (Gutierrez 2004; Singh 2006)
	<i>L. major</i> (Santiago 2005)	<i>T. cruzi</i> (Santiago 2005)	
	<i>T. cruzi</i> (Santiago 2005)	<i>M. tuberculosis</i> (MacMicking 2003)	
	<i>L. monocytogenes</i> (Collazo 2001)	<i>S. typhimurium</i> (Henry 2007)	
	<i>M. tuberculosis</i> (MacMicking 2003)	<i>C. trachomatis</i> (Coers Manuscripts in preparation)	
	<i>M. avium</i> (Feng 2004) <i>S. typhimurium</i> (Henry 2007)		
Irgm2	<i>C. psittaci</i> (Henry 2007)	<i>C. psittaci</i> (Miyairi 2007)	
Irgm3	<i>T. gondii</i> (Taylor 2000)	<i>T. gondii</i> (Halonen 2001; Butcher 2005; Ling 2006)	-Vacuole vesiculation (Martens 2005; Ling 2006) -lysosomal fusion (Ling 2006) -Autophagy (Ling 2006)
	<i>L. major</i> (Taylor 2007)	<i>C. Trachomatis</i> (Bernstein-Hanley 2006)	
Irga6		<i>T. gondii</i> (Martens 2005)	-Vacuole vesiculation (Martens 2005) -Membrane trafficking (Nelson 2005)
		<i>C. trachomatis</i> (Nelson 2005)	
Irgd	<i>T. gondii</i> (chronic, (Collazo 2001))	<i>T. cruzi</i> (Koga 2006)	
Irgb10	<i>C. psittaci</i> (Miyairi 2007)	<i>C. trachomatis</i> (Bernstein-Hanley 2006)	

### 1.7 *Toxoplasma gondii* infection as a model to study the functions of IRG proteins

Infections by the protozoan parasite *Toxoplasma gondii* are widely prevalent in humans and animals worldwide. The definitive host of *T. gondii* is the cat, but the parasite can be carried by a vast majority of warm-blooded animals. Toxoplasmosis, the disease caused by *T. gondii*, is usually minor and self-limiting but can have serious or even fatal effects on an immunocompromised host or on a fetus whose mother is infected during pregnancy. Infection with this parasite proceeds in two phases in immunocompetent hosts (Luft 1992). During the acute phase its rapidly proliferating form, the tachyzoite, disseminates throughout the host; subsequently, during the chronic phase its dormant form, the bradyzoite, becomes established mainly in the central nervous system. This obligate parasite invades host cells, both haematopoietic and non-haematopoietic, by actively creating and entering into a unique non-fusogenic membrane-bounded cytoplasmic compartment, the parasitophorous vacuole (Sibley 2004).

Once inside of the host, *T. gondii* is a potent stimulus for cell-mediated immunity, and IL-12-dependent IFN- $\gamma$  induction is vital for resistance to the parasite (Denkers 2003; Aliberti 2005). IL-12 is produced mainly by dendritic cells, neutrophils and macrophages and is the main cytokine to further stimulate the production of IFN- $\gamma$ . *T. gondii* possesses two mechanisms for triggering IL-12. One is dependent upon adaptor protein MyD88 and involves Toll-like

receptors (Scanga 2002). The other is a more unusual pathway that involves CCR5 by a parasite cyclophilin molecule (Aliberti 2000; Aliberti 2003). *T. gondii* has several mechanisms to down-regulate immunity. Intracellular infection causes a blockage STAT1 activation, therefore suppress the IFN- $\gamma$  signaling (Luder 2001). In addition, intracellular parasite can subtly modify host cell NF $\kappa$ B signaling pathway (Denkers 2003). NF $\kappa$ B is normally associated with transcription of proinflammatory mediators and resistance to infection. However, NF $\kappa$ B can also induce expression of several anti-apoptotic proteins, including inhibitor of apoptosis proteins (IAPs) and cFLIP, which behaves like a dominant-negative form of caspase-8 (Karin 2002; Hayden 2004). It is well-established that *T. gondii* triggers rapid phosphorylation and degradation of the NF $\kappa$ B inhibitor I $\kappa$ B on parasitophorous vacuole membrane, which depends on both the host IKK and a parasite kinase activity, TgIKK (Molestina 2005b; Molestina 2005a). However, there are seemingly controversial reports concerning the activity of NF $\kappa$ B triggered by the parasites. Some groups reported that *T. gondii*-infected cells exhibit increased NF $\kappa$ B activation and gene expression (Gazzinelli 1996; Blader 2001; Kim 2001), while several other groups reported that they are unable to observe NF $\kappa$ B activation despite infection-dependent increased I $\kappa$ B degradation (Butcher 2001; Goebel 2001; Shapira 2005). This may reflect the ability of *T. gondii* to establish a beneficial niche for their long-term survival, as the modification of host cell physiology may differ in different host cell types and in different stages of infection. For example, one interesting publication reported that, in macrophages, activated form of NF $\kappa$ B fails to translocate into the host nucleus despite of I $\kappa$ B degradation. However, after 24 hours, the blockade in NF $\kappa$ B nuclear import is lifted and translocation of activated NF $\kappa$ B is observed (Butcher 2002). Notably there is no dispute regarding the induction of NF $\kappa$ B once infection is established and parasite replication is initiated.

*T. gondii* infection can result in an anti-apoptotic state in host cells to facilitate the parasite intracellular growth. *T. gondii* infected cells are resistant to numerous, both intrinsic and extrinsic, apoptotic stimuli (Carmen 2007). In addition to the activation of NF $\kappa$ B-dependent pro-survival mechanisms mentioned above, *T. gondii* has been suggested to inhibit caspase-9 activation through direct inhibition of apoptosome in *in vitro* reconstitution (Keller 2006) and by inhibiting the release of cytochrome c (Goebel 2001; Carmen 2006). The activation of the

PI3-kinase pathway has also been suggested as a mechanism of induction of anti-apoptotic state during the early stage of infection (Kim 2006a), as the NF $\kappa$ B activation is blocked during that stage. Extracellular pathways of suppressing host immunity by *T. gondii* infection have been reported as well. These involve the infection-induced host production of IL-10 and lipoxins that have potent IL-12 down-regulatory effects (Figure 1.4)(Aliberti 2002a; Aliberti 2002b). Interestingly and surprisingly, no studies have been reported investigating how IFN- $\gamma$  pretreatment influence the anti-apoptotic state conferred by *T. gondii* infection, considering IFN- $\gamma$  is the most potent inducer for *T. gondii* resistance *in vivo* and *in vitro*.

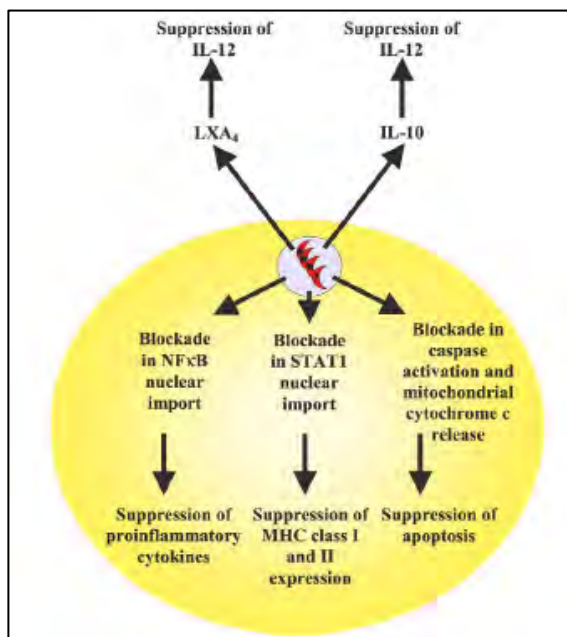


**Figure 1.4 Intracellular and extracellular pathways of immunosuppression during *T. gondii* infection (from Denkers 2003).**

Intracellular infection leads to a blockade in NF $\kappa$ B and STAT1 activation pathways. While I $\kappa$ B is phosphorylated and degraded, and STAT1 undergoes phosphorylation-dependent activation, neither NF $\kappa$ B nor STAT1 translocate into the nucleus during early infection. As a result, production of IL-12 and TNF- $\alpha$  is suppressed, and expression of MHC molecules is down-regulated. *T. gondii* infection also renders cells resistant to apoptosis, as shown by reduced caspases proteolytic activation and mitochondrial cytochrome c release. Extracellular pathways of immunosuppression involve *Toxoplasma*-induced host production of LXA<sub>4</sub> and IL-10. These soluble mediators are potent down-regulators of IL-12 production that can act on infected and noninfected cells alike.

*T. gondii* is an excellent system to analyze the functions of IRG proteins. The host resistances for both phases of infection *in vivo*, as well as in cultured cells, are IFN- $\gamma$  dependent (Suzuki 1988; Scharon-Kersten 1996). Either Irgm1 or Irgm3 deficient mice succumb to *T. gondii* avirulent strain infection within 9-11 days, which is comparable to the time frame as *T. gondii* infected mice lacking either IL12 or IFN- $\gamma$ -signaling machinery (Taylor 2000; Collazo 2001). In addition, Irgd-deficient mice can survive acute phase of *T. gondii* infection, but have impaired resistance during chronic infection (Collazo 2001). On the cellular level, Irgm1 and Irgm3 deficient macrophages and astrocytes lose resistance against *T. gondii* infection upon IFN- $\gamma$  induction, which correlates with loss of resistance in mice (Halonen 2001; Butcher 2005). At least five members of IRG proteins are concentrated on *T. gondii* PVM rapidly after the parasite invasion in murine astrocytes and primary embryonic fibroblasts (Martens 2005).

Vesiculation and stripping of parasitophorous membrane have been observed in *T. gondii* infected astrocytes and macrophages (Martens 2005; Ling 2006). An autophagolysosomal process has been suggested in macrophages after stripping of *T. gondii* vacuolar membranes (Ling 2006). However, no lysosomal fusion has been observed in astrocytes (Martens 2005), and the question how naked parasites free in the cytosol are killed remains to be illustrated. Furthermore, although *Irgm1* is indispensable for resistance against *T. gondii in vivo*, this protein is absent from *T. gondii* PVM indicating that IRGs may function in multiple layers of resistance (Butcher 2005; Martens 2005).

### **1.8 Aims of this study**

Immunity-related GTPases (IRG) are powerful, non-redundant resistance factors against a variety of intracellular pathogens in mice. This is manifested by well-documented analyses using gene-targeted mice and cells for individual members of IRGs. Cell-autonomous control of pathogens is a predominant function of IRG proteins, although the exact mechanisms are still not known. *Irgm1* is the most prominent member in IRG family for resistance as mice lacking this protein are susceptible to all bacterial and protozoal pathogens tested so far. Possible mechanisms have been suggested for functions of *Irgm1* such as: (i) lysosome fusion and/or acidification of the vacuole (MacMicking 2003; Deghmane 2007), (ii) induction of autophagy (Gutierrez 2004; Singh 2006), (iii) regulation of the adhesion and motility of activated macrophages (Henry 2007), (iv) negatively regulation of TLR4-triggered proinflammatory cytokine production and prevention of endotoxemia (Bafica 2007) and (v) regulation of haematopoiesis during chronic infection (Feng 2004; Santiago 2005).

*Irgm1* has been reported to localize to Golgi apparatus, ER and vesicular structures in resting cells. During phagocytosis it is rapidly relocalized to F-actin-rich plasma membrane ruffles associated with phagocytic cups in macrophages and fibroblasts (Martens 2004b). In the present study subcellular localization of *Irgm1* and corresponding mechanisms are further investigated in depth. In addition, localization influenced by N and C terminal tag is analyzed, as proposed pro-autophagic function of *Irgm1* is based on experiments using EGFP-tagged protein and correct subcellular localization was not confirmed. Furthermore, role of *Irgm1* in cell-autonomous resistance to *T. gondii* infection in fibroblasts is studied. Finally, live cell

imaging system is established and employed to investigate the involvement of IRG proteins in resistance against *T. gondii* infection on a single cell level.

## **2. Material and Methods**

### **2.1 Reagents and Cells**

#### **2.1.1 Chemicals, Reagents and Accessories**

All chemicals were purchased from Aldrich (Steinheim), Amersham-Pharmacia (Freiburg), Applichem (Darmstadt), Baker (Deventer, Netherlands), Boehringer Mannheim (Mannheim), Fluka (Neu-Ulm), GERBU (Gaiberg), Merck (Darmstadt), Pharma-Waldhof (Düsseldorf), Qiagen (Hilden), Riedel de Haen (Seelze), Roth (Karlsruhe), Serva (Heidelberg), Sigma-Aldrich (Deisenhofen) or ICN biochemicals, Oxoid, (Hampshire UK). Developing and fixing solutions for Western Blot detection were from Amersham Pharmacia (Freiburg), Luminol from Sigma Aldrich (Deisenhofen), Coumaric acid from Fluka (Neu-Ulm). Deionised and sterile water (Seral TM) was used for all the buffers and solutions, Ultra pure water derived from Beta 75/delta UV/UF from USF Seral Reinstwassersysteme GmbH, (Baumbach) equipped with UV (185/254nm) and ultrafiltration (5000 kd cut off), or from Milli-Q-Synthesis (Millipore).

#### **2.1.2 Equipments**

Centrifuges used were: Biofuge 13, Heraeus; Sigma 204; Sigma 3K10; Labofuge 400R, Heraeus; Sorvall RC-5B, Du Pont instruments; Optima TLX Ultracentrifuge, Beckmann and Avanti J-20 XP, Beckman. BioRAD Gel dryer, Model-583; BioRad Power pack 300 or 3000; electrophoresis chambers from FMC Bioproducts (Rockland Maine US); Gel Electrophoresis Chamber, Cambridge electrophoresis; Biorad Mini Protean II; PTC-100, MJ Research Inc.; ÄKTA P-920, OPC-900, Frac-950, Amersham; Centrifuge tubes 15ml, TPP Switzerland; 50ml Falcon, BectonDickenson; Zeiss Axioplan II microscope equipped with AxioCam MRm camera (Zeiss). Zeiss Axiovert 200M motorized microscope equipped with AxioCam MRm camera (Zeiss). ELISA reader (Vmax, Molecular Devices)

### **2.1.3 Materials**

Sterile filters FP 030/3 0,2 µm and ME 24 0,2 µm (Schleicher und Schüll, Dassel); Nitrocellulose transfer membrane PROTRAN (Schleicher und Schüll, Dassel); 3MM Whatmann Paper (purchased via LaboMedic); 100 Sterican 0,50 x 16mm hypodermic needles (Braun AG, Melsungen); 0.2µm and 0.45µm sterile filters (Schleicher und Schuell, Dassel); X-OMAT LS and AR X-ray films, Kodak. All plastic ware for cell culture was from Sarstedt (Nümbrecht) or Greiner (Solingen).

### **2.1.4 Enzymes and Proteins**

Restriction enzymes (New England Biolabs); Pyrococcus furiosus (Pfu) DNA Polymerase (Promega, Mannheim); T4 DNA ligase (New England Biolabs); RNase A (Sigma); shrimp alkaline phosphatase (SAP) (USB, Amersham); PageRuler™ Prestained Protein Ladder (Fermentas); PageRuler™ Protein Ladder (Fermentas); SigmaMarker™ Wide Range (Sigma); GeneRuler™ DNA Ladder Mix (Fermentas).

### **2.1.5 Kits**

Plasmid Maxi and Midi kit (Qiagen, Hilden),  
Terminator-cycle Sequencing kit version 3 (ABI),  
QuikChange™ Site directed mutagenesis kit (Stratagen),  
Rapid PCR product purification Kit (Roche, Mannheim),

### **2.1.6 Vectors and constructs used in the present study**

pGW1H (British Biotech),  
pEGFP-C3, pEGFP-N3 (Clontech),  
pmDsRed-C3, pmDsRed-N3, pCherry-C3, pCherry-N3  
pF25: gift from Dr. Gregory A. Taylor, Duke University, coding for the N-terminally EGFP-tagged Irgm1 (Irgm1-EGFP).  
EGFP-Irgm1, EGFP-Irgm1  $\alpha$ K, EGFP-LC3, Irga6-ctag1-EGFP

### 2.1.7 Cell lines, bacterial and protozoan strains

Murine embryonic fibroblasts (MEFs) derived from C57/BL6 mice, L929 (CCL-1) and gs3T3 (Invitrogen) mouse fibroblasts were cultured in DMEM supplemented with 10% FCS (Biochrom AG, Berlin), 2 mM L-Glutamine, 1 mM sodium pyruvate, 100 U/ml penicillin and 100 µg/ml streptomycin, all from Gibco BRL. Human foreskin fibroblasts (Hs27, ATCC CRL-1634) were cultured in IMDM supplemented with 5% FCS and 2mM L-glutamine. Sterile trypsin/EDTA solution in PBS (10x trypsin/EDTA solution: 0.05% (w/v) trypsin (1:250, Gibco BRL)/17 mM EDTA/145 mM NaCl)) was used to detach adherent cells from culture flasks.

*Escherichia coli* DH5 $\alpha$ : 80dlacZ  $\Delta$ M15, recA1, endA1, gyrA96, thi-1, hsdR17 (rB-, mB+), supE44, relA1, deoR,  $\Delta$ (lacZYA-argF)U169

*Toxoplasma gondii*: Type II strain ME49, Type I strain RH-YFP

### 2.1.8 Media

Luria Bertani (LB) medium:

10 g bacto tryptone, 5 g yeast extract, 10 g NaCl, distilled water 1L

LB plate medium:

10 g bacto tryptone, 5 g yeast extract, 10 g NaCl, 15 g agar, distilled water 1L

IMDM (Iscove's Modified Dulbecco's Medium) supplemented with 10% FCS (Biochrom AG, Berlin), 2 mM L-glutamine, 1 mM sodium pyruvate, 1x non-essential amino acids, 100 U/ml penicillin, 100 µg/ml streptomycin (all from Gibco BRL)

DMEM (Dulbecco's Modified Eagle Medium) supplemented with 10% FCS (Biochrom AG, Berlin), 2 mM L-glutamine, 1 mM sodium pyruvate, 1x non-essential amino acids, 100 U/ml penicillin, 100 µg/ml streptomycin (all from Gibco BRL)

## 2.1.9 Serological reagents

### Primary antibodies and antisera

Name	Immunogen	Species	Concentration	Dilution	Origin
P20	N-terminus peptide of Irgm1	Goat polyclonal	0.2 mg/ml	IF: 1:100	Santa Cruz Sc-11074
1B2	Irgm1	Mouse monoclonal		IF: undiluted supernatant from hybridoma cell culture	Dr. Gregory Taylor Duke University
165	Recombinant Irga6	Rabbit polyclonal	1-3 mg/ml	WB: 1:25000 IF: 1:8000	
H53	N-terminus peptide of Irgm2	Rabbit polyclonal		IF: 1:1000	
$\alpha$ IGTP clone 7	aa 283-423 of Irgm3	Mouse monoclonal	0.25 mg/ml	WB: 1:2000	BD Transduction laboratories
A20	N-terminal peptide of Irgb6	Goat polyclonal	0.2 mg/ml	WB: 1:500 IF: 1:100	Santa Cruz sc11079
GM130	C-terminus of rat GM130	Mouse monoclonal IgG1		IF: 1:1000 WB: 1:250	BD transduction Lab. 610822
S-20	C-terminus peptide from rat TGN38 origin	Goat polyclonal	0.2 mg/ml	IF: 1:100	Santa Cruz Sc-27681
CI-M6PR antibody	CI-M6PR	Rabbit polyclonal		IF: 1:100	Albert Hass, Bonn
1D4B	Mouse LAMP1	Rat monoclonal		IF: 1:1000	DSHB, Iowa
SPA-865	Peptide from canine calnexin aa 50-68	Rabbit polyclonal		WB: 1:10000 IF: 1:200	Stressgen
GRA7	GRA7	Mouse monoclonal		IF: 1:1000	Gaby Reichmann Düsseldorf
Cytochrome C antibody	Rat cytochrome c	Mouse monoclonal	0.5 mg/ml	IF: 1:1000	BD PharMingen 556432 Clone: 6H2.B4
HMGB1 antibody	aa150 to the C-terminus of human HMGB1	Rabbit polyclonal	0.5 mg/ml	WB: 2 $\mu$ g/ml	Abcam ab18256
Cleaved Caspase-3 antibody	N-terminal peptide adjacent to Asp175 of human Caspase-3	Rabbit polyclonal		WB: 1:1000	Cell signaling Technology, Inc. #9661
PARP antibody	Peptide corresponding to the caspase cleavage site	Rabbit polyclonal		WB: 1:1000	Cell signaling Technology, Inc. #9542

### Secondary antibodies and antisera

The following secondary immunoreagents were used: goat anti-mouse Alexa 488 and 546, goat anti-rabbit Alexa 488 and 546, goat anti-rat Alexa 555, donkey anti-rat Alexa 488, donkey anti-goat Alexa 350, 488, 546 and 647, donkey anti-mouse Alexa 488, 555 and 647, donkey anti-rabbit Alexa 488, 555 and 647 (Molecular Probes; all used 1:1000 for immunofluorescence). Donkey anti-rabbit HRP (Amersham), donkey anti-goat HRP (Santa Cruz) and goat anti-mouse HRP (PIERCE) (all horse radish peroxidase (HRP)-coupled sera were used 1:5000 for immunodetection of Western blots). 4',6-Diamidino-2'-phenylindole dihydrochloride (DAPI, Invitrogen) was used for nuclear counterstaining at a final concentration of 0.5  $\mu$ g/ml.

### 2.1.10 Peptides

The following peptides are synthesized by JPT Peptide Technologies GmbH, Berlin

Irgm1  $\alpha$ K: H-SKLRLMTCAIVNAFFRLLRFLPCVCC-OH

Irgm1  $\alpha$ K ins362E: H-SKLRLMTCAIVNAEFFRLLRFLPCVCC-OH

Irgm2  $\alpha$ K: Biotin-SKVLARLYRTGTRVGSIGFDYMKCCFTSH-OH

Irgm3  $\alpha$ K: Biotin-SKMMCFAVNKFLRLLESSWWYGLWNVVTR-OH

The Irgm1  $\alpha$ K and Irgm1  $\alpha$ K ins362E peptides are biotinylated at the second residue Lysine.

## 2.2 Molecular Biology

### 2.2.1 Agarose gel electrophoresis

DNA was analysed by agarose gel electrophoresis (1x TAE; 0.04 M Tris, 0.5 mM EDTA, pH adjusted to 7.5 with acetic acid) The DNA was stained with ethidium bromide (0.3  $\mu$ g/ml), a fluorescent dye which intercalates between nucleotide bases, and the migration of the DNA molecules was visualized by using bromophenol blue.

### 2.2.2 Generation of the expression constructs

The following primers were used to generate the Irgm1 S90N mutant in EGFP-Irgm1 and Irgm1-EGFP (pF25) constructs.

Forward: 5'- gggactctggcaatggcatgaattctttcatcaatgcacttcg -3'

Reverse: 5'- cgaagtgcattgatgaaagaattcatgccattgccagagctcc -3'

Following mutations were introduced into EGFP-Irgm1  $\alpha$ K construct using the listed primers:

**L366A** Forward: 5'-gcaattgtgaatgctttctccgtttggcgagatttctccc -3'

Reverse: 5'-cgtaaacacttacgaaagaaggcaaacgctctaaagaggg -3'

**L365A** Forward: 5'-gcaattgtgaatgctttctccgcttgagatttctccc -3'

Reverse: 5'-cgtaaacacttacgaaagaaggcacgcaactctaaagaggg -3'

**R367A** Forward: 5'-gcaattgtgaatgctttctccgtttggcatttctcccatgc -3'

Reverse: 5'-cgtaaacacttacgaaagaaggcaacaaccgtaagaggggtacg -3'

**R364A** Forward: 5'-gcaattgtgaatgctttctccgctttgtgagatttctccc -3'

Reverse: 5'-cgttaacacttacgaaagaagcgaacaactctaaagaggg -3'

**F363A** Forward: 5'-gcaattgtgaatgctttcgcccgtttgttgagatttctccc -3'

Reverse: 5'-cgttaacacttacgaaagcgggcaacaactctaaagaggg -3'

**F362A** Forward: 5'-gcaattgtgaatgcagcattccggtttgttgagatttctccc -3'

Reverse: 5'-cgttaacacttacgtcgtgaaggcaacaactctaaagaggg -3'

**N360A** Forward: 5'-catgtgcaattgtggcagcatttctccg -3'

Reverse: 5'-gtacacgttaacaccgtcgtagaagggc -3'

**L365A, L366A**: Forward: 5'- gcaattgtgaatgctttcttcgctggcgagatttctccc -3'

Reverse: 5'-cgttaacacttacgaaagaaggcagccgctctaaagaggg -3'

**F362A, F363A** Forward :5'- gcaattgtgaatgcagcagcccgtttgttgagatttctccc -3'

Reverse: 5'-cgttaacacttacgtcgtcgggcaacaactctaaagaggg -3'

**N360A, R364A, R367A** Forward: 5'- gtgcaattgtggctgcatttctcgtttgttgagatttctccc -3'

Reverse: 5'-cacgttaacaccgacgtaagaagcgaacaaccgtaaagaggggtacgc -3'

**N360A, R364A** Forward: 5'- gtgcaattgtggctgcatttctcgtttgttgagatttctccc -3'

Reverse: 5'-cacgttaacaccgacgtaagaagcgaacaactctaaagaggg -3'

**R364A, R367A** Forward: 5'-gcaattgtgaatgctttcttcgctttgttgagatttctccc -3'

Reverse: 5'-cgttaacacttacgaaagaagcgaacaaccgtaaagaggggtacgc -3'

**F362A, F363A, L365A, L366A**

Forward: 5'- gcaattgtgaatgcagcagcccgtcggcgagatttctccc -3'

Reverse: 5'-cgttaacacttacgtcgtcgggacgcccgtctaaagaggggtacgc -3'

pmDsRed-C3, pmDsRed-N3, pCherry-C3, pCherry-N3 constructs were made by amplification of mDeRed or mCherry sequences from pDsRed-Monomer-N In-Fusion (Clontech) or mCherry-pRsetB (gift from Tsien 2005), respectively, by using the following primers. pmDsRed-C3 and pCherry-C3 PCR products were digested with NheI and ScaI, and ligated into the NheI/ScaI digested pEGFP-C3 vector. pmDsRed-N3 and pCherry-N3 PCR products were digested with BamHI and NotI, and ligated into the BamHI/NotI digested pEGFP-N3 vector.

pmDsRed-C3 Forward: 5'- cccccccc gctagc gccacc atg gacaacaccgaggacgtcat -3'

Reverse: 5'-cccccccc agtact t ctgggagccggagtggcgggc -3'

pmDsRed-N3 Forward: 5'-cccccccc ggatcc atg gacaacaccgaggacgtcat -3'

Reverse: 5'-cccccccc gcggccgc ctactgggagccggagtgggcgggc -3'

pCherry-C3 Forward: 5'-cccccccc gctagc gccacc atg gtgagcaagggcgaggagga -3'

Reverse: 5'-cccccccc agtact t cttgtacagctcgtccatgc -3'

pCherry-N3 Forward: 5'-cccccccc ggatcc atg gtgagcaagggcgaggagga -3'

Reverse: 5'-cccccccc gcggccgc ctactgtacagctcgtccatgc -3'

### **2.2.3 Cloning of PCR amplification products**

Amplified PCR products were purified using the rapid PCR purification Kit (Roche) and eluted with 100 µl 10mM Tris, pH 8.5. DNA yield was monitored by agarose gel electrophoresis and DNA fragments were digested with the appropriate restriction endonuclease (New England Biolabs) according to the suppliers' protocol. Restriction enzymes were used at a 5-10 fold over-digestion. Following restriction, DNA fragments were again column purified using the rapid PCR purification Kit (Roche) and DNA yield was monitored by agarose gel electrophoresis.

### **2.2.4 Purification of DNA fragments from agarose gels**

DNA fragments were loaded on agarose gels of the suitable percentage after incubation with appropriate restriction endonucleases. After proper separation of the fragments, DNA was visualized under a low energy UV source and cut out of the gel using a clean blade. DNA fragments were eluted from the gel with the rapid PCR purification Kit (Roche) according to the manufactures protocol. Purity and yield of the DNA was determined by agarose gel electrophoresis and UV spectroscopy.

### **2.2.5 Ligation**

The appropriate cloning vector was cut with the respective restriction enzyme(s) (10 U/ 1 µg DNA) for 1 h under according to the restriction enzyme suppliers' protocol. After the first hour the same amount of restriction enzyme and 0.1 U of shrimp alkaline phosphatase were added to the reaction followed by 1.5 h incubation. Following restriction, DNA fragments were column purified using the rapid PCR purification Kit (Roche) and DNA yield was

monitored by agarose gel electrophoresis. Vector and the appropriate cut insert were mixed at a ratio of 1:3 and ligated with T4-DNA ligase in a total volume of 10  $\mu$ l at 16°C over-night according to the manufactures protocol. As control, the same reaction without insert was carried out which should not yield any colonies after transformation into competent DH5 $\alpha$ .

### **2.2.6 Preparation of competent cells**

A single colony from a particular *E. coli* strain was grown over-night in 2 ml LB medium with 0.02 M MgSO<sub>4</sub>/ 0.01 M KCl with vigorous shaking (~300 rpm). It was diluted 1:10 into fresh medium with the same constituents and grown for 90 min, at 37°C to an OD<sub>600</sub> of 0.45. Cultures were incubated on ice for 10 min after which the cells were pelleted by centrifugation at 6000 rpm at 4°C for 5 min. Cells were resuspended in TFB I (30 ml/ 100 ml culture), incubated 5 min on ice, pelleted again by centrifugation at 6000 rpm at 4°C for 5 min and finally resuspended in TFB II (4 ml per 100 ml culture). 100  $\mu$ l aliquots of the competent bacteria were frozen at -80°C.

Composition of the buffers:

TFB I (30 mM KOAc/50 mM MnCl<sub>2</sub>/100 mM RbCl<sub>2</sub>/10 mM CaCl<sub>2</sub>/15% w/v glycerin, pH 5.8)

TFBII (10 mM MOPS, pH 7.5/ 75 mM CaCl<sub>2</sub>/ 100 mM RbCl<sub>2</sub>/ 15% w/v glycerin)

Both the solutions were sterilized and stored at 4°C.

### **2.2.7 Transformation of competent bacteria**

100  $\mu$ l of competent bacteria were thawed on ice and gently mixed 3-4 times. 5  $\mu$ l of the ligation reaction was added to the cells followed by incubation for 20 min on ice. Cells were then heat-shocked for 45 sec at 42°C followed by a further incubation on ice for 2 min. Antibiotic free LB medium was added to a total volume of 1 ml and cells were rolled at 37°C for 1 h. The culture was spun at 9000 rpm for 2 min and 800  $\mu$ l of the supernatant was removed. The cell pellet was resuspended in the remaining 200  $\mu$ l medium in the 1.5 ml reaction tube and plated on a LB agar plate supplemented with the appropriate antibiotics.

### **2.2.8 Plasmid isolation**

For screening a large number of cultures for clones containing the desired insert, 4 ml LB cultures with the appropriate antibiotics were inoculated with single colonies picked from a ligation plate and grown over-night at 37°C, 250 rpm. All following steps were performed at room temperature. 1.5 ml of the cultures was transferred into a 1.5 ml reaction tube and pelleted by centrifugation at 23000 g for 5 min. The supernatant was discarded and pellet resuspended in 100 µl P1 (50 mM Tris, pH 8.0/ 10 mM EDTA/ 100µg/ml RNase A). After addition of 100 µl P2 (200mM NaOH/ 1% SDS) the reaction was gently mixed and incubated for 5 min. 140 µl of P3 (3M potassium acetate, pH 5.5) was added and the reaction was spun for 15 min at 23000 g. The supernatant (~340 µl) was transferred into a new tube and 700 µl of 100% ethanol was added. After mixing, the reaction was spun for 15 min at 23000 g and the supernatant was removed. The pellet was washed by addition of 700 µl of 70% ethanol and spun at 23000 g. After removal of the supernatant the pellet was air-dried and resuspended in 50 µl 10mM Tris pH 8.0. 5 µl of the plasmid preparation was cut with the appropriate restriction enzyme(s) in a total volume of 50 µl for 1 h and 10 µl of the reactions were subjected to agarose gel electrophoresis to identify insert-containing clones.

For preparation of large amounts of plasmid, the Qiagen Midi and Maxi Plasmid Preparation Kits were used according to the manufactures instructions.

### **2.2.9 Determination of the concentration of DNA**

The concentration of DNA was measured using a spectrophotometer at 260 nm. The purity of the DNA solution was determined using the ratio of OD readings at 260 nm and 280 nm. Pure preparations of DNA have an  $OD_{260}/OD_{280}$  ratio of 1.8. The concentration was calculated according to the following equation.  $c = A_{260} \times 50 \mu\text{g/ml} \times \text{dilution factor}$ .

### **2.2.10 Site directed mutagenesis**

Site directed mutagenesis was carried out using a modified protocol supplied with “Quik-Change™ XL Site-Directed Mutagenesis” Kit from Stratagene. The amplification was carried out using 20 ng plasmid as template, 125 ng of the sense and antisense oligonucleotide as

primers and 2.5 U of Pfu-polymerase (Promega) in a total volume of 50  $\mu$ l. The following program was used: 1. 95°C, 30 sec; 2. 95°C, 30 sec; 3. 55°C, 60 sec; 4. 68°C, 15 to 20 min (back to step 2., 15 to 18 times); 5. 68°C, 15 min. After amplification 1  $\mu$ l *DpnI* (20 U, New England Biolabs) was added to the reaction and incubated for 1.5 h at 37°C. 5  $\mu$ l of the reaction was used to transform 200  $\mu$ l competent DH5 $\alpha$ . As control the whole procedure was carried out without addition of Pfu-polymerase. Ideally no colonies are found on the final LB agar plate for the control reaction.

### **2.2.11 DNA Sequencing**

All constructs generated were verified by sequencing. DNA was sequenced using the *ABI Prism<sup>R</sup> BigDye<sup>TM</sup> Terminator Cycle Sequencing Ready Reaction Kit* (PE Applied Biosystems), using fluorescently labeled dideoxynucleotides based on the dideoxy-chain termination. Template DNA (0.5  $\mu$ g), the respective primer (10 pmole) and 2  $\mu$ l *Big Dye<sup>TM</sup>* terminator ready reaction mix (ABI) were combined in a total volume of 10  $\mu$ l and the sequencing reaction was carried out as follows: 25x (96°C, 30 sec; 50°C, 15 sec; 60°C, 4 min). Sequencing was done on an automated sequencer (ABI 373A).

## **2.3 Cell biology**

### **2.3.1 Transfection**

Cells were transiently transfected for 24 h at 37°C using FuGENE 6 Transfection Reagent (Roche) according to the manufacturer's protocol. DNA ( $\mu$ g): FuGENE6 ( $\mu$ l) ratio was always 1:3. For transfection of cells in 6 well plates or in 60 mm dish 1  $\mu$ g or 2  $\mu$ g of DNA was used respectively.

### **2.3.2 Transferrin uptaking experiments**

Cells were grown on coverslips and starved for 1 hour in the FCS-free medium. To label the early endosomes, Alexa-546 labeled human Transferrin (Molecular Probes) was then diluted to the final concentration of 5  $\mu$ g/ml into the FCS-free medium, and cells were incubated at

37°C, 7.5% CO<sub>2</sub> for 5 minutes. Cells were then fixed with ice-cold 3% PFA in PBS for 20 minutes.

To label the recycling endosomes, the cells were incubated with FCS-free medium with diluted transferrin for 10 minutes after starvation, then washed with ice-cold PBS for 3 times. The full medium was added afterwards and the cells were incubated at 37°C, 7.5% CO<sub>2</sub> for 30 minutes. Finally cells were fixed with ice-cold 3% PFA in PBS for 20 minutes followed by three times washing with PBS and subjected to the immunofluorescence staining.

### **2.3.3 LysoTracker loading experiments**

LysoTracker Red DND-99 (Molecular Probes) was diluted to a final concentration of 50 nM in the full medium and the cells were incubated at 37°C, 7.5% CO<sub>2</sub> for 20 minutes. Cells were then fixed with ice-cold 3% PFA in PBS for 20 minutes followed by three times washing with PBS and subjected to the immunofluorescence staining.

### **2.3.4 Latex beads phagocytosis experiments**

MEFs were grown on the coverslips, treated with 200 U/ml IFN- $\gamma$  and/or transfected with indicated constructs for 24 hours. During the IFN- $\gamma$ -treatment and/or transfection procedure, 2  $\mu$ m carboxylated latex beads (Polysciences) were added to the culture at a dilution of 1:1000, and the cells were incubated with the latex beads at 37°C overnight. The latex beads were extensively phagocytosed by the MEFs through unidentified receptors. Finally the cells were fixed with 3% paraformaldehyde (PFA) for 20 minutes at room temperature and subjected to the immunofluorescence staining.

### **2.3.5 Immunocytochemistry**

Cells were grown on coverslips, fixed with PBS/ 3% paraformaldehyde (PFA) for 20 min and subsequently washed three times with PBS. Cells were permeabilized with PBS/0.1% saponin (washing buffer) followed by a blocking step with PBS/0.1% saponin/1% BSA (fractionV) (blocking buffer) for 1 hour. Coverslips were incubated with primary antibodies (diluted in blocking buffer) in a humid chamber for 1 h at RT and subsequently washed 3x 5 min with washing buffer. Incubation with secondary antibodies was done as described for primary

antibodies for 30 min at RT and washed 3x as described above. Coverslips were mounted on slides with ProLong<sup>®</sup> Gold antifade reagent (Invitrogen), sealed with nail polish and cleaned with deionized water. DAPI, used to stain DNA (300 nM), was added to the secondary antibody solution. Images were taken with a Zeiss Axioplan II fluorescence microscope equipped with an AxioCam MRm camera (Zeiss). Images were processed with Axiovision 4.6 software (Zeiss).

### **2.3.6 Peptide-streptavidin complex experiments**

The peptides were dissolved in 10mM NaAc pH4.5 buffer with 10mM TCEP as reducing agent and stored at -80°C with a stock concentration of ~100 µM. The absolute absorbance of the Irgm1 αK peptide at 230 nm in the dissolving buffer is ~0.46/100 µM.

The peptide-streptavidin complex was made in the blocking buffer used in the immunofluorescence staining (PBS pH7.4/0.1% saponin/1% BSA with additional 2 mM DTT). The C3-labelled streptavidin (Sigma, S6402) was first diluted in the blocking buffer to a final concentration of 20 µg/ml (0.33 µM). The peptide stocking solution was then added to the streptavidin solution with a titration from 4:1 to 50:1 molar ratio (peptide to streptavidin). The optimum ratio was experimentally determined based on the staining signals (8 µM peptide in the Figure 3.18). The peptide-streptavidin solution was well-mixed and then spun down at 45.000 rpm for 30 minutes. The supernatant was recovered and antibodies against indicated proteins were added. This solution was used as the primary antibody in the immunofluorescence staining, and was incubated with the PFA-fixed saponin permeabilized cells at 37°C for 1 hour. The peptide-streptavidin images were obtained through Cy3 channel in the Zeiss Axioplan II fluorescence microscope.

### **2.3.7 *In vitro* passage and infection of *Toxoplasma gondii***

Tachyzoites from *T. gondii* strains ME49 and RH-YFP were maintained by serial passage in confluent monolayer of human foreskin fibroblasts (HS27, ATCC number CRL-1634). RH-YFP parasites were propagated in presence of Chloramphenicol (3.2 µg/ml, Sigma-Aldrich) to maintain the stably integrated YFP expression plasmid containing a chloramphenicol acetyltransferase selection marker.

The *T. gondii* replicate intracellularly and egress from their host cells approximately 3 days later. Extracellular parasites were harvested from the supernatant and purified from host cell debris by differential centrifugation (5 minutes at 100g, 15 minutes at 500g). The parasites were resuspended in medium, counted using a Neubauer chamber and immediately used for the infection of the host cells.

### **2.3.8 Live cell imaging**

All the live cell imaging experiments were performed in  $\mu$ -slide I (ibidi, München). Cells were incubated in phenol-red-free DMEM supplemented with 10% FCS, 20 mM HEPES pH 7.4, 2 mM L-glutamine, 1 mM sodium pyruvate, 1x non-essential amino acids, 100 U/ml penicillin, and 100  $\mu$ g/ml streptomycin.  $1 \times 10^5/100 \mu$ l MEFs were seeded in the channel of the  $\mu$ -slide I and 500  $\mu$ l medium was then added to each of the reservoirs. For the transfection experiments, 2  $\mu$ g DNA/6  $\mu$ l Fugene6 in 100  $\mu$ l FCS-free medium was prepared and 50  $\mu$ l of the transfection reagent was added to the channel of one  $\mu$ -slide I. The cells were simultaneously stimulated with 200 U/ml IFN- $\gamma$  for 24 hours. After infection with *T. gondii*, the cells were observed under the Zeiss Axiovert 200M motorized microscope with the objective EC “Plan-Neofluar” 40 $\times$ /1.30 Oil Ph3 (Zeiss). The time-lapse images were obtained and processed by Axiovision 4.6 software (Zeiss).

Phosphatidylserine exposure were detected by adding 1% (v/v) annexin-V-Alexa555 (Molecular Probes) with 2.5 mM CaCl<sub>2</sub> into the medium. Propidium iodide (0.4 mg/ml) was added into the medium to detect the loss of cell plasma membrane integrity.

### **2.3.9 Quantification of IRG signals on *T. gondii* parasitophorous vacuoles**

The signal intensities for the specific IRG proteins on the *T. gondii* parasitophorous vacuoles were quantified using the ImageJ software (Wayne Rasband, NIH). The images are processed in 16-bit (Zeiss Axioplan II microscope) or 12 bit (Zeiss Axiovert 200M motorized microscope) gray-scale TIFF format. Two intensity profiles orthogonal to each other were generated per vacuole followed by subtraction of the background values. The average of the 4 peak values was obtained for each vacuole. The average pixel intensity of each vacuole was plotted for each IRG protein in a scatter plot using Excel (Microsoft).

### **2.3.10 Cell viability assay**

7500 cells/well MEFs were seeded into 96-well plates and treated with IFN $\gamma$  or control condition for 24 hours. The cells were then infected with *T. gondii* avirulent strain ME49 or virulent strain RH-YFP for 8 or 20 hours. Thereafter, the viable cells were quantified by the CellTiter 96 AQueous non-radioactive cell proliferation assay (Promega) according to the manufacturer's instructions. The absorption of the bio-reduced form (formazan) of a substrate (MTS) generated by metabolically active cells during incubation at 37°C for 2-4 hours was measured in an ELISA reader (Molecular Devices) at 490 nm. The quantity of formazan product is directly proportional to the number of living cells in the culture.

### **2.3.11 Western blotting**

After SDS-PAGE, proteins were transferred to nitrocellulose transfer membranes (Schleicher & Schuell) by electroblotting. The gel was placed in contact to a nitrocellulose transfer membrane, and was sandwiched between four sheets of 3 mm Whatmann paper, two porous pads, and two plastic supports on either side, soaked in a transfer buffer containing 25 mM Tris/ 190 mM glycine. The sandwich was then placed between platinum plate electrodes, with the nitrocellulose membrane facing the anode, and the transfer was carried out at RT for 1 h with a current of 0.5 V. Ponceau S staining was used to locate proteins (0.1% (w/v) Ponceau S (Sigma) in 5% (v/v) acetic acid) after Western blotting. Membranes were blocked with PBS/ 5% milk powder/ 0.1% Tween 20 or Western Blotting Blocking Reagent (Roche) at room temperature for 1 h or over-night at 4°C. Antisera/ antibodies were diluted in PBS/ 5% FCS/ 0.1% Tween 20 or PBS/ 5% Western Blotting Blocking Reagent. Bands were visualized with enhanced chemiluminescence (ECL) substrate.

## Results-I

### 3.1 Irgm1 localizes to Golgi apparatus and late endocytic/lysosomal compartments.

Irgm1 (LRG-47) was reported to be exclusively in membrane-bound form and localized to the Golgi apparatus in L929 fibroblasts, TIB-75 hepatocytes and Raw 264.7 macrophages. This localization is mediated by an amphipathic helix near the C-terminus (Martens 2004b). It was also noted that in addition to the Golgi localization, there is a distributed granular signal throughout the cell periphery, of which the subcellular localization remained to be identified. In order to investigate in detail the intracellular distribution of Irgm1, C57BL/6 embryonic fibroblasts were used in the present study, which is microscopically favorable. Compared to L929 cells or macrophages that are morphologically round and small (~25µm), MEFs are much larger (50-100µm) and spread flat on the cover slips. In IFN-γ treated MEFs, both goat polyclonal anti-Irgm1 antiserum P20 and mouse monoclonal anti-Irgm1 antibody 1B2 gave a focused perinuclear signal and additional distributed granular signals. The perinuclear signal accurately overlaps with both cis-Golgi matrix protein GM130 and trans-Golgi/trans-Golgi network protein TGN38 (Figure 3.1, a-f). Less accurate colocalization was seen with cation-independent mannose 6 phosphate receptor (CI-M6PR), which is predominantly distributed in the late endosomes, less in the trans-Golgi network and ~10% at plasma membrane. Irgm1 localizes rather to places adjacent to or partially overlapping with CI-M6PR positive compartments (Figure 3.1, g-l). Furthermore, the distributed granular signal of Irgm1 accurately colocalized with the late endosome/lysosome marker LAMP1 (Figure 3.2). By comparison, Irgm2 localizes exclusively to Golgi apparatus, with no extra signal overlapping with LAMP1 (Figure 3.2, c). To confirm the apparent lysosomal localization of Irgm1, the acidotropic dye LysoTracker was loaded and cells were costained with anti-Irgm1 antibody 1B2. Irgm1 was found to accumulate around the LysoTracker enriched compartments (Figure 3.2, e-g). Hence, Irgm1 is associated with late endocytic/lysosomal compartments in addition to Golgi apparatus.

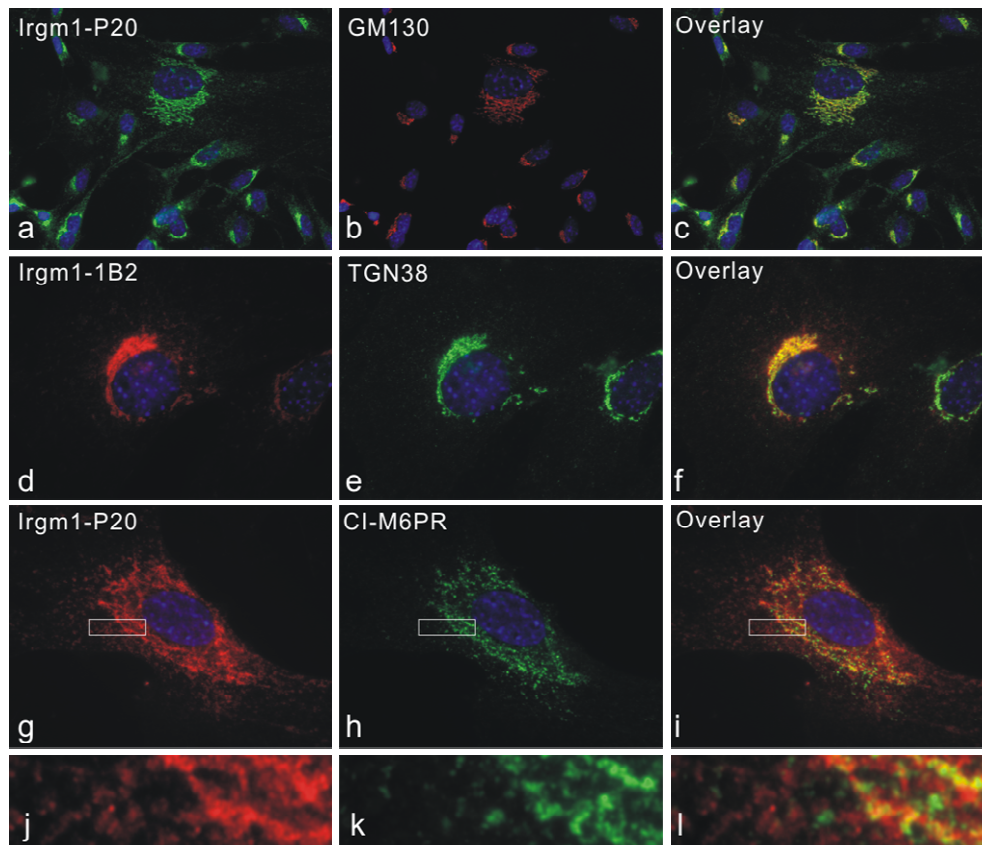


**Figure 3.1 Irgm1 localizes to Golgi apparatus.**

MEFs were treated with 200U/ml IFN- $\gamma$  for 24 hours, fixed with 3% PFA in PBS, and stained for Irgm1 by goat antiserum P20 (a-c, g-l) or mouse monoclonal antibody 1B2 (d-f) and indicated marker proteins by indirect immunofluorescence. Irgm1 accurately colocalized with GM130 (a-c) and TGN38 (d-e), and localized to adjacent places or partially colocalized with the CI-M6PR positive compartments (j-l are the enlargement of the squares in g-i, respectively). Magnification: a-c 400x, d-l 630x. Nuclei were labelled with DAPI.

To examine whether Irgm1 also localizes to the early and recycling endocytic compartments, IFN- $\gamma$  induced MEFs were labeled either with Alexa-Fluor-546-labelled transferrin for 5 minutes or pulsed with transferrin for 10 minutes, then chased for 30 minutes, to label early or recycling endosomes, respectively. Transferrin is a serum glycoprotein that binds Fe<sup>3+</sup> ions for delivery to the cells through receptor-mediated endocytosis into early endosomes. In acid environment (endosomes) the Fe<sup>3+</sup> is released from transferrin-receptor complex and the transferrin is recycled to the plasma membrane through the recycling endosomes (Rothenberger 1987). Fluorescent transferrin conjugates can therefore be used to label early and/or recycling endosomes. The diffuse granular signal of Irgm1 showed no manifest overlapping with early or recycling endosomes (Figure 3.3). Therefore, Irgm1 is not distributed in early/recycling endocytic compartments at a detectable level.

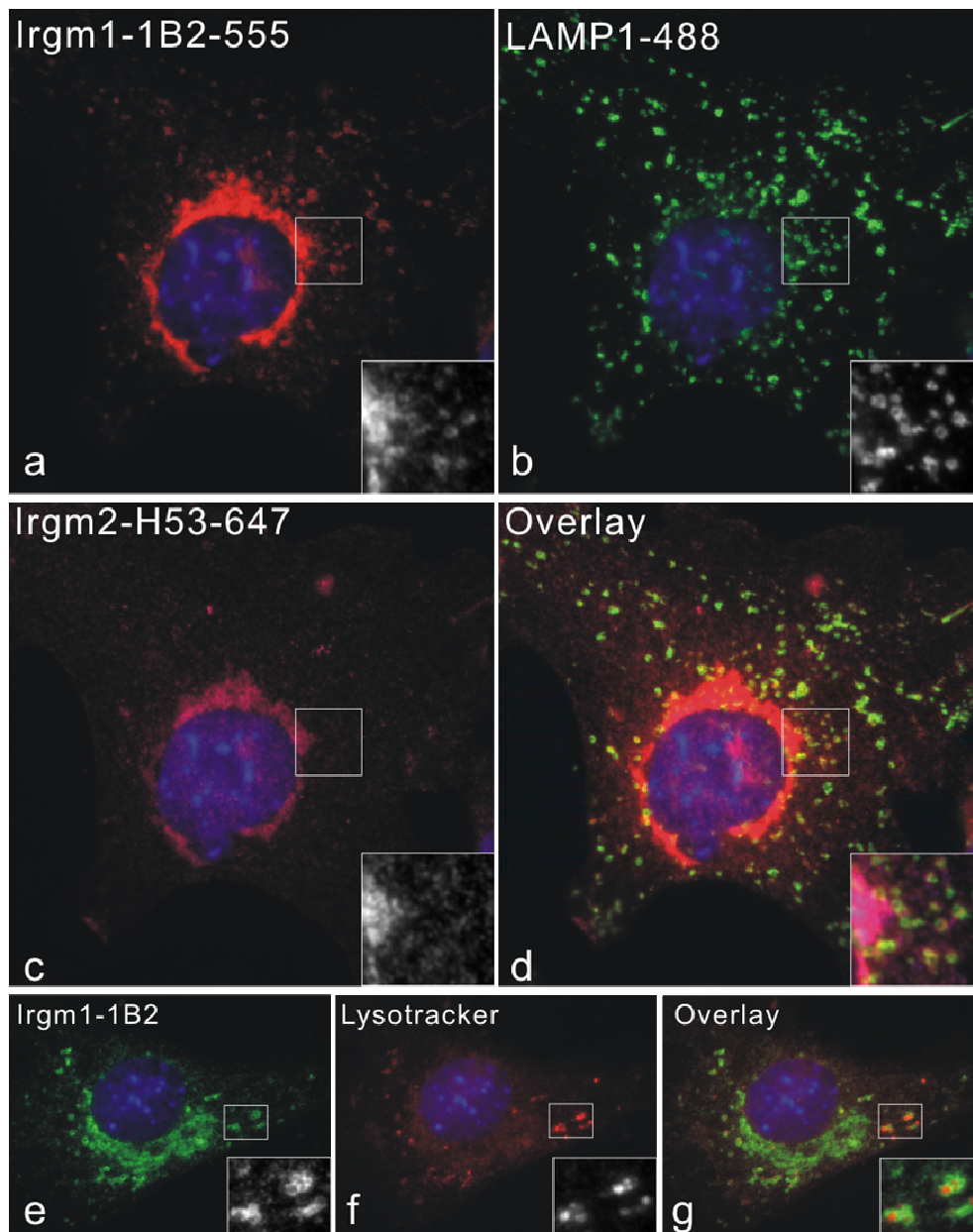


**Figure 3.2 Irgm1 localizes to late endocytic/lysosomal compartments in addition to Golgi apparatus.**

a-d, MEFs were treated with 200U/ml IFN- $\gamma$  for 24 hours, fixed with 3% PFA in PBS, and stained by indirect immunofluorescence using 1B2, 1D4B, and H53 against Irgm1, LAMP1 and Irgm2, respectively. Secondary Alexa Fluor 555 labelled donkey anti-mouse, Alexa Fluor 488 labelled donkey anti-rat, and Alexa Fluor 647 labelled donkey anti-rabbit antiserum were used, respectively. e-g, after treatment with 200U/ml IFN- $\gamma$  for 24 hours, cells were incubated with 50 nM LysoTracker Red DND-99 for 30 minutes in the full medium, fixed with 3% PFA in PBS, and stained for Irgm1 by 1B2 antibody. Irgm1 was found to associate with LAMP1 positive compartments (a-d) and accumulate around the LysoTracker enriched compartments (e-g) in addition to Golgi localization. Irgm2 localizes exclusively to Golgi apparatus (c). Magnification: 630x. Nuclei were labelled with DAPI.

To conclude, Irgm1 localizes to Golgi apparatus, including *cis*-Golgi and *trans*-Golgi networks. In addition, Irgm1 also localizes to the late endocytic/lysosomal compartments, but scarcely, if at all, to the early/recycling endocytic compartments.

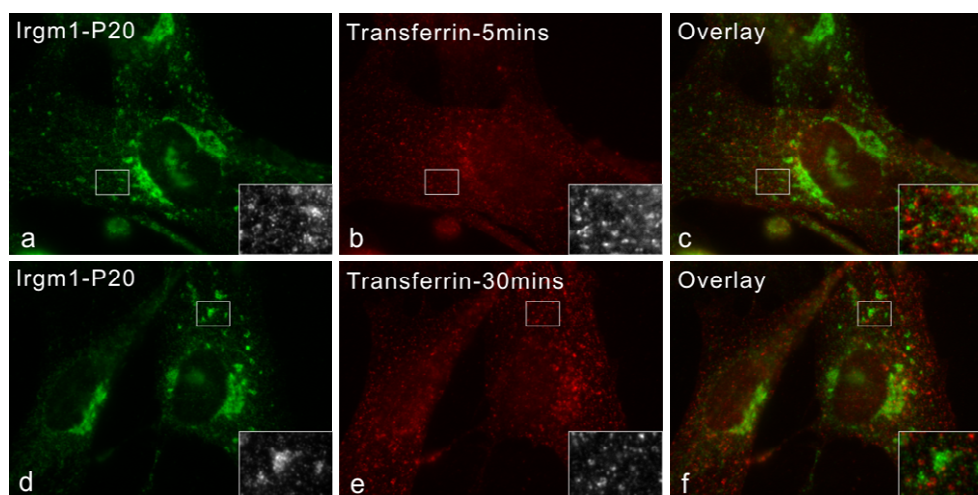


**Figure 3.3 Irgm1 is not associated with early or recycling endosomes.**

After treatment with 200U/ml IFN- $\gamma$  for 24 hours, MEFs were incubated with Alexa-Fluor-546-labelled transferrin for 5 minutes (a-c) or pulsed with transferrin for 10 minutes, then chased for 30 minutes (d-f). Cells were then fixed with 3% PFA in PBS and P20 goat antiserum was used to stain Irgm1 by indirect immunofluorescence. The granular signals from Irgm1 were not found to associate with transferrin positive compartments. Magnification: 630x.

### 3.2 Both N and C terminal EGFP-tag lead to the mislocalization of Irgm1

Deretic *et al* reported that Irgm1 (LRG-47) is required to initiate an interferon-induced autophagic process as a protection mechanism against *Mycobacterium tuberculosis* infection (Gutierrez 2004; Singh 2006). This claim was based on over-expression experiments using C-terminally EGFP-tagged Irgm1. However, Martens reported earlier that both N and C terminally tagged Irgm1 misbehave in cells (Martens 2004b). To investigate in depth which compartments tagged Irgm1 localize in cells, both N and C terminally EGFP-tagged Irgm1 were expressed in MEFs and co-stained with Golgi marker protein GM130 and TGN38 by indirect immunofluorescence. EGFP-Irgm1 and Irgm1-EGFP both showed diffuse vesicular and dotty expression pattern throughout the cytoplasm. Colocalization with Golgi protein GM130 and TGN38 was abolished (Figure 3.4 and Figure 3.5). Many of those vesicular and dotty signals strongly colocalized with transferrin labeled early endosomes and recycling endosomes (Figure 3.6). As mentioned earlier, no colocalization was found between native IFN- $\gamma$  induced Irgm1 and early and recycling endosomes (Figure 3.3). Furthermore, Irgm1-EGFP construct showed strong colocalization with lysosomal marker LAMP1 while in EGFP-Irgm1 version, lysosomal association was largely abolished (Figure 3.7). Since Irgm1 associates with membrane independent of IFN- $\gamma$  induced factors, we asked whether IFN- $\gamma$  could influence the mislocalization of EGFP-Irgm1 and Irgm1-EGFP. Two constructs

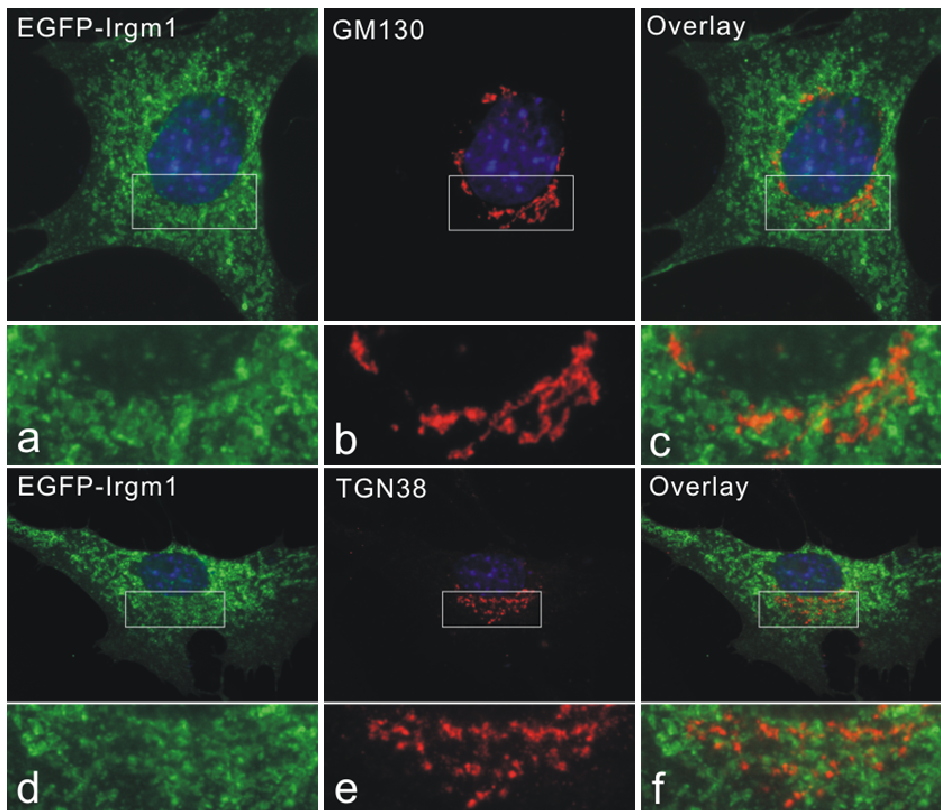


**Figure 3.4 N-terminally EGFP-tagged Irgm1 is dislodged from Golgi apparatus.**

EGFP-Irgm1 was transiently transfected into MEFs by using Fugene 6 transfection reagent. 24 hours later, cells were fixed with 3% PFA in PBS, stained for GM130 (a-c) and TGN38 (d-f) by indirect immunofluorescence. EGFP-Irgm1 was found to be absent from Golgi apparatus. Magnification: 630x. Nuclei were labelled with DAPI.

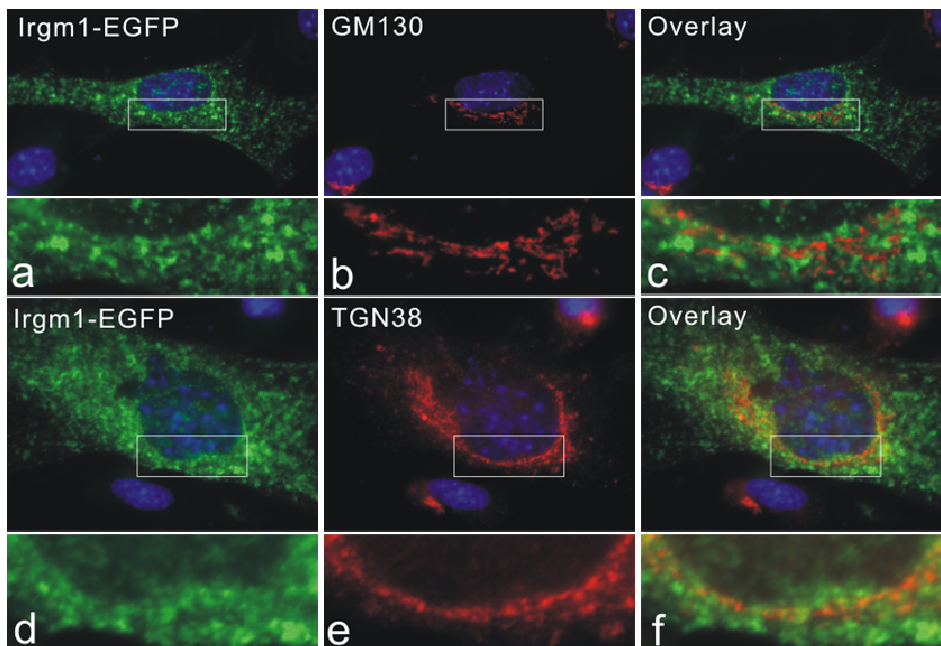


**Figure 3.5 C-terminally EGFP-tagged Irgm1 is not localized to Golgi apparatus.**

Irgm1-EGFP (pF25) was transiently transfected into MEFs by using Fugene 6 transfection reagent. 24 hours later, cells were fixed with 3% PFA in PBS, stained for GM130 (a-c) and TGN38 (d-f) by indirect immunofluorescence. Irgm1-EGFP was not colocalized with GM130 or TGN38. Magnification: 630x. Nuclei were labelled with DAPI.

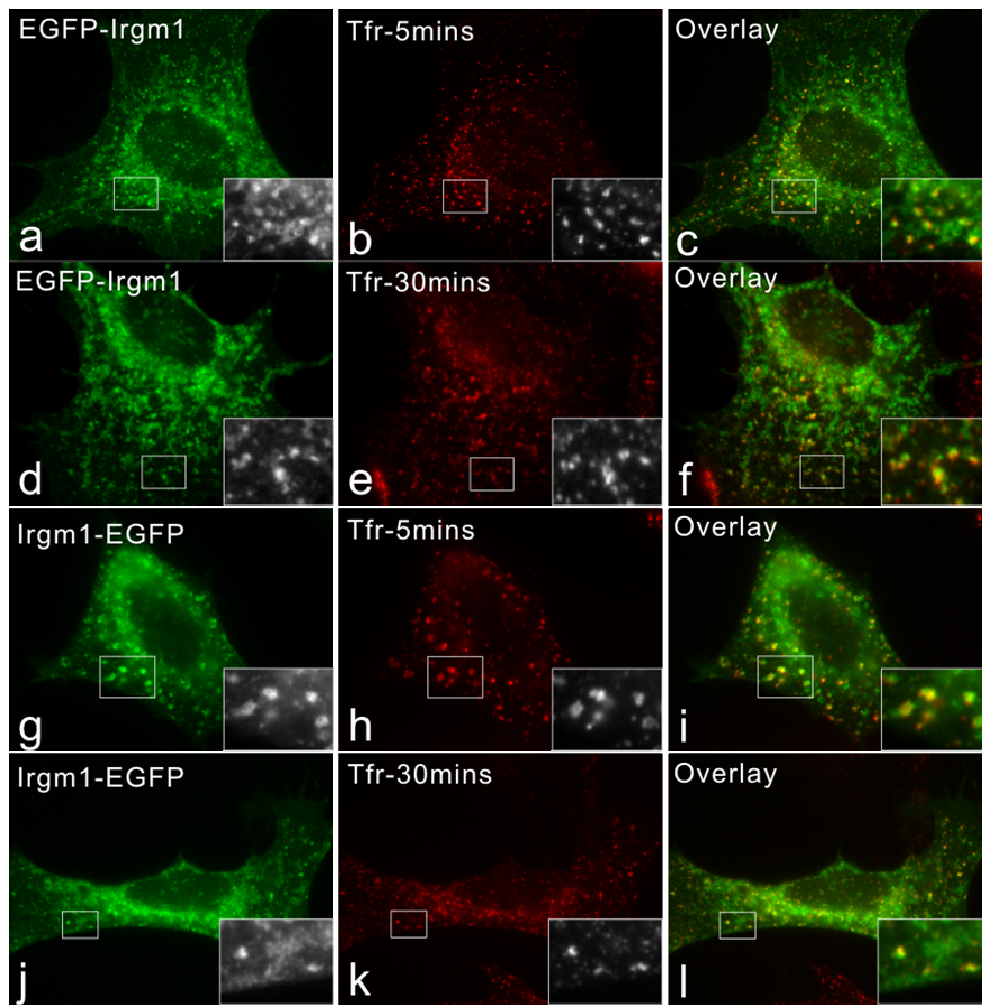


**Figure 3.6 N or C terminally EGFP-tagged Irgm1 mislocalize to early and recycling endosomes.**

EGFP-Irgm1 (a-f) and Irgm1-EGFP (pF25, g-l) was transiently transfected into MEFs by using Fugene 6 transfection reagent. 24 hours later, cells were incubated with Alexa-Fluor-546-labelled transferrin for 5 minutes (a-c, g-i) or pulsed with transferrin for 10 minutes, then chased for 30 minutes (d-f, j-l). Cells were then fixed with 3% PFA in PBS and directly observed under microscope. The vesicular and dotted signals from EGFP-Irgm1 and Irgm1-EGFP strongly overlap with transferrin-labelled early and recycling endosomes. Magnification: 630x.

were transfected into MEFs simultaneously induced with IFN- $\gamma$ . The same manner of mislocalization of EGFP-Irgm1 and Irgm1-EGFP was observed (data not shown).

In conclusion, N or C terminally EGFP-tagged Irgm1 does not localize to Golgi apparatus, and mislocalizes to early and recycling endocytic compartment. And this mislocalization is IFN- $\gamma$  independent.

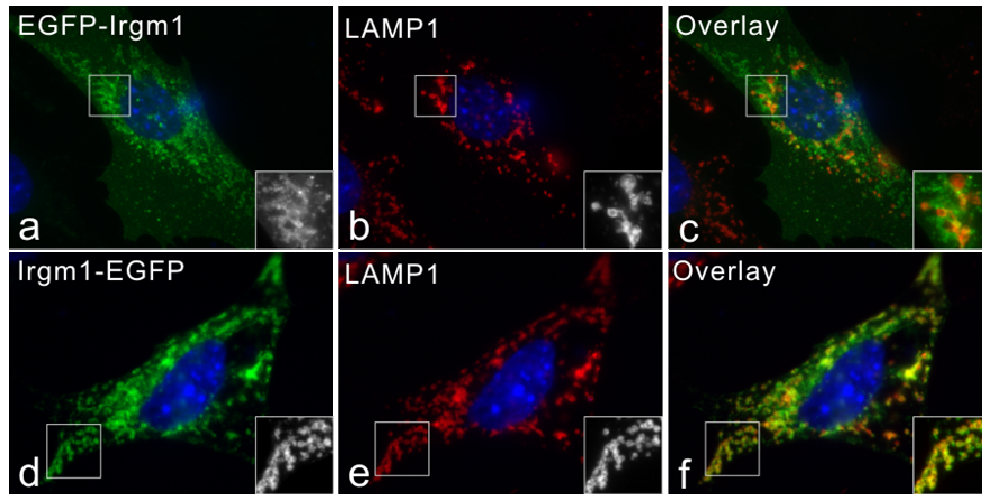


**Figure 3.7 Irgm1-EGFP strongly associates with lysosomes, while EGFP-Irgm1 is largely absent from lysosomal compartments.**

EGFP-Irgm1 (a-c) and Irgm1-EGFP (d-f, pF25) was transiently transfected into MEFs by using Fugene 6 transfection reagent. 24 hours later, cells were fixed with 3% PFA in PBS, stained for LAMP1 by indirect immunofluorescence. Irgm1-EGFP is strongly colocalized with LAMP1 while lysosomal association of EGFP-Irgm1 was largely abolished. Magnification: 630x. Nuclei were labelled with DAPI.

### 3.3 Mislocalization of Irgm1 by EGFP tagging is nucleotide dependent.

Irgm1 is associated with Golgi apparatus independent of nucleotide binding (Martens 2004b). To test whether mislocalization of Irgm1 caused by EGFP tagging is influenced by nucleotide binding, Irgm1 nucleotide binding deficient mutant (S90N) tagged with EGFP at N or C terminus were expressed in the cells. Notably more cytoplasmic reticular and vesicular signals were seen. However, Golgi localization of native Irgm1 was restored as shown by costaining with Golgi protein TGN38 (Figure 3.8) and GM130 (data not shown). The expression patterns of EGFP-Irgm1 (S90N) and Irgm1-EGFP (S90N) were similar to the localization of untagged nucleotide-binding deficient Irgm1 (S90N) (compare Figure 3.8 a, d with Figure 3.9 e, as well as Martens 2004b).

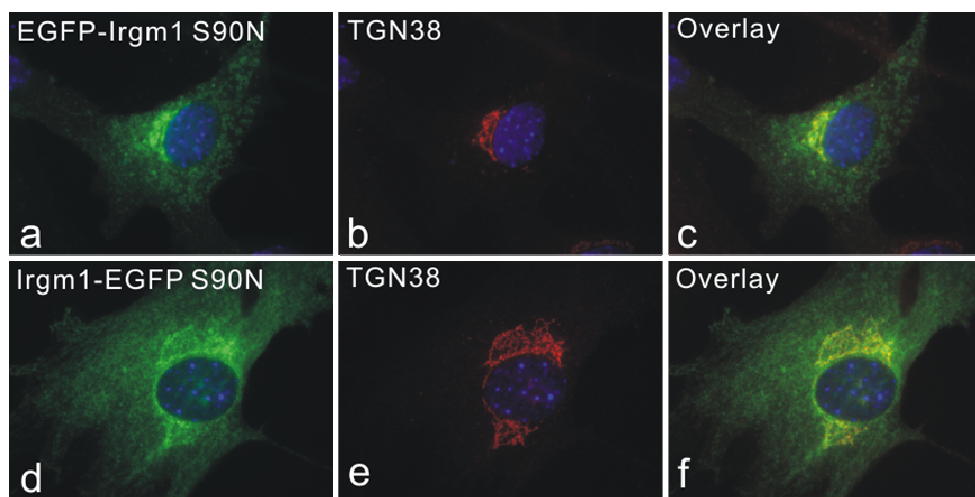


**Figure 3.8 EGFP-Irgm1 S90N and Irgm1-EGFP S90N localize to Golgi apparatus.**

EGFP-Irgm1 S90N (a-c) and Irgm1-EGFP S90N (d-f) was transiently transfected into MEFs by using Fugene 6 transfection reagent. 24 hours later, cells were fixed with 3% PFA in PBS, stained for TGN38 by indirect immunofluorescence. Both constructs colocalize with Golgi marker TGN38, although significant proportion of transfected proteins display additional cytoplasmic reticular and vesicular signals. Magnification: 630x. Nuclei were labelled with DAPI.

### **3.4 Phagosomal accumulation of Irgm1 is nucleotide dependent, but IFN- $\gamma$ independent.**

In L929 and Raw264.7 cells, IFN- $\gamma$  induced Irgm1 is rapidly recruited to active plasma membrane upon phagocytosis and remains associated with phagosomes as they mature. It was also reported that Irgm1 associates with Golgi apparatus in an IFN- $\gamma$  and nucleotide independent manner (Martens 2004b). It was therefore attempted to analyze whether Irgm1 can accumulate on the phagosomes independent of IFN- $\gamma$  and if so, whether the association with phagosomes is regulated by the nucleotide binding motif. Due to expression of undefined phagocytic receptors in primary murine embryonic fibroblasts, 2- $\mu$ m latex beads are extensively taken up after 4 hours of incubation (data not shown). Therefore, this phenomenon was used to study the accumulation of IRG proteins on the phagosomes. Irgm1 wild type and nucleotide binding deficient mutant S90N were expressed in MEFs in the absence of IFN- $\gamma$  and phagocytosis was initiated by incubating with 2- $\mu$ m latex beads overnight. Indirect immunofluorescence was performed and LAMP1 staining was used as a marker for latex beads-containing phagosomes. Wild type Irgm1 strongly associated with latex beads-containing phagosomes while Irgm1 S90N lost the phagosomal accumulation (Figure 3.9). Transfected Irgm1 also colocalized with LAMP1 positive compartments in unstimulated phagocytic cells (Figure 3.9, arrows), as well as in cells not involved in phagocytosis (Figure 3.13). Irgm1 S90N still showed Golgi localization while lysosomal

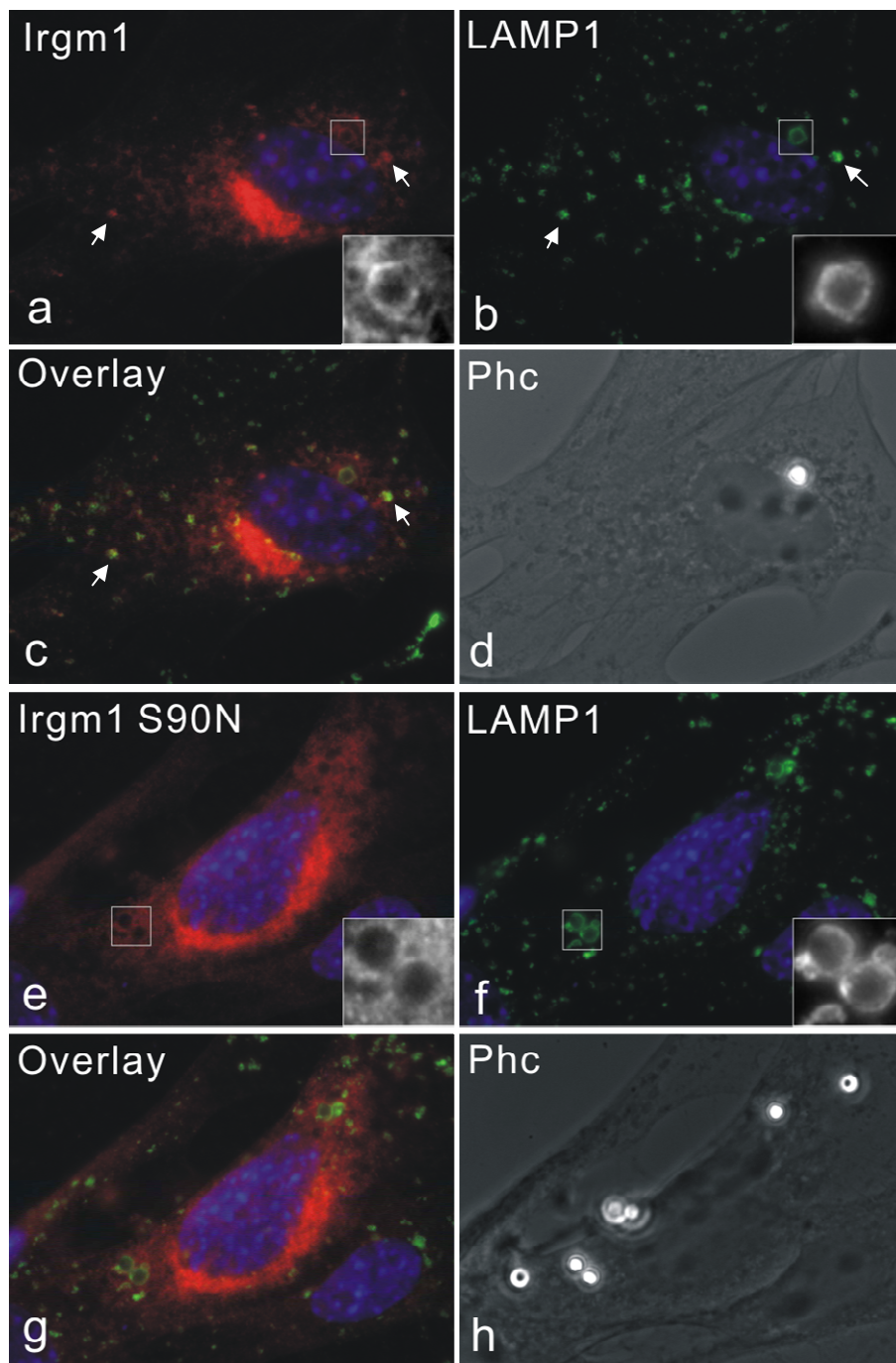


**Figure 3.9 Accumulation of Irgm1 on phagosomes is nucleotide dependent.**

Irgm1 wild type (a-d) and S90N mutant (e-h) in pGW1H vector were transiently transfected into MEFs for 24 hours by using Fugene 6 transfection reagent. During transfection, cells were incubated with 2- $\mu$ m latex beads overnight. Cells were then fixed with 3% PFA in PBS and staining for Irgm1 and LAMP1. Irgm1 accumulates around the latex beads phagosomes while the destroying of the nucleotide binding site completely abolished the phagosomal accumulation. Arrows indicate the colocalization of transfected wild type Irgm1 with LAMP1 positive compartments. Magnification: 630x. Nuclei were labelled with DAPI.

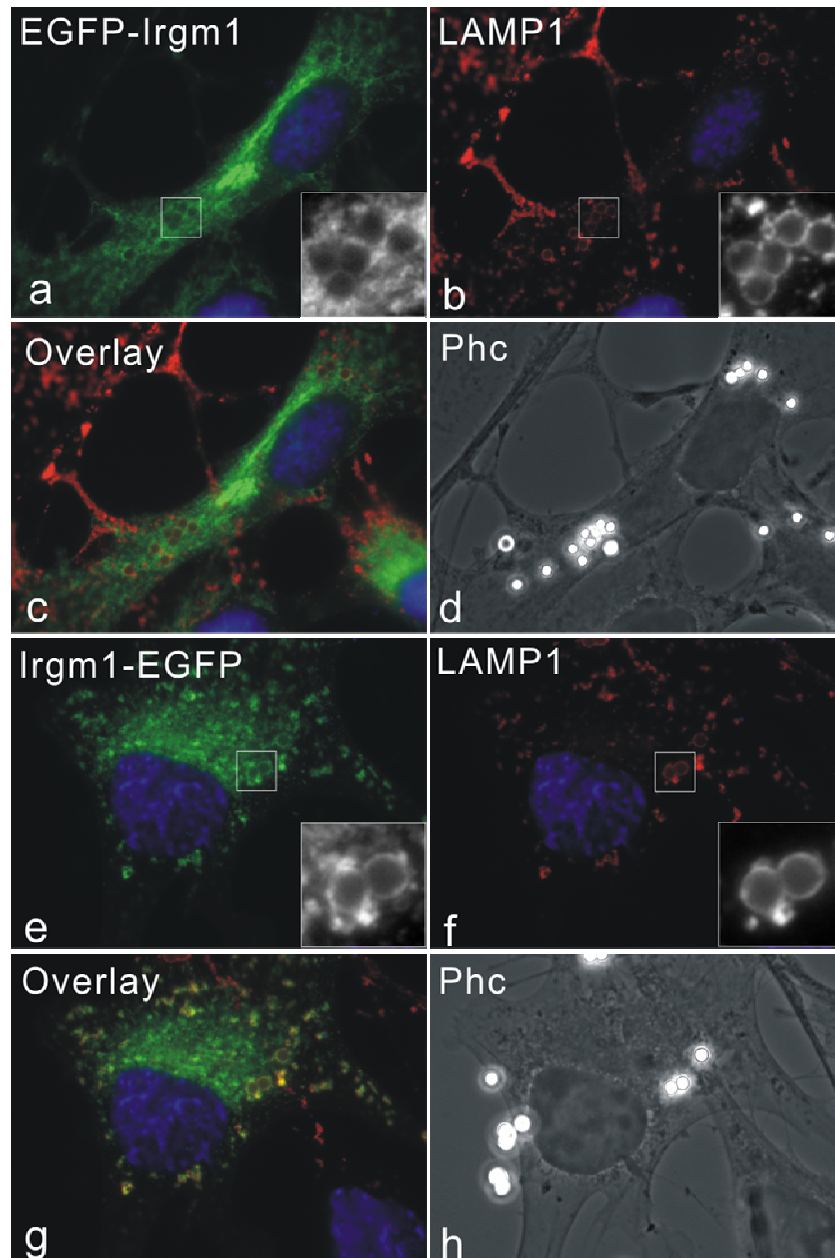


**Figure 3.10 Irgm1-EGFP accumulates on phagosomes while EGFP-Irgm1 does not.**

EGFP-Irgm1 (a-d) and Irgm1-EGFP (e-f) were transiently transfected into MEFs for 24 hours using Fugene 6 transfection reagent. During transfection, cells were incubated with 2- $\mu$ m latex beads overnight. Cells were then fixed with 3% PFA in PBS and staining for LAMP1. Irgm1-EGFP accumulated around the latex beads phagosomes while EGFP-Irgm1 did not. Magnification: 630x. Nuclei were labelled with DAPI.

distribution was largely abolished (Figure 3.9). To conclude, accumulation of Irgm1 on phagosomes is nucleotide dependent, but IFN- $\gamma$  independent.

As showed in Figure 3.7, Irgm1-EGFP showed strong lysosomal association, while EGFP-Irgm1 did not. Consistent with this observation, Irgm1-EGFP showed strong accumulation on latex beads-containing phagosomes whereas EGFP-Irgm1 was absent from phagosomes (Figure 3.10). Like untagged Irgm1, the accumulation of Irgm1-EGFP on phagosomes is also

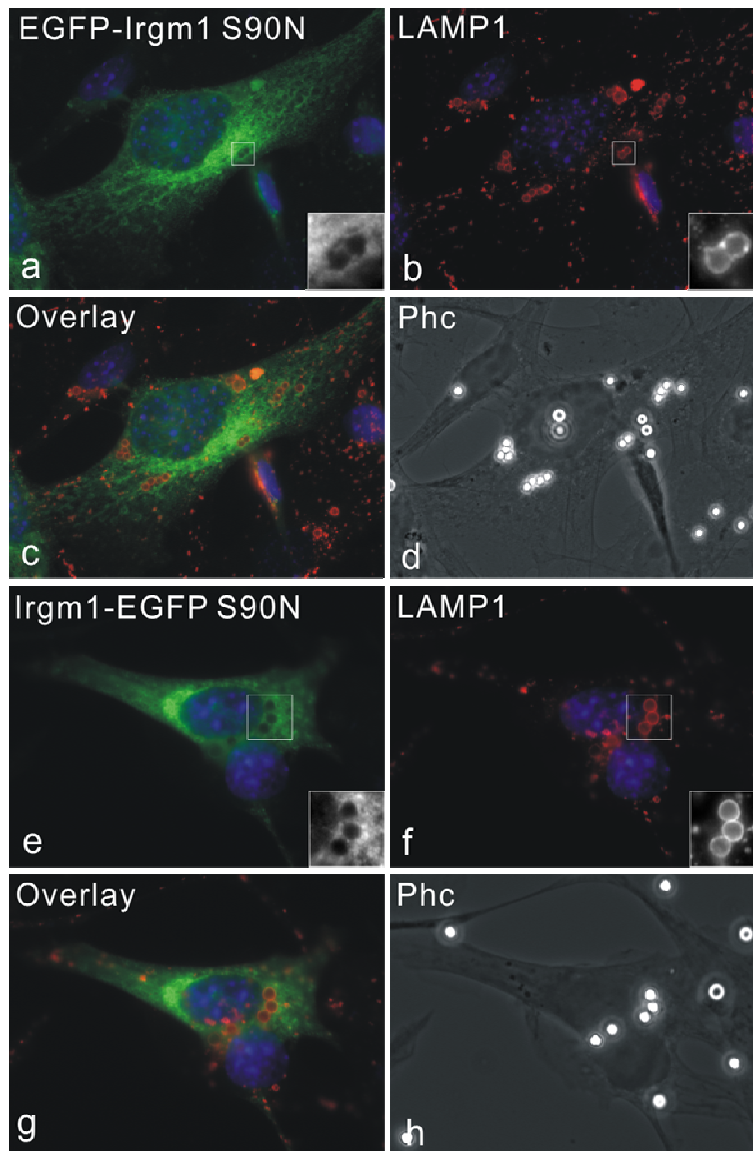


**Figure 3.11 Irgm1-EGFP association with phagosomes is nucleotide dependent.**

EGFP-Irgm1 S90N (a-d) and Irgm1-EGFP S90N (e-f) were transiently transfected into MEFs for 24 hours by using Fugene 6 transfection reagent. During transfection, cells were incubated with 2- $\mu$ m latex beads overnight. Cells were then fixed with 3% PFA in PBS and staining for LAMP1. Both constructs were absent from latex beads phagosomes. Magnification: 630x. Nuclei were labelled with DAPI.

regulated by nucleotide binding. EGFP-Irgm1 S90N not longer associates with latex beads-containing phagosomes (Figure 3.11). The different association of EGFP tagged Irgm1 wild type and nucleotide binding deficient mutant (S90N) to the latex beads-containing phagosomes were not changed when cells were treated simultaneously with IFN- $\gamma$  (data not shown).

In conclusion, the recruitment of Irgm1 to phagosomes is regulated by nucleotide binding and independent of IFN- $\gamma$  induced factors. Phagosomal accumulation of Irgm1 is abolished by N-terminal, but not by C-terminal EGFP-tag.

### **3.5 Amphipathic helix near the C-terminus is responsible for both Golgi and lysosomal targeting of Irgm1.**

It was previously reported that a predicted amphipathic helix near the C terminus (named  $\alpha$ K helix after the analogy to Irga6 structure) is responsible for the proper Golgi localization of Irgm1. As a C-terminal tag, the  $\alpha$ K helix is sufficient to target EGFP to the Golgi apparatus as defined by GM130. Disruption of amphipathicity by glutamate insertion into helical region abolished the Golgi localization in both EGFP-Irgm1  $\alpha$ K construct and Irgm1 full length protein (Martens 2004b). Since endogenous Irgm1 also exhibits lysosomal localization besides Golgi association in murine embryonic fibroblasts (Figure 3.2), the localization of EGFP Irgm1  $\alpha$ K construct was examined in MEFs. 46% of the cells transfected with EGFP- $\alpha$ K construct indeed localized to the Golgi apparatus as showed by costaining of GM130 (Figure 3.12, a-f and m-o). However, in other transfected cells (54%), EGFP-Irgm1  $\alpha$ K showed punctate structures throughout the cytoplasm. Many of those structures displayed accurate colocalization with lysosomal protein LAMP1 (Figure 3.12, j-i). In 14% of transfected cells, EGFP-Irgm1  $\alpha$ K expressing showed both Golgi and lysosomal localization (Figure 3.12, b-f and m-o). This is consistent with the observation that endogenous, IFN- $\gamma$ -induced Irgm1 has Golgi as well as lysosomal distribution. It has to be pointed out that some punctate structures showed neither co-localization with LAMP1-positive compartments nor early/recycling endosomes (data not shown), of which the cellular localization remained undefined.

To test whether the  $\alpha$ K helix is not only enough, but also necessary, for both Golgi and lysosomal localization, full length Irgm1 and ins 362,367E mutant, in which the amphipathicity of the  $\alpha$ K targeting helix was destroyed by two glutamate insertions (Martens 2004b), were transiently expressed in the cells without IFN- $\gamma$  treatment. Wild type Irgm1 showed both Golgi and lysosomal association like the endogenous IFN- $\gamma$  induced protein (Figure 3.13). Irgm1 ins 362, 367E mutant was distributed as dotted structures throughout the cytoplasm that showed neither Golgi nor lysosomal localization (Figure 3.13 and (Martens 2004b)). Thus the native amphipathic K helix is required for both Golgi and lysosomal targeting of full length Irgm1 protein.

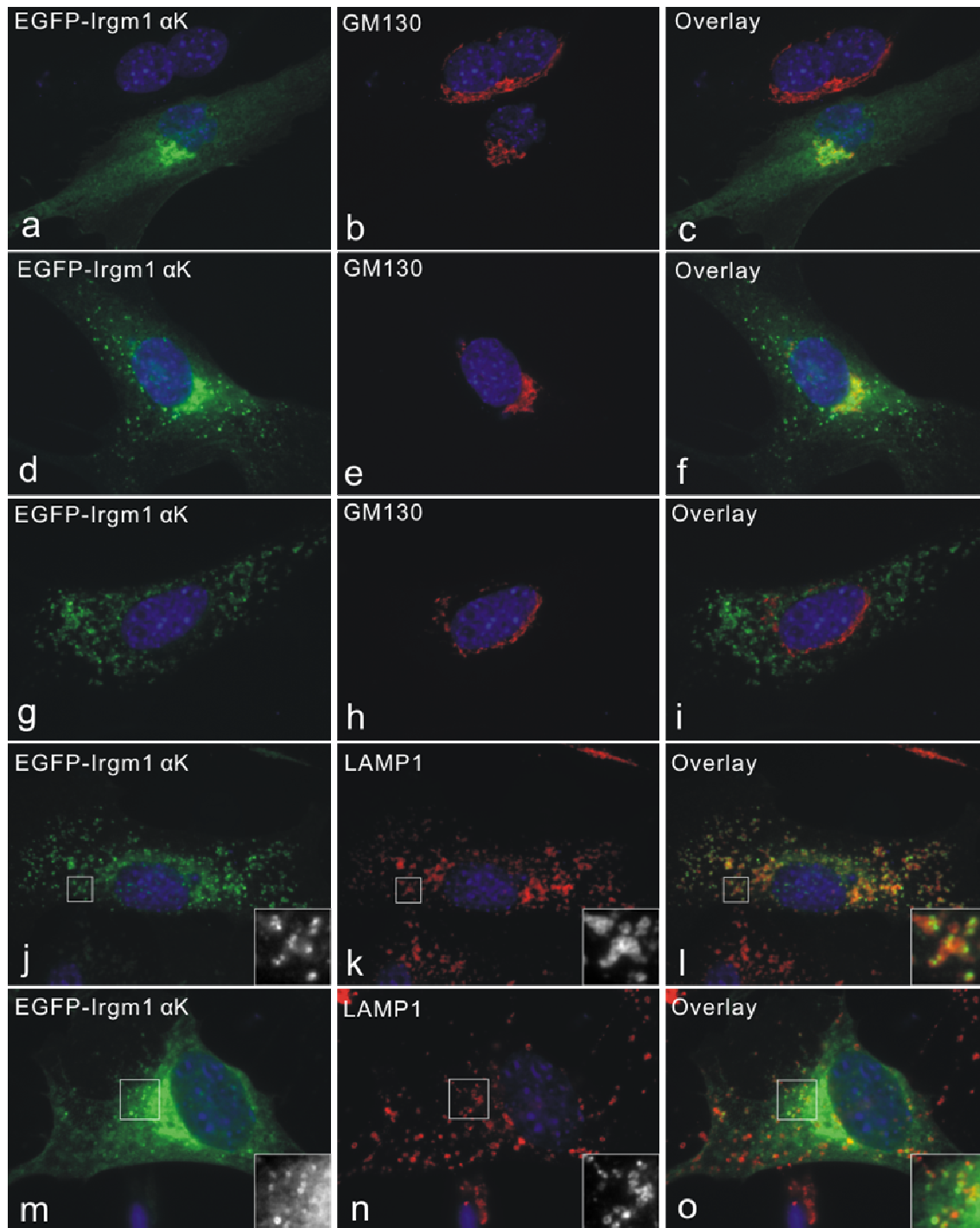


**Figure 3.12 EGFP-Irgm1  $\alpha$ K showed both Golgi and lysosomal localization.**

EGFP-Irgm1  $\alpha$ K construct was transiently transfected into MEFs for 24 hours by using Fugene 6 transfection reagent. Cells were then fixed with 3% PFA in PBS and staining for GM130 (a-i) and LAMP1 (j-o). 32% transfected cells (a-c) showed only Golgi localization and 54% (g-l) showed only dotty structures among which strong lysosomal localization was observed. Expression in 14% (d-f and m-o) transfected cells showed both Golgi and lysosomal localization. Magnification: 630x. Nuclei were labelled with DAPI.

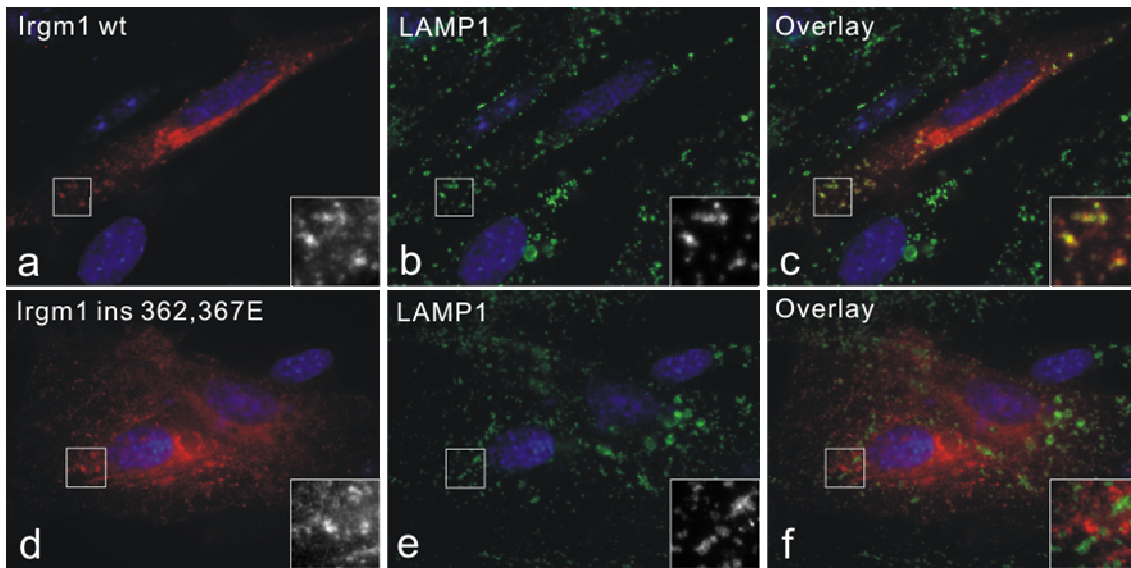


**Figure 3.13 Amphipathic K helix is responsible for lysosomal targeting of full length Irgm1 protein.**

Irgm1 wild type (a-c) and ins 362, 367E mutant (d-f) in pGW1H vectors were transiently transfected into MEFs for 24 hours by using Fugene 6 transfection reagent. Cells were then fixed with 3% PFA in PBS and staining for Irgm1 and LAMP1. Wild type Irgm1 is strongly associated with LAMP1 positive compartment, while Irgm1 ins 362, 367E mutant showed granular signals throughout cytoplasm which are overlapping with LAMP1 signals. Magnification: 630x. Nuclei were labelled with DAPI.

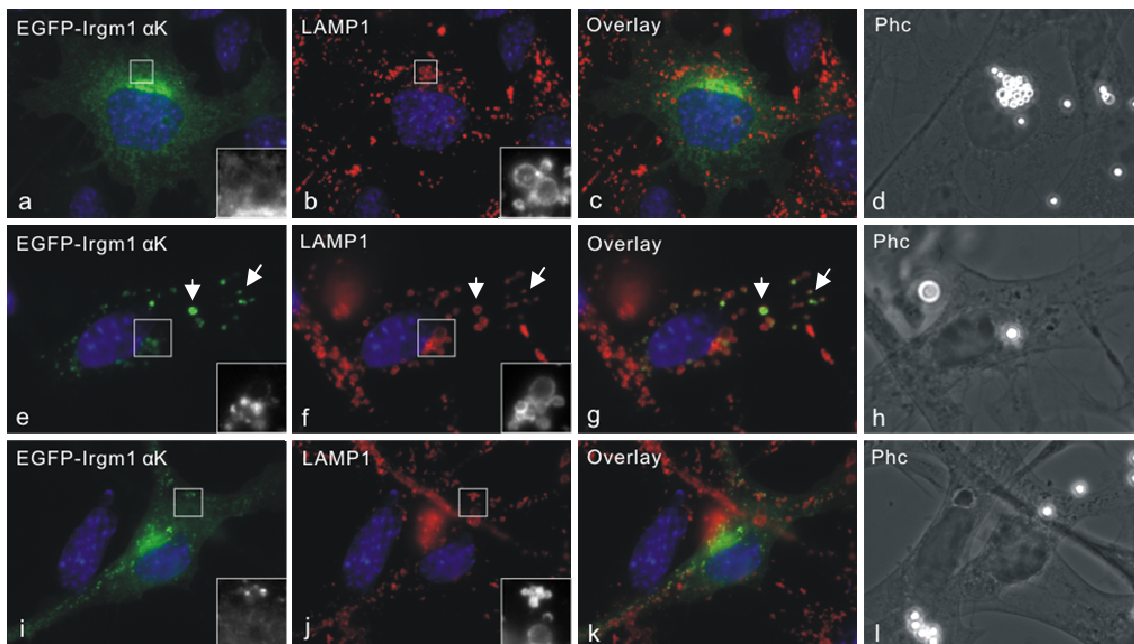


**Figure 3.14 EGFP-Irgm1  $\alpha$ K is not recruited to phagosomes.**

EGFP-Irgm1  $\alpha$ K was transiently transfected into MEFs for 24 hours by using Fugene 6 transfection reagent. During transfection, cells were incubated with 2- $\mu$ m latex beads overnight. Cells were then fixed with 3% PFA in PBS and staining for LAMP1. Golgi only state (a-d), lysosomal state (e-h) and Golgi plus lysosomal state (i-l) of EGFP-Irgm1  $\alpha$ K are exclusively found to be absent from latex beads phagosomes, even though colocalization with LAMP1 outside of phagosomes was seen (arrows). Magnification: 630x. Nuclei were labelled with DAPI.

EGFP-Irgm1  $\alpha$ K showed Golgi and lysosomal localization that mimicked the full length protein. The next question was whether the  $\alpha$ K helix is also responsible for phagosomal accumulation of Irgm1. EGFP-Irgm1  $\alpha$ K was expressed and cells were induced to phagocytose 2- $\mu$ m latex beads. Interestingly, even though colocalization was seen between EGFP-Irgm1  $\alpha$ K and LAMP1 in phagocytic cells (Figure 3.14, arrows), latex beads phagosomes remained blank for EGFP-Irgm1  $\alpha$ K (Figure 3.14). This result indicates Irgm1  $\alpha$ K helix alone is not sufficient for the phagosomal accumulation of full-length protein.

To investigate the possible mechanisms of subcellular localization of Irgm1, an alanine mutagenesis scan was performed based on the targeting construct EGFP-Irgm1  $\alpha$ K. Single mutations of hydrophobic residues (C356A; I358A; V359A; F362A; F363A; L365A; L366A) and hydrophilic residues (N360A; R364A; R367A) had no influence on EGFP-Irgm1  $\alpha$ K localization (Golgi and/or Lysosome, Figure 3.16, only single hydrophilic mutant showed). Furthermore, double mutants of hydrophobic residues (F362A F363A and L365A L366A, not shown) and surprisingly, even the quadruple mutant (F362A F363A L365A L366A, Figure 3.15) did not change the Golgi/lysosomal localization of the EGFP- $\alpha$ K construct. However, if more than one charged residues were mutated to alanine (N360A, R364A; R364A, R367A; N360A, R364A, R367A; Figure 3.17), both Golgi and lysosomal

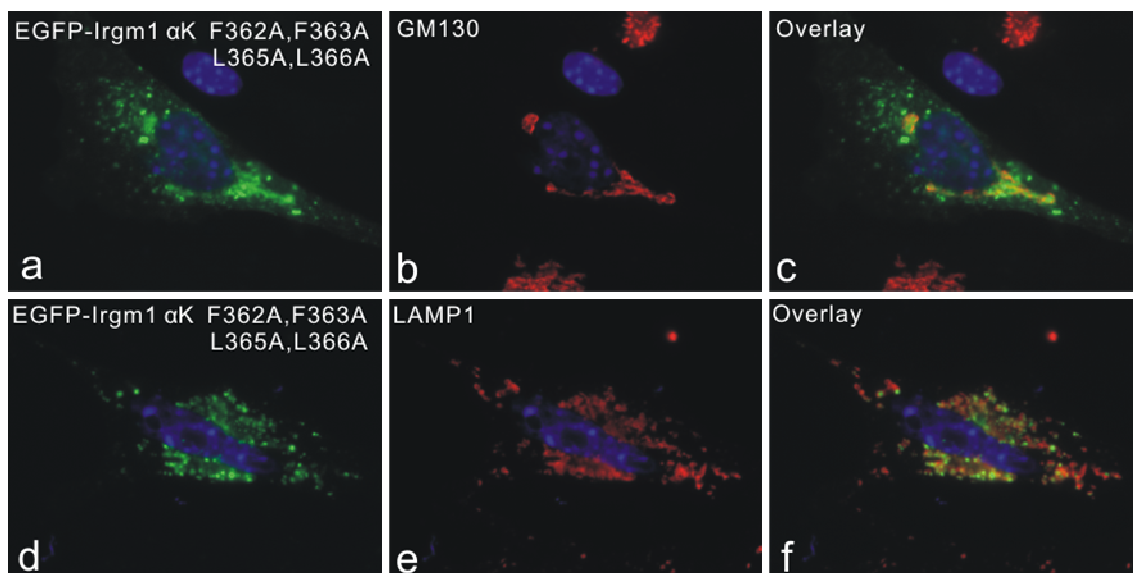


**Figure 3.15** Quadruple mutant EGFP-Irgm1  $\alpha$ K F362A F363A L365A L366A still localizes to Golgi and/or lysosomes. EGFP-Irgm1  $\alpha$ K quadruple mutant F362A F363A L365A L366A was transiently transfected into MEFs for 24 hours by using Fugene 6 transfection reagent. Then cells were fixed with 3% PFA in PBS and staining for GM130 (a-c) or LAMP1 (d-f). Four hydrophobic residues mutation still showed localization at Golgi and/or lysosomes as wild type EGFP-Irgm1 $\alpha$ K. Magnification: 630x. Nuclei were labelled with DAPI.

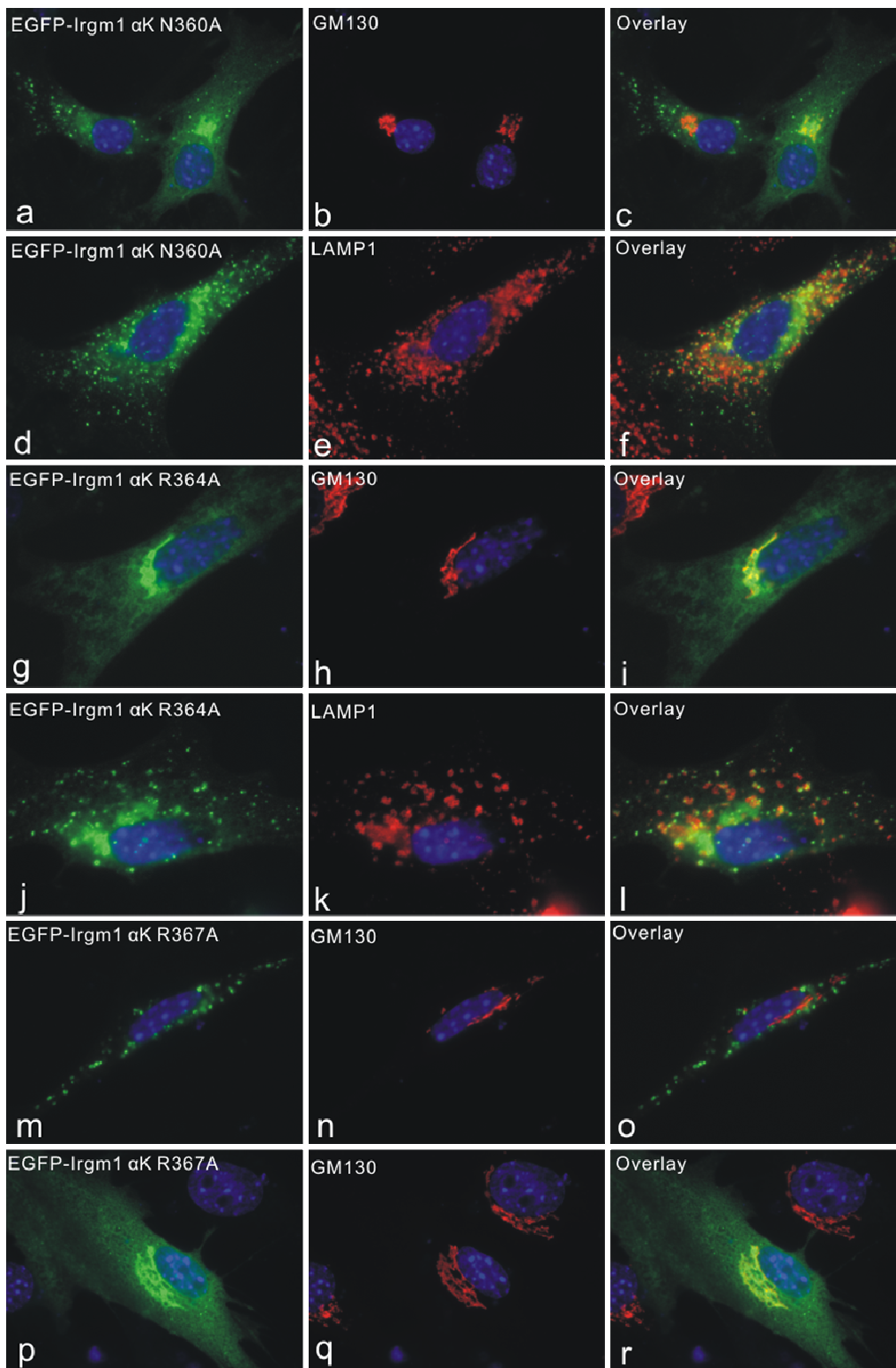


**Figure 3.16 Mutations of single hydrophilic residue do not change the Golgi/lysosomal localization of EGFP-Irgm1  $\alpha$ K.** EGFP-Irgm1  $\alpha$ K N360A (a-f), EGFP-Irgm1  $\alpha$ K R364A (g-l) and EGFP-Irgm1  $\alpha$ K R367A (m-r) were transiently transfected into MEFs for 24 hours by using Fugene 6 transfection reagent. Then cells were fixed with 3% PFA in PBS and staining for GM130 or LAMP1. The Golgi and/or lysosomal localization were not influenced by these mutations. Magnification: 630x. Nuclei were labelled with DAPI.

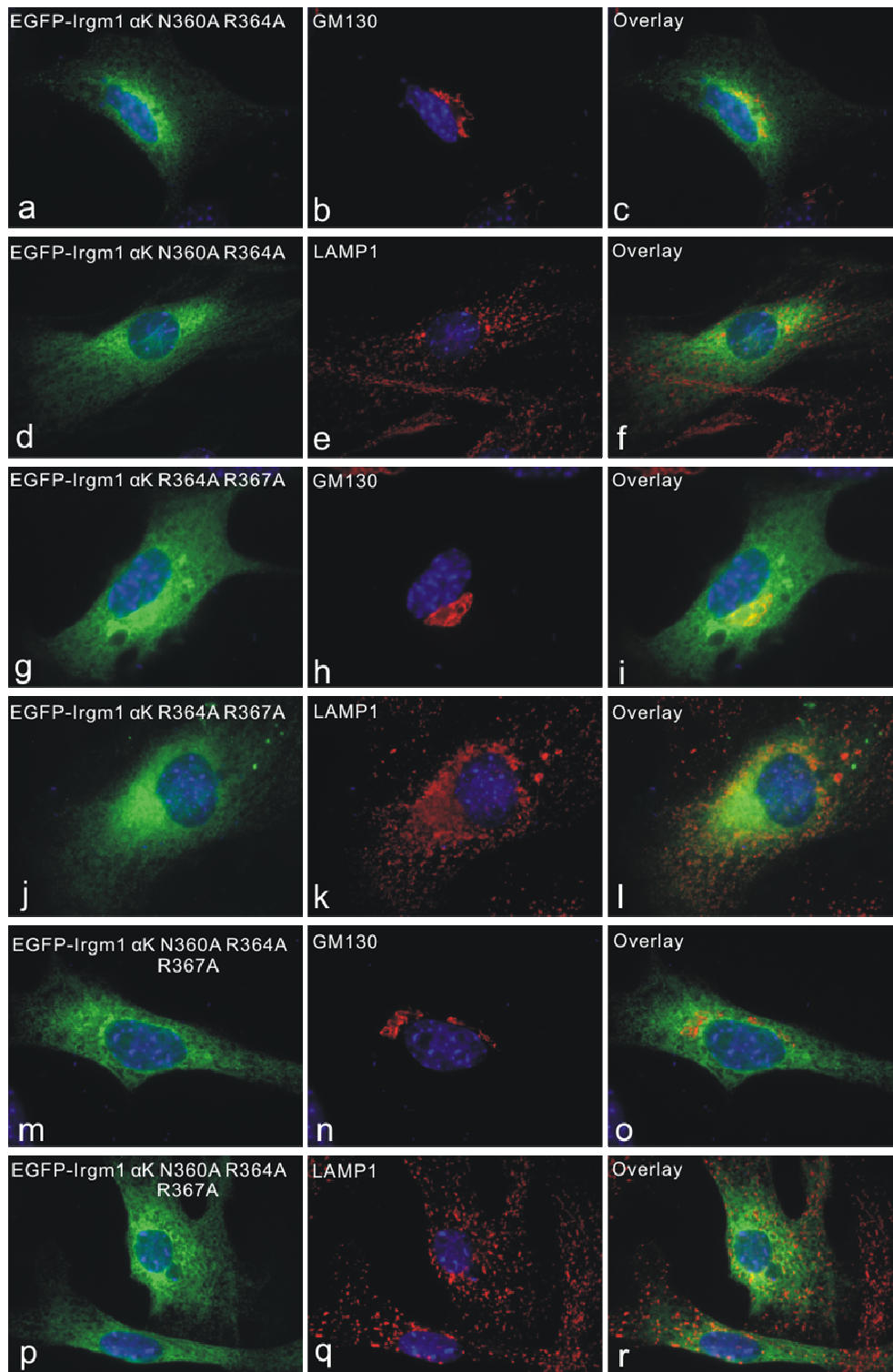


**Figure 3.17 Golgi and lysosomal localization are simultaneously abolished when more than two hydrophilic residues are mutated in amphipathic helix of EGFP-Irgm1  $\alpha$ K.**

EGFP-Irgm1  $\alpha$ K N360A R364A (a-f), EGFP-Irgm1  $\alpha$ K R364A R367A(g-l) and EGFP-Irgm1  $\alpha$ K N360A R364A R367A (m-r) were transiently transfected into MEFs for 24 hours by using Fugene 6 transfection reagent. Cells were then fixed with 3% PFA in PBS and staining for GM130 or LAMP1. The Golgi and lysosomal localization were completely abolished. The signals rather showed unspecific reticular structures throughout the cytoplasm. Magnification: 630x. Nuclei were labelled with DAPI.

localization were completely abolished simultaneously. Those mutants were rather distributed in an unspecific reticular structure throughout the cytoplasm. These results suggest that both the overall amphipathicity of the  $\alpha$ K helix and the identity of the non-hydrophobic residues contribute together to the membrane and Golgi/lysosome localization of the  $\alpha$ K helix.

To summarize, the predicted amphipathic  $\alpha$ K helix near the C-terminus is responsible for Golgi and lysosomal localization of Irgm1, and is in turn dependent on the amphipathic property of the helical region. It is possible that the specificity to Golgi and lysosomal membranes is determined by the identity of the polar residues.

### **3.6 Artificial $\alpha$ K amphipathic peptide mimics the localization of endogenous Irgm1.**

Biochemical studies showed that Irgm1 behaves like an integral membrane protein, even though no transmembrane domain has been identified within the protein sequence. It was demonstrated that Irgm1 exclusively associates with membrane fraction of the cells (Martens 2004b). In addition, attempts to purify recombinant Irgm1 protein failed due to insolubility. To investigate the possible mechanisms of Irgm1 localization, peptide corresponding to the targeting amphipathic sequences (SKLRLMTCAIVNAFFRLLRFLPCVCC) of Irgm1 was synthesized. The lysine in position 2 was covalently conjugated with biotin. Therefore the peptide could be loaded onto the tetrameric streptavidin protein, which has four biotin binding sites, to form a peptide-streptavidin tetrameric complex. This complex was further used as the antibody in standard immunofluorescence staining to test whether this artificial complex can mimic the localization of endogenous Irgm1 as well as EGFP-Irgm1- $\alpha$ K construct. Fluorochrome-labelled streptavidin was used as read-out. The detailed procedure to make peptide-streptavidin complex and fluoro-cytochemistry staining using this tetramer system are described in materials and methods. Figure 3.18 shows the staining pattern of Cy3 labelled streptavidin-Irgm1  $\alpha$ K tetrameric complex. Cy3-labeled streptavidin alone was used as control and pictures were taken with the same exposure time. The streptavidin-Irgm1  $\alpha$ K complex staining shows both perinuclear and vesicular structures which was similar to the localization of endogenous Irgm1 protein and the EGFP-Irgm1  $\alpha$ K targeting construct. Figure 3.18 shows the costaining of Streptavidin-Irgm1  $\alpha$ K with endogenous Irgm1 together with Golgi marker GM130 and lysosomal protein LAMP1. Essentially, Streptavidin-Irgm1  $\alpha$ K

showed accurate localization with full length Irgm1 at both Golgi apparatus and lysosomes, although higher background was seen probably due to the intrinsic hydrophobic property of the peptide. To conclude, the streptavidin-peptide complex mimics the localization of endogenous Irgm1 and provides a valuable novel method to investigate the function of targeting motifs of proteins, especially those with unknown biochemical properties.

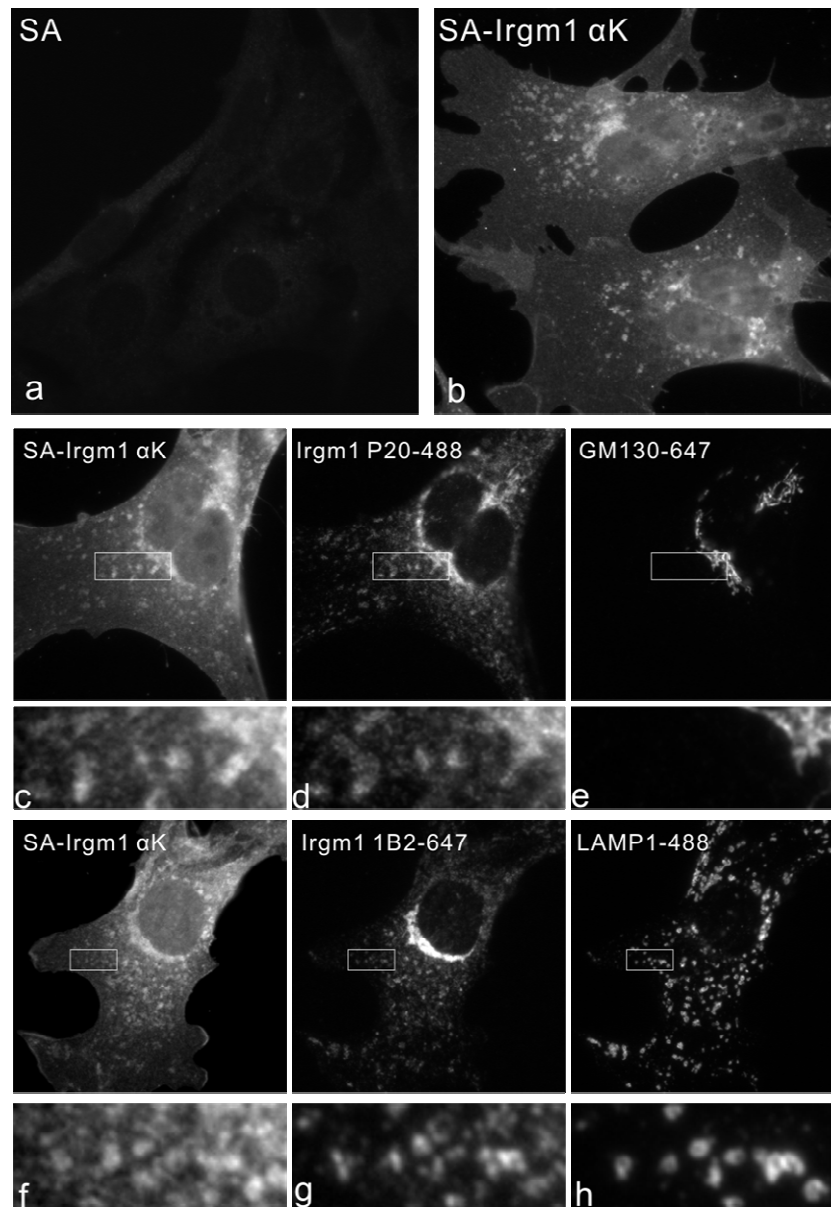


**Figure 3.18 Artificial  $\alpha$ K amphipathic peptide mimics the localization of endogenous Irgm1.**

MEFs were treated with 200U/ml IFN- $\gamma$  for 24 hours, fixed with 3% PFA in PBS. 8 $\mu$ M Irgm1- $\alpha$ K peptide (final concentration, b-h) was loaded on 20  $\mu$ g/ml (0.33 $\mu$ M final) C3-streptavidin in PBS and spun down at 45,000 rpm for 30 minutes. Then antibodies against indicated proteins were added into streptavidin-peptide solution and it was used as primary antibodies in immunofluorescence staining. 20  $\mu$ g/ml Streptavidin (0.33 $\mu$ M final) alone (a) was used as control. Image a and b were taken by same exposure time. Colocalization was seen between streptavidin-Irgm1  $\alpha$ K peptide and endogenous Irgm1 at both Golgi apparatus and lysosomes. Magnification: 630x.

### **3.7 Irgm1 is not recruited to *Toxoplasma gondii* ME49 strain vacuoles and is not absolutely necessary for IFN- $\gamma$ -dependent cell-autonomous resistance against *T. gondii* ME49 strain.**

IRG proteins accumulate onto *T. gondii* parasitophorous vacuoles membrane and contribute to the vacuolar vesiculation and disruption, which lead to the elimination of parasites itself. At least five members of IRG family, namely Irga6, Irgb6, Irgd, Irgm2, and Irgm3 were found to accumulate onto the *T. gondii* PVM in primary astrocytes (Martens 2005). Irgm1 was not detected on the PVM (Butcher 2005; Martens 2005). However this observation was technically less satisfactory because the A19 antiserum had a significant cross-reaction with *T. gondii* itself. Therefore another goat anti-Irgm1 antiserum, P20, and monoclonal anti-Irgm1 antibody 1B2 were used in the present studies to further confirm the absence of Irgm1 from *T. gondii* PVM. Figure 3.19 shows one image of P20 staining, in which Irgm1 is not present on GRA7 positive *T. gondii* vacuole. The same results were also obtained with the monoclonal antibody 1B2 (Stefii, personal communication). As Irgm1 also localizes to lysosomal compartments, lysosomal fusion with *T. gondii* PVM was examined. Neither LAMP1 nor Irgm1 was present on *T. gondii* vacuole at 2, 4 and 6 hours after infection (Figure 3.19). This is consistent with the observation in primary astrocytes (Martens 2005).

To test whether Irgm1 is necessary for IFN- $\gamma$ -dependent cell autonomous resistance against *T. gondii* infection, the *T. gondii* proliferation assay was performed in Irgm1-deficient primary MEFs (performed by Stephanie Könen-Waisman). Surprisingly, even though Irgm1 is indispensable *in vivo* for mice to survive *T. gondii* infection, Irgm1 is not absolutely necessary *in vitro* at cellular level for the resistance against *T. gondii* (Figure 3.20). To examine whether other members of IRG proteins still accumulate on *T. gondii* vacuoles in the absence of Irgm1, Irgm1 MEFs deficient in Irgm1 were treated with 200U/ml IFN- $\gamma$  for 24 hours, infected with *T. gondii* ME49 strain and indirect immunofluorescence were performed. Figure 3.21 shows that in Irgm1 deficient MEFs, Irga6, Irgb6 and Irgm2 still accumulate on *T. gondii* vacuole membrane and the same disrupted morphology of PVM is observed as in the wild type MEFs. However, punctate Irga6 and Irgb6 signals were noticed that is absent in wild-type MEFs (arrows). To get a quantitatively information, wild type and Irgm1 deficient MEFs were treated with IFN- $\gamma$  for 24 hours, infected with *T. gondii* ME49 strain and stained for

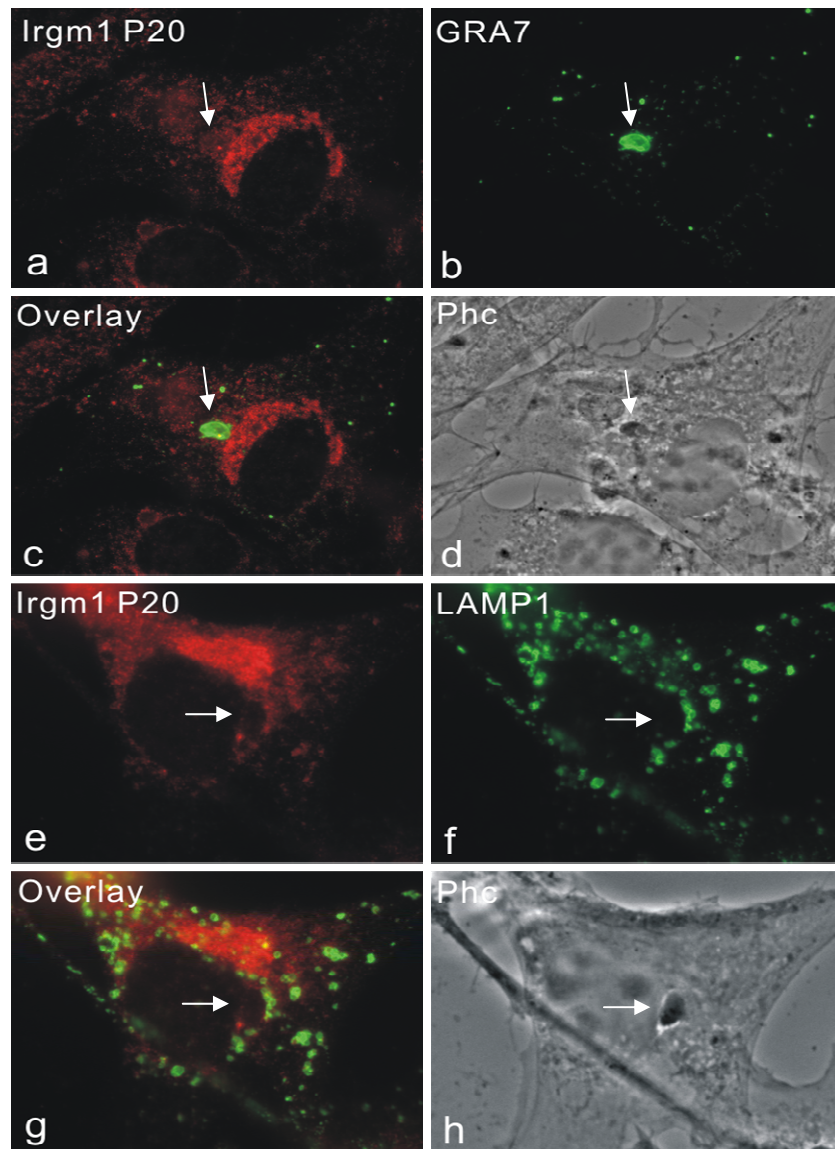


**Figure 3.19 Irgm1 is not recruited to *T. gondii* parasitophorous vacuole membrane.**

MEFs were treated with 200U/ml IFN- $\gamma$  for 24 hours and then infected with ME49 for 2 (a-d) or 4 (e-h) hours. Cells were fixed with 3% PFA in PBS and stained for indicated proteins. Irgm1 was found not to associate with *T. gondii* vacuolar membrane (a-d), and no lysosomal fusion was seen for *T. gondii* vacuoles (e-h). Arrows indicate the intracellular parasites. Magnification: 630x.

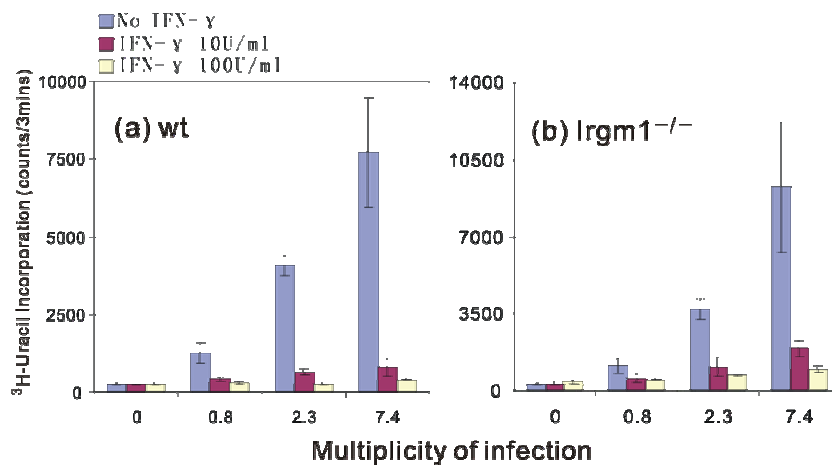


**Figure 3.20 Irgm1 is not absolutely necessary for IFN- $\gamma$ -dependent cell-autonomous resistance against *T. gondii* ME49 strain in MEFs. (performed by Stephanie Könen-Waisman)**

MEFs isolated from wild-type (a) or Irgm1 knock-out (b) mice were induced with the indicated concentrations of IFN- $\gamma$  for 24 hours and infected with *T. gondii* ME49 strain by different multiplicities of infection. 48 hours later, 1 $\mu$ Ci/well [ $^3$ H]-uracil were added to the culture and incubated for additional 24 hours. The amount of incorporated uracil, which is directly in proportion to *T. gondii* growth, was determined by liquid scintillation counting. The IFN- $\gamma$ -treated Irgm1-deficient MEFs can control ME49 growth to a similar level in the wild-type cells.

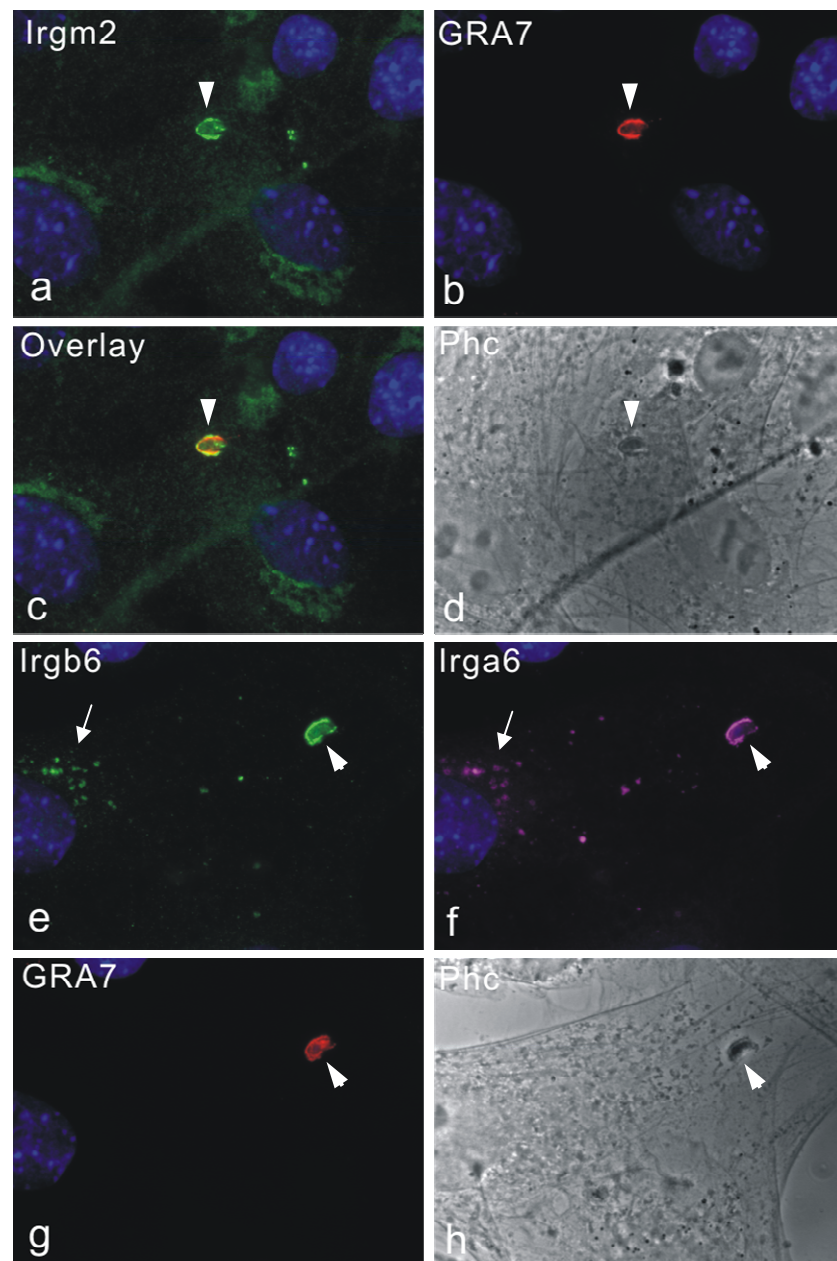


**Figure 3.21 Other IRG proteins still accumulate onto *T. gondii* ME49 strain vacuoles in Irgm1 deficient MEFs.**

Irgm1 deficient MEFs were treated with 200U/ml IFN- $\gamma$  for 24 hours and then infected with ME49 for 2 hours. Cells were fixed with 3% PFA in PBS and stained for indicated proteins. Even in the absence of Irgm1, at least three members of IRG family, namely Irgm2 (detected by rabbit antiserum H53, a-d), Irga6 (rabbit antiserum 165, f) and Irgb6 (goat antiserum A20, e) are still accumulated on *T. gondii* vacuolar membranes (arrow heads indicate the intracellular *T. gondii*). Aggregated Irga6 and Irgb6 were noticed (arrows). Magnification: 630x. Nuclei were labelled with DAPI.

Irga6 and Irgb6. Images were taken with same exposure time and signal intensities were measured for Irga6 and Irgb6 on *T. gondii* vacuoles. Figure 3.22 shows that in Irgm1 deficient MEFs, the loading of Irga6 and Irgb6 onto the PVM is decreased by about 30% compared to those in wild type cells. However, this decrease in loading of other members of IRGs on PVM seems not to have a significant influence on the cell-autonomous control of *T. gondii* growth, since Irgm1 deficient MEFs control intracellular *T. gondii* ME49 strain essentially as efficiently as the wild type cells.

We therefore conclude that Irgm1 is not absolutely required for IFN- $\gamma$ -dependent cell-autonomous resistance against *T. gondii* ME49 strain in murine fibroblasts.

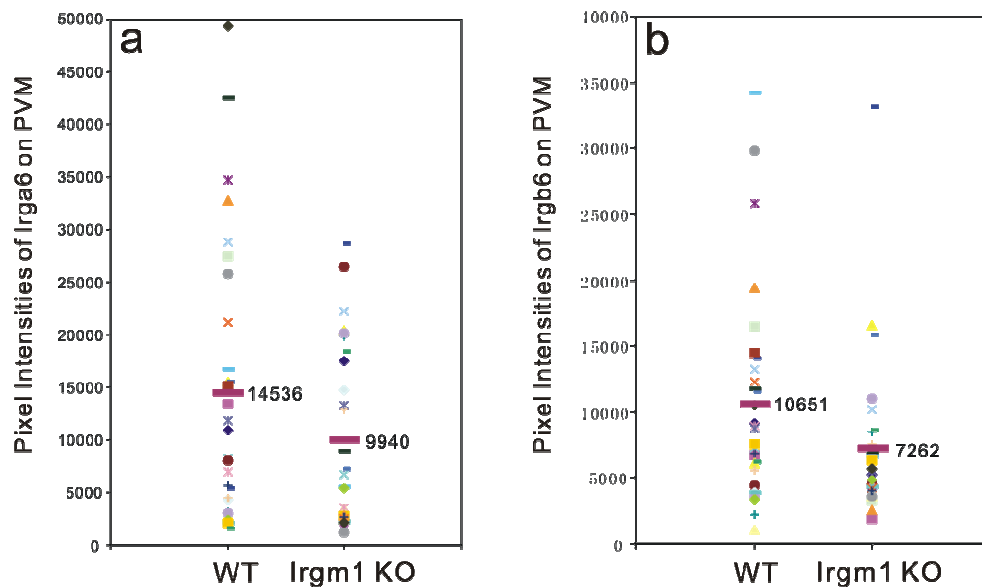


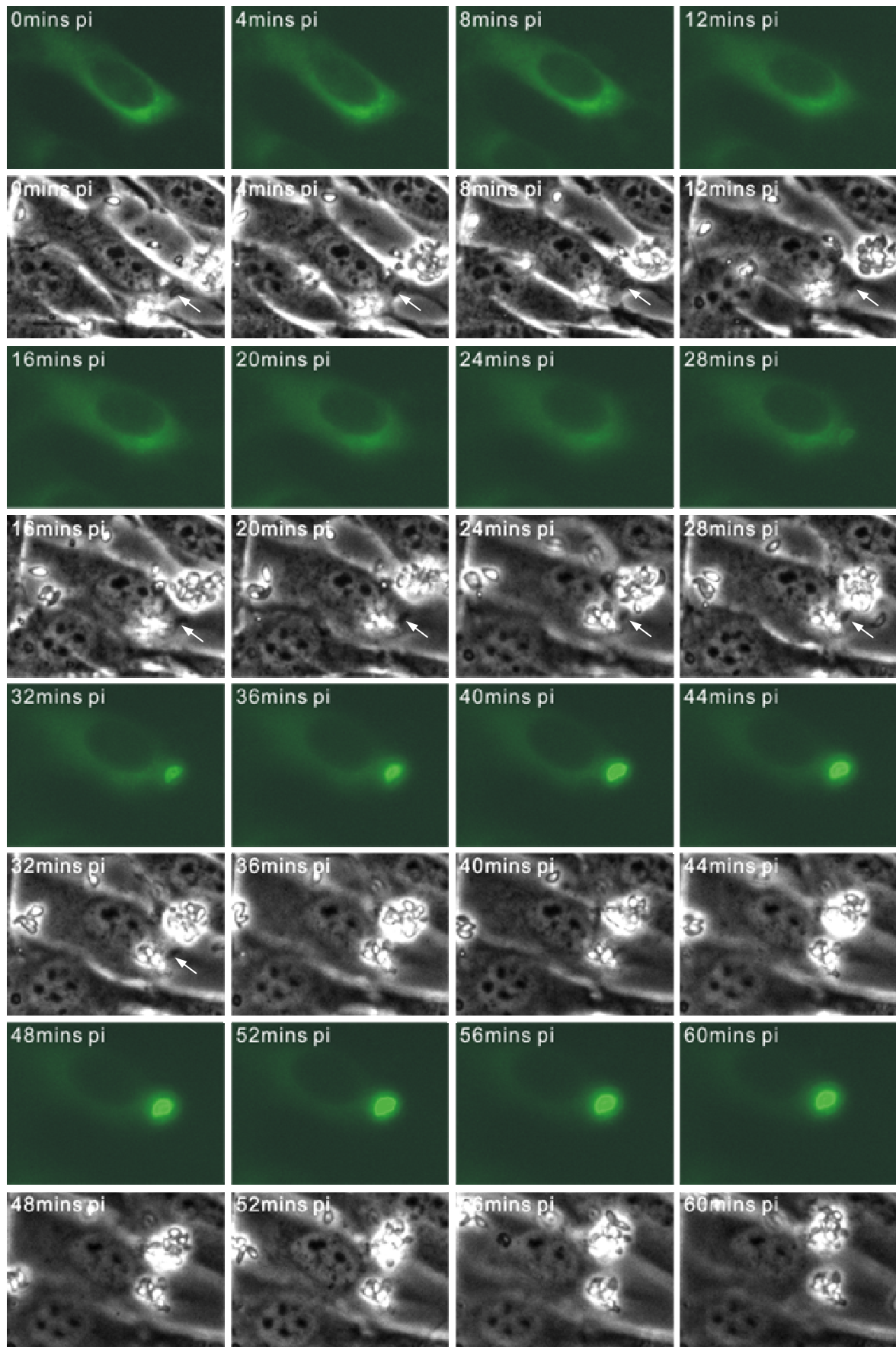
**Figure 3.22 The accumulation of Irga6 and Irgb6 on PVM is decreased in Irgm1 deficient MEFs.**

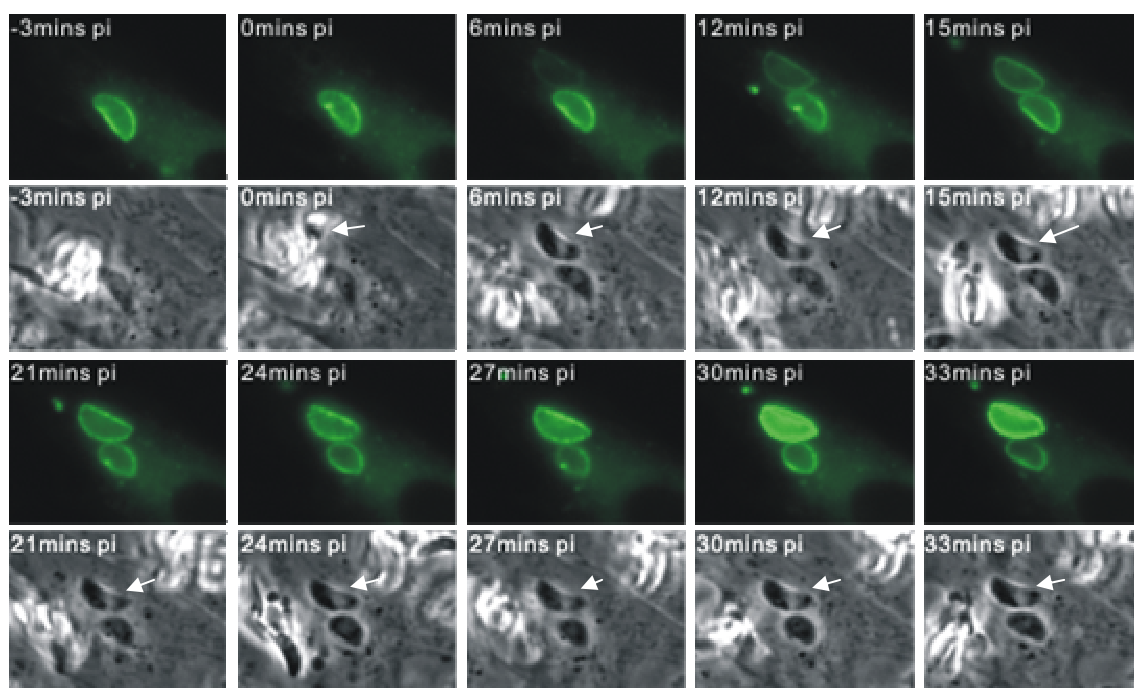
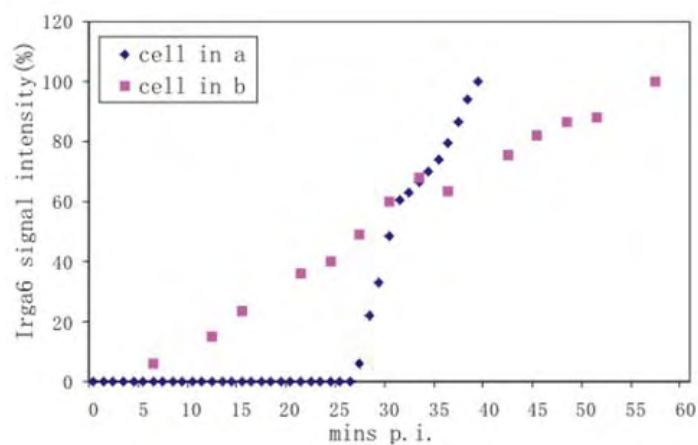
Wild type and Irgm1 deficient MEFs were treated with 200U/ml IFN- $\gamma$  for 24 hours and then infected with *T. gondii* ME49 strain for 2 hours. Cells were fixed with 3% PFA in PBS and stained for Gra7 to identify intracellular parasites, as well as 165 for Irga6 and A20 for Irgb6. Gra7 positive vacuoles were randomly selected and images were taken at same exposure time for either Irga6 or Irgb6. Signals intensities of Irga6 (a) and Irgb6 (b) on PVM were measured by pixel counting and plotted as showed. Mean values are depicted by violet bars. Both Irga6 and Irgb6 signals on PVM were decreased by about 30%.

## 4. Results-II

### 4.1 Dynamics of the Irga6-loading onto the *T. gondii* ME49 strain parasitophorous vacuolar membrane

At least 5 members of the IRG family have been reported to accumulate onto the *T. gondii* parasitophorous vacuolar membrane and contribute to the disruption of the vacuole, resulting in the death of the parasites by unknown mechanisms (Martens 2005). To investigate the mechanisms of IFN- $\gamma$ -dependent cell autonomous resistance against *T. gondii* infection and the role of IRG proteins in this process, a live cell imaging system was established. This method allowed us to document the accumulation of IRG proteins onto *T. gondii* vacuoles and the disruption of vacuoles by time-lapse microscopy. EGFP-ctag1-Irga6 fusion protein has the same ER-localization as endogenous Irga6 and is recruited to *T. gondii* PVM as well, and was therefore used in the present live cell imaging experiments. Mouse embryonic fibroblasts were transfected with EGFP-tagged-Irga6 construct and simultaneously treated with 200U/ml IFN- $\gamma$ . Twenty four hours later, cells were infected with *T. gondii* avirulent ME49 strain and observed in the live cell imaging system. Figure 4.1 shows two examples of Irga6 accumulation onto the *T. gondii* vacuoles. In the first movie, signal of Irga6 on the PVM was detectable from 26 minutes after the infection, and signal increased rapidly to the maximum capacity of the camera within 15 minutes. The accumulation of Irga6 on the PVM was accompanied by a global reduction of cytoplasmic Irga6 signal. In the second movie, one parasite invaded a host cell that is already infected by an earlier parasite, which is already coated with Irga6. Signal of Irga6 started to accumulate on the second *T. gondii* PVM around 6 minutes after the invasion of this parasite. For this individual it took 50 minutes for Irga6 to reach the plateau. Quantification of Irga6 signal intensities on PVM is shown in Figure 4.1 c. Interestingly, the directly observed lag phase between the entry of the parasites and the initiation of accumulation of Irga6 on PVM varied from less than 6 minutes to more than 12 hours and some parasite vacuoles remained uncoated with Irga6 as long as the conditions of cell culture allowed (more than 12 hours, data not shown).

**a**

**b****c**

**Figure 4.1 Accumulation of Irga6 on the *T. gondii* ME49 strain parasitophorous vacuole membrane.**

MEFs were transiently transfected with Irga6-ctag1-EGFP and treated with 200U/ml IFN- $\gamma$ . 24 hours later cells were infected with ME49. Images were taken by time-lapse microscopy. (a) The time-lapse images were taken immediately after infection and one intracellular parasite (arrows) was already observed when the first frame started. (b) When the video was running, an extracellular *T. gondii* invaded the host cell, which already had one parasite infected and Irga6 accumulated on it. Timing was set as zero when this invading parasite was observed. Arrows showed the second invaded *T. gondii*. (c) Quantification of signal intensities of Irga6 on the vacuoles in (a) and (b). Magnification: 400x.

## 4.2 Disruption of the Irga6-positive *T. gondii* vacuoles is followed by parasite deterioration and host cell death

Compared to the variable accumulation of Irga6 onto the *T. gondii* PVM, the disruption of parasitophorous vacuole is fast and uniform. Figure 4.2 shows two examples of *T. gondii* PVM disruption processes. Consecutive time-lapse images were taken with one minute intervals. In both cases, the disruption processes of Irga6-positive *T. gondii* vacuoles happen within 3 minutes. The initially intact Irga6-positive vacuolar membranes suddenly break on one end and the parasites are exposed to the cytosol.

To observe the fate of the stripped parasites in the cytosol, longer intervals between consecutive time-lapse images (3-5 minutes) were further taken to minimize the toxic effect of the illuminating light beam. The *T. gondii* apparently deteriorate in the cytosol as the phase behavior of the parasite changes. The *T. gondii* tachyzoites initially with high phase density changed to a phase-transparent form after stripping of the PVM (Figure 4.3). This deterioration of *T. gondii* has been observed only after the disruption of Irga6-positive vacuoles.

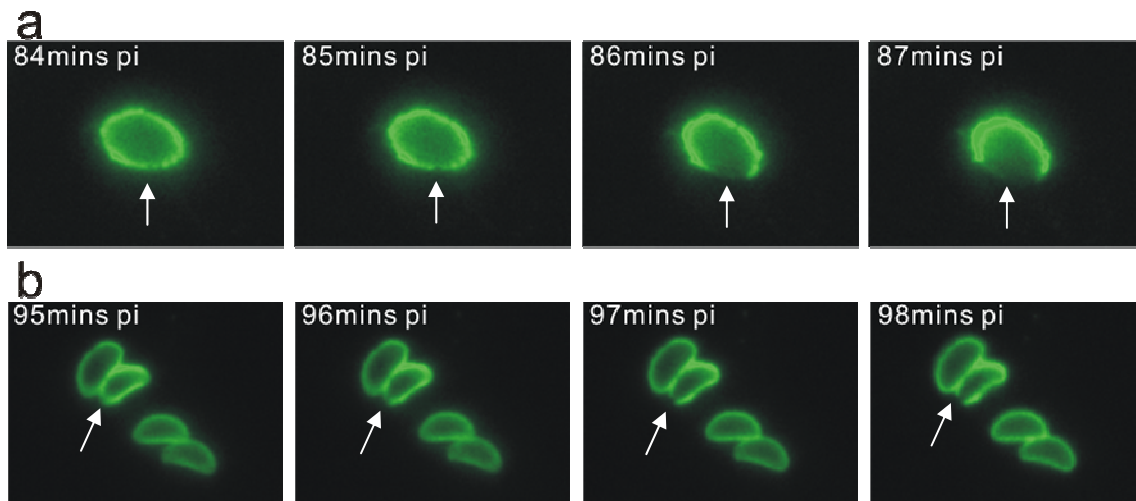


**Figure 4.2 Disruption of Irga6-positive *T. gondii* ME49 strain vacuoles**

MEFs were transiently transfected with Irga6-ctag1-EGFP and treated with 200U/ml IFN- $\gamma$ . 24 hours later cells were infected with ME49. Images were taken by time-lapse microscopy. (a) and (b) show the disruption of the *T. gondii* vacuoles from two individual experiments (arrows). Magnification: 400x.

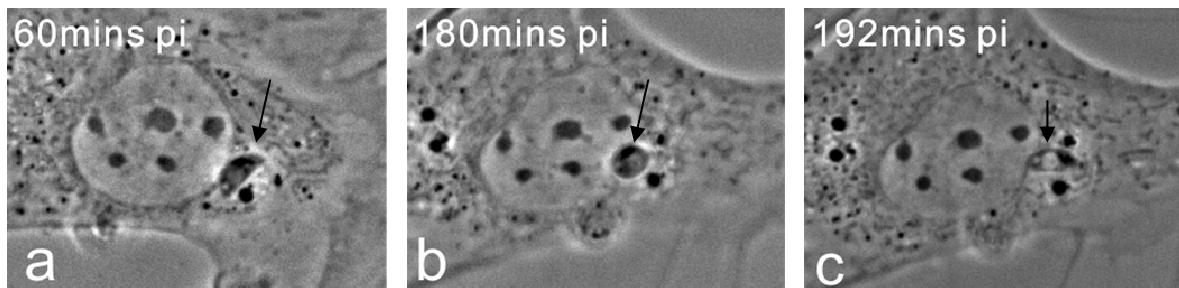


**Figure 4.3** *T. gondii* deteriorates in the cytosol after the disruption of vacuoles.

MEFs were transiently transfected with Irga6-ctag1-EGFP and treated with 200U/ml IFN- $\gamma$ . 24 hours later cells were infected with ME49. 1 hours after infection, images were taken by time-lapse microscopy. (a) shows the *T. gondii* in the beginning of the experiments. Disruption of the vacuole happened at 135 minutes p.i. After that the parasite underwent morphological changes. It was rounded up (b) and appeared to be in a transparent form (c) in the cytosol. Arrows indicate the *T. gondii*. Magnification: 400x.

Surprisingly, but uniformly, dying of the infected host cells was further observed after the *T. gondii* vacuoles had been disrupted and the parasites deteriorated. The dying of the host cells was confirmed by propidium iodide staining and possible effect of deteriorating culture conditions was excluded, since the infected cell death was observed repeatedly and the uninfected neighboring cells were always alive. The dying host cells showed characteristics of shrinkage of nuclei, condensed cytoplasm, overall breakdown of cellular structures, and loss of mobility. Figure 4.4 shows consecutive frames from one infected cell in which Irga6 was already accumulated on the PVM when the movie started. Propidium iodide was present in the medium, but was initially excluded. Between 190 and 210 minutes p.i. the cell became permeate to PI indicating the loss of plasma membrane integrity. The *T. gondii* vacuole was disrupted at 170 minutes after infection and the host cell die between 20 and 40 minutes later. The Irga6 signals disappeared completely shortly after the cell became PI-permeable, suggesting that PVM-associated Irga6 was either completely disassembled from membrane and released from the dead cell, or else was proteolytically digested.

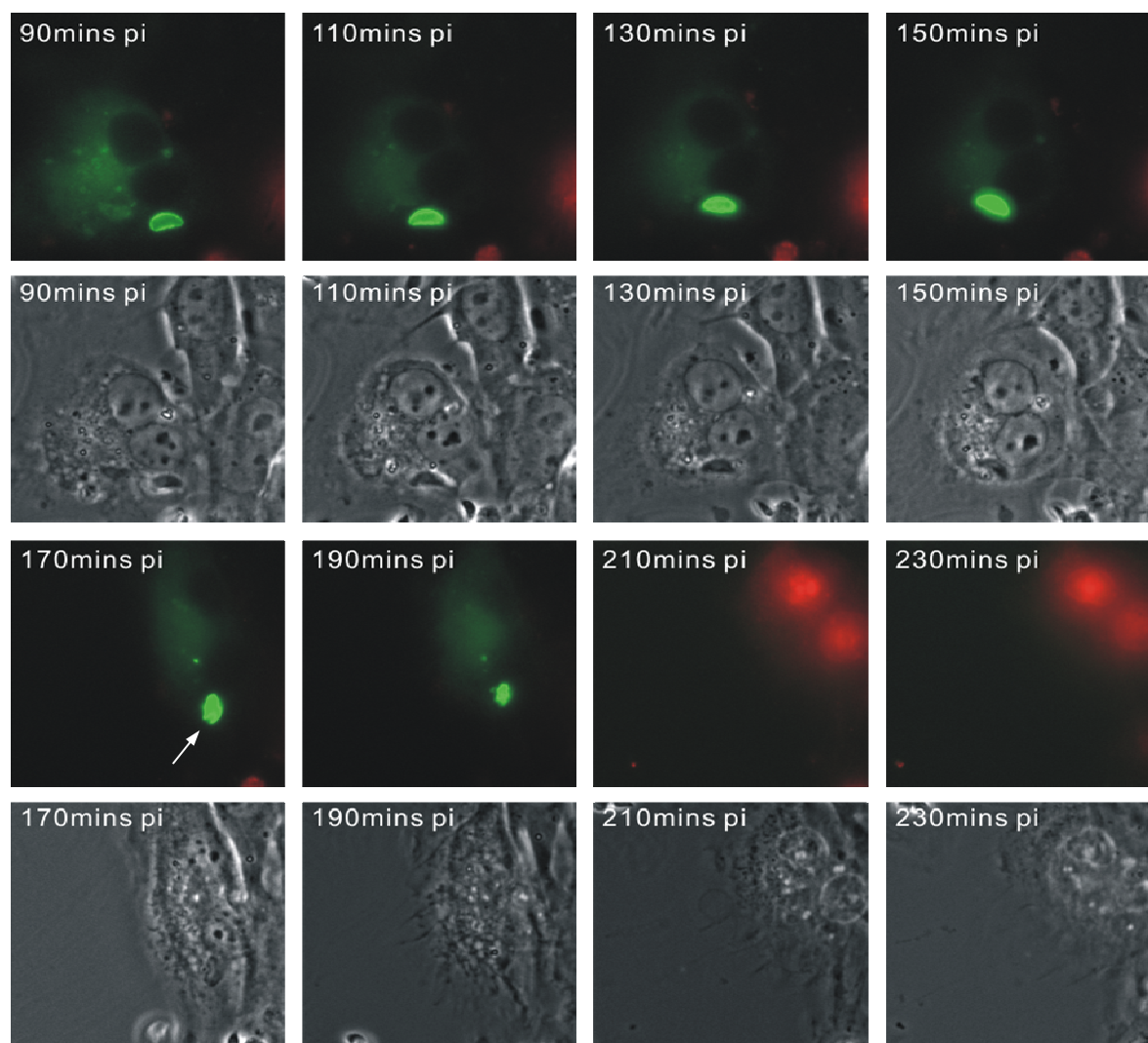


**Figure 4.4** Host cells lose plasma membrane integrity and die after the disruption of *T. gondii* vacuole.

MEFs were transiently transfected with Irga6-ctag1-EGFP and treated with 200U/ml IFN- $\gamma$ . 24 hours later cells were infected with ME49 for 90 minutes and images were taken by time-lapse microscopy. Propidium iodide (1 $\mu$ g/ml) was present in the medium. 210 minutes after infection, the nucleus of host cell became positive for PI and overall cellular structures collapsed. Arrow shows the disruption of Irga6 positive vacuole. Magnification: 400x.

### 4.3 EGFP-LC3 associates with a proportion of *T. gondii* ME49 strain vacuoles independent of IFN- $\gamma$

Recent publications reported that autophagy plays a role in elimination of intracellular *T. gondii*. A process of indentation, vesiculation, disruption and stripping of the parasite PVM has been observed in primed effector macrophages. Denuded parasites were apparently enveloped in autophagosome-like vacuoles, which ultimately fused with lysosomes (Ling 2006). Similar PVM vesiculation and disruption processes have been reported in primary astrocytes as well. Although lysosomal fusion with *T. gondii* parasites were not observed in this study, EGFP-LC3, a marker for autophagosomes, was found to accumulate in the vicinity

of denuded parasites (Martens 2005). To investigate the role of autophagy in IFN- $\gamma$  mediated resistance against *T. gondii*, EGFP-LC3 was again used in the present study by immunofluorescence staining in fixed samples, as well as in the established live cell imaging system. MEFs were transfected with EGFP-LC3 construct, induced with 200U/ml IFN- $\gamma$  or left untreated. Twenty four hours later, cells were infected with ME49 *T. gondii* strain and EGFP-LC3 immunofluorescence was observed. Figure 4.5 shows that EGFP-LC3 can accumulate on some, but not all, *T. gondii* vacuoles. In (a) and (b), the cells were not treated with IFN- $\gamma$ . Arrows indicate the EGFP-LC3 coated *T. gondii* vacuoles and arrow heads indicate the other EGFP-LC3-negative vacuole in the same cell. *T. gondii* vacuoles in this cell are obviously not disrupted. Cells in (c-d) are treated with IFN- $\gamma$  and infected with *T. gondii* for 2 hours. Arrows indicate the disrupted, Irga6-coated *T. gondii* vacuole, and EGFP-LC3 is weakly associated with this disrupted vacuole. In e-h, cells were treated with IFN- $\gamma$  and infected with *T. gondii* for 6 hours. Arrows in (e and f) indicate the EGFP-LC3 positive, but Irga6 negative vacuole and arrow heads indicate the Irga6-positive, but EGFP-LC3 negative vacuole. Notice that there are two more vacuoles in the same cell which are not coated with either Irga6 or EGFP-LC3. In (g and h), the arrows indicate the disrupted, Irga6-positive *T. gondii* vacuole. EGFP-LC3 is negative for this vacuole; despite that enhanced EGFP-LC3 aggregates are obviously visible in this cell.

In live cell imaging experiment, EGFP-LC3 has been found to be weakly associated with *T. gondii* PVM as well as denuded parasite itself (Figure 4.6, arrows). Again the host cell died eventually and no manifest high level of autophagy was observed. EGFP-LC3 was then released completely from dead host cells implying that the host cell plasma membrane was permeabilized. We noticed, however, that before the permeabilization of host cell plasma membrane, the intracellular parasite itself was penetrated by EGFP-LC3 (arrows). This seemed to imply that the *T. gondii* membrane itself became permeable to a soluble protein, confirming that the *T. gondii* was now dead. This effect had nothing special to do with the LC3 moiety of the EGFP-LC3 fusion protein since, in repeated experiments, it was observed that the parasites from stripped vacuoles became permeable to EGFP or other fluorescent proteins alone. These results show that the disruption and the stripping of the *T. gondii* vacuoles in IFN- $\gamma$ -treated cells leads directly to the death of parasites in the cytosol. In

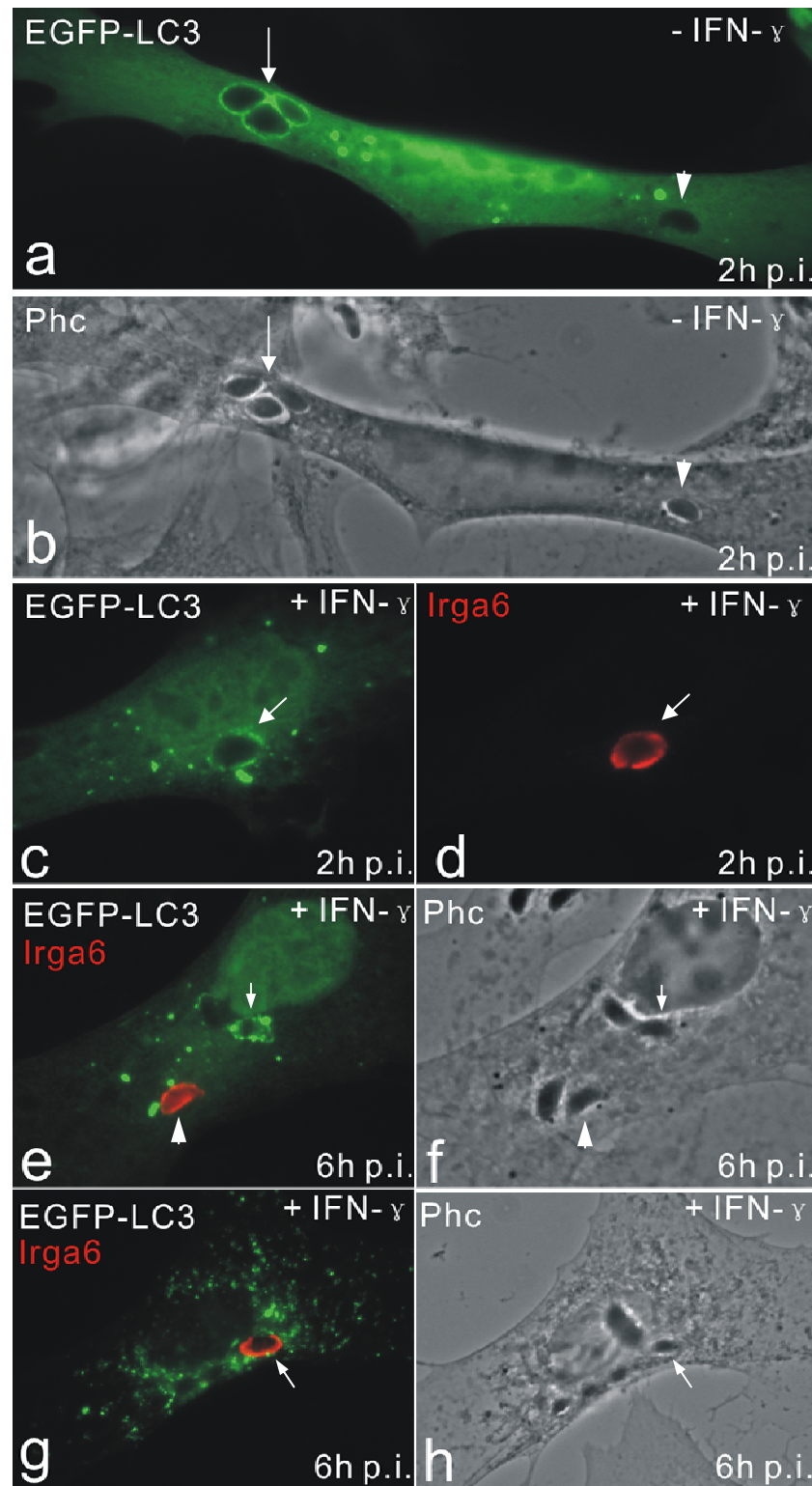


**Figure 4.5 EGFP-LC3 associates with some *T. gondii* vacuoles in MEFs**

MEFs were transfected with EGFP-LC3 and treated with 200U/ml IFN- $\gamma$  (c-h) or left untreated (a-b). 24 hours later cells were infected with ME49 for 2 hours (a-f) or 6 hours (g-h). (a-b) arrows indicate the EGFP-LC3 coated *T. gondii* vacuoles and arrow heads indicate the other EGFP-LC3-negative vacuole. (c-d) arrows indicate the disrupted, Irga6-coated and weakly EGFP-LC3 associated *T. gondii* vacuole. (e-f) arrows indicate the EGFP-LC3 positive, but Irga6 negative vacuole and arrow heads indicate the Irga6-positive, but EGFP-LC3 negative vacuole. Notably, there are two more vacuoles which are not coated with either Irga6 or EGFP-LC3. (g-h) arrows indicate the disrupted, Irga6-positive and EGFP-LC3 negative *T. gondii* vacuole and enhanced EGFP-LC3 aggregates are visible. Magnification: 630x.

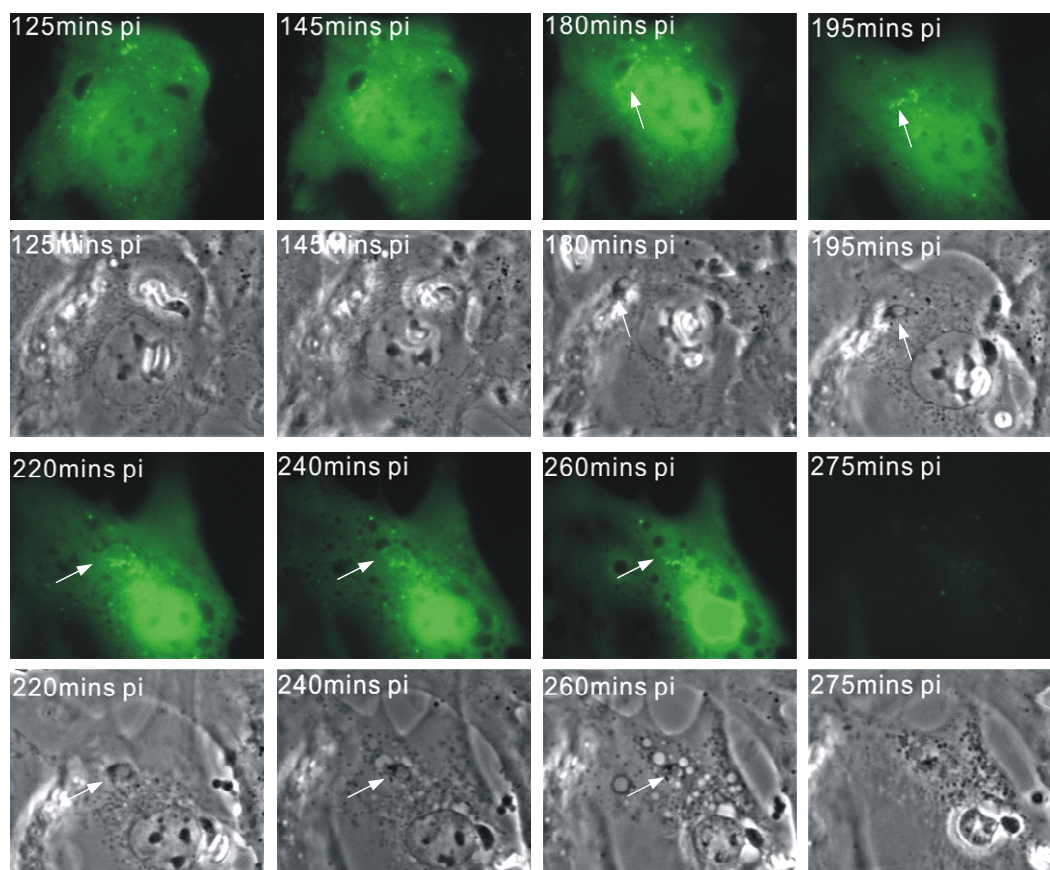


**Figure 4.6 EGFP-LC3 weakly associates with *T. gondii* vacuole as well as denuded parasite in IFN- $\gamma$  treat MEFs**

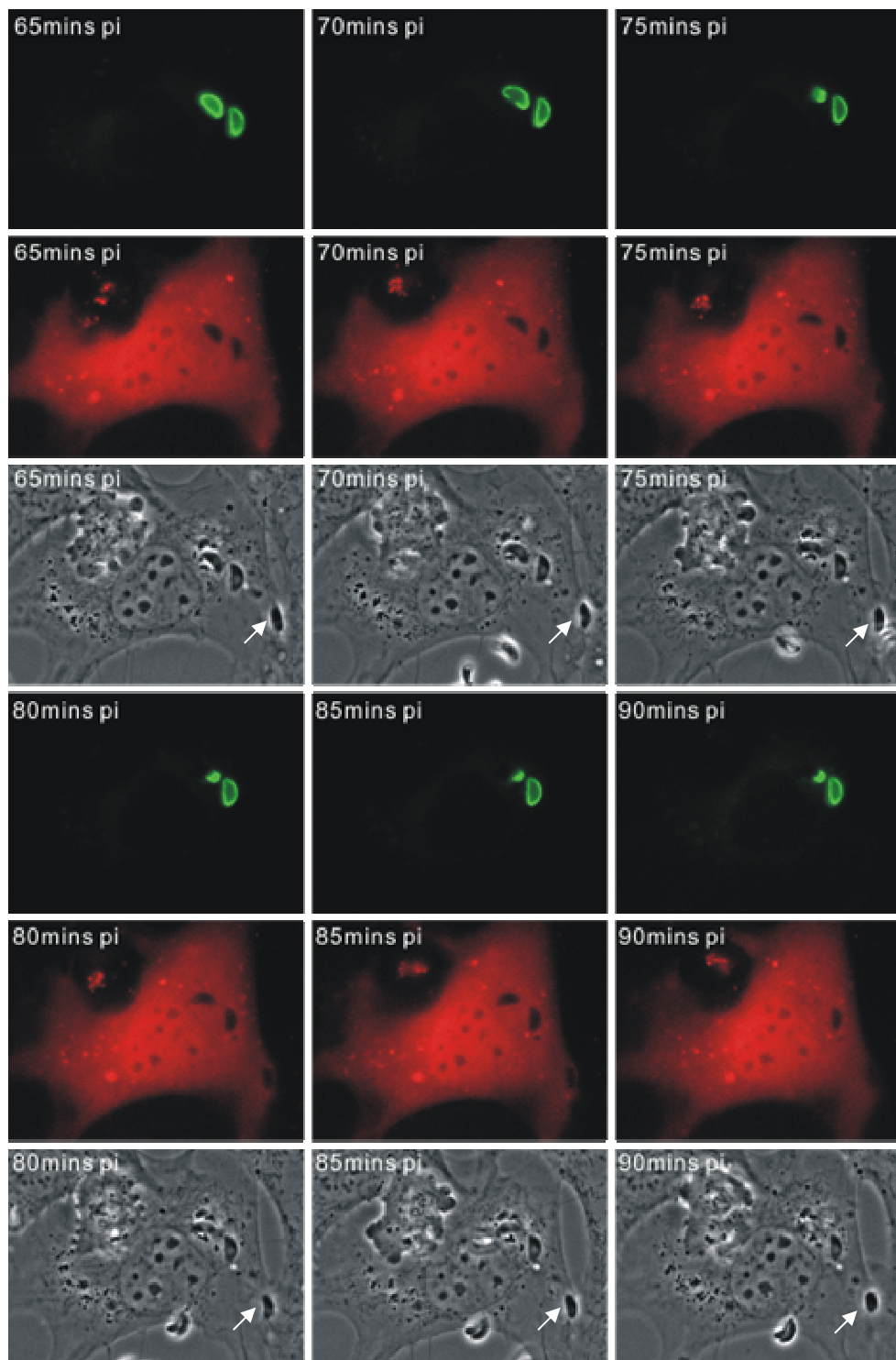
MEFs were transiently transfected with EGFP-LC3 and treated with 200U/ml IFN- $\gamma$ . 24 hours later cells were infected with ME49 for 120 minutes and images were taken by time elapse microscopy. Weak association was observed with *T. gondii* vacuole as well as denuded parasite (arrows). 180 minutes after infection, intracellular *T. gondii* was permeabilized as EGFP-LC3 diffused into the vacuole and parasite itself accompanied by phase contrast change of the Toxoplasma. Host cell died 275 minutes after the infection and EGFP-LC3 signal was vanished from dead cell. No eminent autophagosome formation was seen in the process of parasite permeabilization and host cell death. Magnification: 400x.

addition, the change in the phase properties of *T. gondii* has roughly the same timing as the entry of soluble proteins. Thus it seemed that entry of soluble fluorescent proteins (EGFP) into individual *T. gondii* could be used as a direct method to give a time point for the death of individual parasites in live cell experiments.

#### **4.4 Intracellular *T. gondii* is killed after the disruption of parasitophorous vacuole**

In order to examine the timing and possible relationship between the disruption of *T. gondii* vacuole and the permeabilization (killing) of the parasite itself, Irga6-ctag1-EGFP and a construct coding for the red fluorescent protein (pmDsRed C3) were co-transfected into MEFs and the whole succession of events was documented by live cell imaging. Figure 4.7 shows one movie in which the evolution of two Irga6 positive *T. gondii* vacuoles in one cell was

documented. One vacuole was disrupted at 70 minutes p.i. and the parasite became permeate to DsRed at 20 minutes later (90mins pi). The other vacuole was disrupted at 100 minutes p.i. and this parasite permeabilized at 145 minutes p.i.. Finally the host cell died at 150 minutes p.i.. It is worth noting that during the whole process, one intracellular parasite remained Irga6 negative and mDsRed negative until the host cell died (arrows). Table 4.1 shows the timing of the experiments that were documented by live cell imaging. Although the time between the



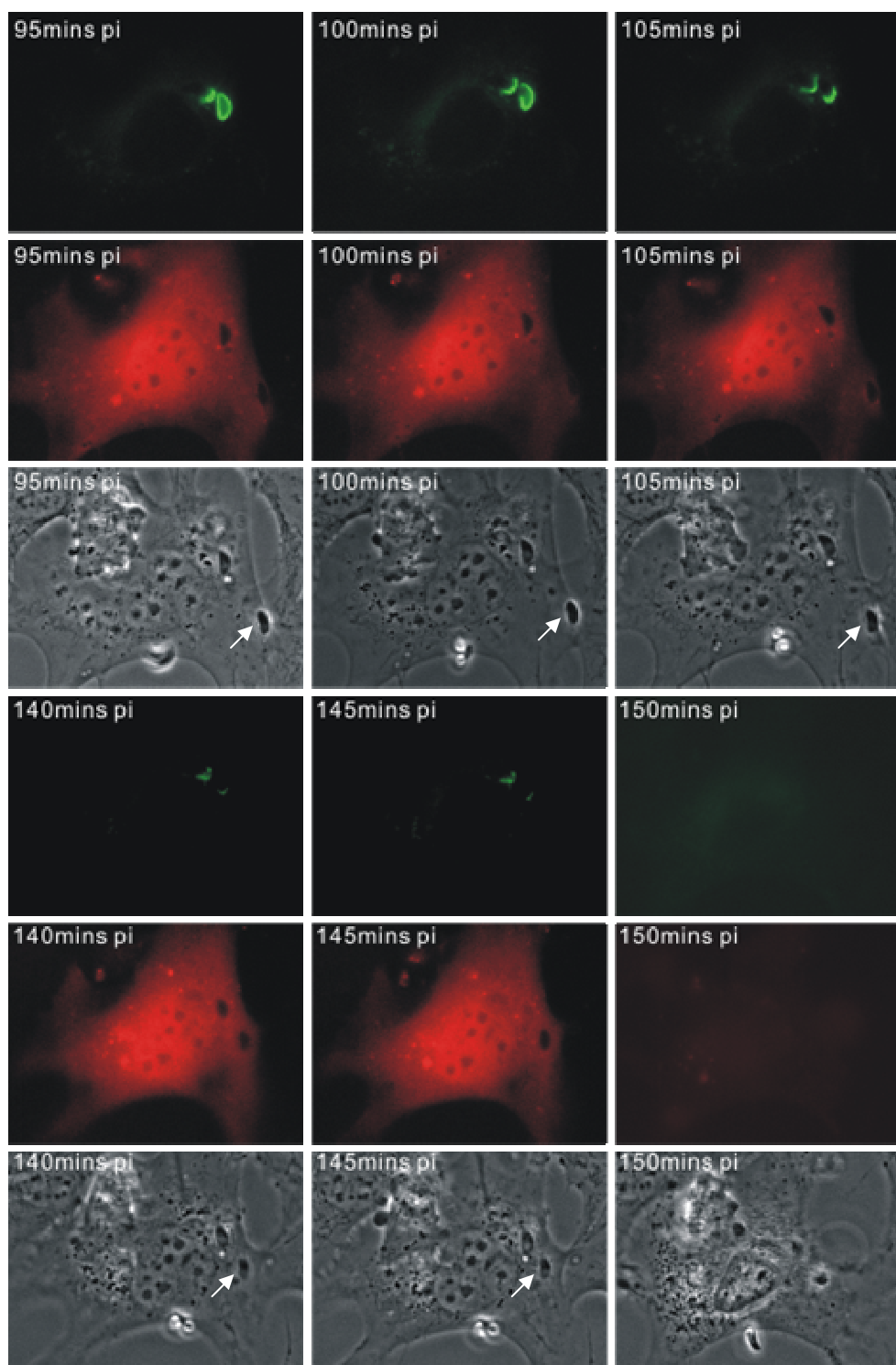


**Figure 4.7 Intracellular *T. gondii* are permeabilized after the disruption of parasitophorous vacuoles.**

MEFs were cotransfected with Irga6-ctag1-EGFP and pmDsRed C3 constructs, treated with 200U/ml IFN- $\gamma$  for 24 hours and infected with *T. gondii* ME49 strain. 60 minutes after infection three intracellular parasites were observed and two of them were coated with Irga6. Images were then taken by time elapse microscopy and consecutive frames are shown. One vacuole was disrupted at 70 min p.i. and parasite was permeabilized at 90 min p.i.. The other vacuole was then disrupted at 100 min p.i. and permeabilized at 145 min p.i.. 5 minutes later the host cell died and the DsRed signal was vanished from the host cell, as showed in the last frame. The Irga6 uncoated *T. gondii* (arrows) remained Irga6 and DsRed negative until the host cell death. Magnification: 400x

**Table 4.1 Timing of the *T. gondii* vacuolar disruption, subsequent permeabilization of stripped parasites and the final host cell death in live cell imaging experiments.**

Nr.	Starting of experiments	Disruption of PV	Entry of EGFP/mDsRed	Cell death
1	120	135		415
2	120	135		220
3	150	160		180
4	120	*		130
5	60	96		120
6	180	*		260
7	90	170		195
8	120		180	265
9	60		80	110
10	60		175/200(135pi <sup>#</sup> )	280
11	0		145	225
12	60	70	90	150
		100	145	150
13	0	44	62	88
14	120	170	185	190
15	240	255	283	328
16	0	36	51	81
17	140	140	155	260

MEFs were treated with 200U/ml IFN- $\gamma$  and transfected with EGFP-cTag1-Irga6 (1-7), pEGFP-C3 (8-11) or cotransfected with EGFP-cTag1-Irga6 and pmDsRed/pCherry (12-17) for 24 hours. Cells were then infected with *T. gondii* ME49 strain and observed by live cell imaging system from indicated time after infection. In Nr.4 and 6, \* indicates that the *T. gondii* vacuole was already disrupted when the movie started. In Nr.10, # indicates that the second parasite invaded the host cell while the film was running and was permeabilized at 135 minutes after its invasion. In Nr.12, there were two intracellular *T. gondii* coated with Irga6 and their timings are given respectively. All numbers have units as minutes after infection.

infection and host cell death ranged in different experiments from 81 to 415 minutes, the time intervals between the disruption of vacuoles and the permeabilization of parasite itself were much more constant, ranging from 15 to 45 minutes (15, 15, 18, 20, 27, 28, 45 minutes).

#### **4.5 Host cell death is a mechanism of IFN- $\gamma$ -dependent cell-autonomous resistance against *T. gondii* avirulent strain.**

The host cell death after the disruption of the *T. gondii* vacuoles seemed to be inevitable despite the fact that the stripped parasite had been killed before host cell death. To document this phenomenon on the population level, MEFs were seeded at the same density, treated with IFN- $\gamma$  or left untreated for 24 hours, and infected with *T. gondii* ME49 strain. 24 hours after infection, the cell monolayer was observed directly under inverted microscope (Figure 4.8). IFN- $\gamma$  treatment alone or *T. gondii* infection alone did not have effects on host cell density. In

*T. gondii* infected IFN- $\gamma$  untreated cells, the multiplication of parasites could be observed (not shown). However, in IFN- $\gamma$ -treated, ME49 infected cells, the cell density was notably decreased. Furthermore, cell debris could be observed and no parasite could be found in remaining live cells.

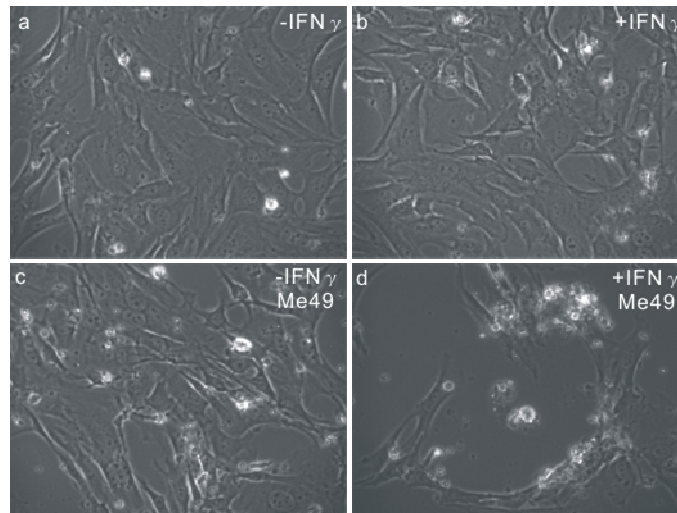


**Figure 4.8 Cell density was decreased in the IFN- $\gamma$ -induced and *T. gondii* ME49 strain infected host cells.**

MEFs ( $1 \times 10^5$ ) were seeded at the same density, treated with IFN- $\gamma$  or left untreated for 24 hours, and infected with ME49 with MOI of 10. 24 hours later, images were taken by inverted Zeiss Axiovert 200M microscope. Cell density was decreased in presence of both IFN- $\gamma$  and ME49 infection and cell debris could be observed. There is no significant density difference between cells only treated with IFN- $\gamma$ , or only infected with ME49, or with control conditions alone. Magnification: 200x.

Quantification of host cell viability was performed based on a standard colorimetric assay. Avirulent *T. gondii* strain ME49 caused a significant decrease of host cell viability in an IFN- $\gamma$  dependent manner (Figure 4.9a). Virulent *T. gondii* strain RH-YFP had no similar death-causing effect on either IFN- $\gamma$  treated or untreated host cells (Figure 4.9b). This is consistent with the observation that IFN- $\gamma$ -treated cells are unable to efficiently control the virulent *T. gondii* strain, like RH-YFP (Figure 4.10). Therefore it is in turn suggesting that the IFN- $\gamma$ -dependent host cell death could be an elimination mechanism against *T. gondii*, which is effective against avirulent strain, but rather ineffective against virulent strain.

Interestingly, IFN- $\gamma$  induced L929 fibroblasts failed to die in presence of ME49 infection (Figure 4.9 c,d). This is, however, consistent with the observation that, unlike other cell lines and primary cells, L929 cells cannot control *T. gondii* ME49 multiplication efficiently upon IFN- $\gamma$  induction (Konen-Waisman 2007), further suggesting that the host cell death is indeed a mechanism for the elimination of intracellular *T. gondii*.

To conclude, host cell death seems to be a novel and important component in the mechanism of IFN- $\gamma$ -dependent cell-autonomous resistance against *T. gondii* avirulent strain infection.

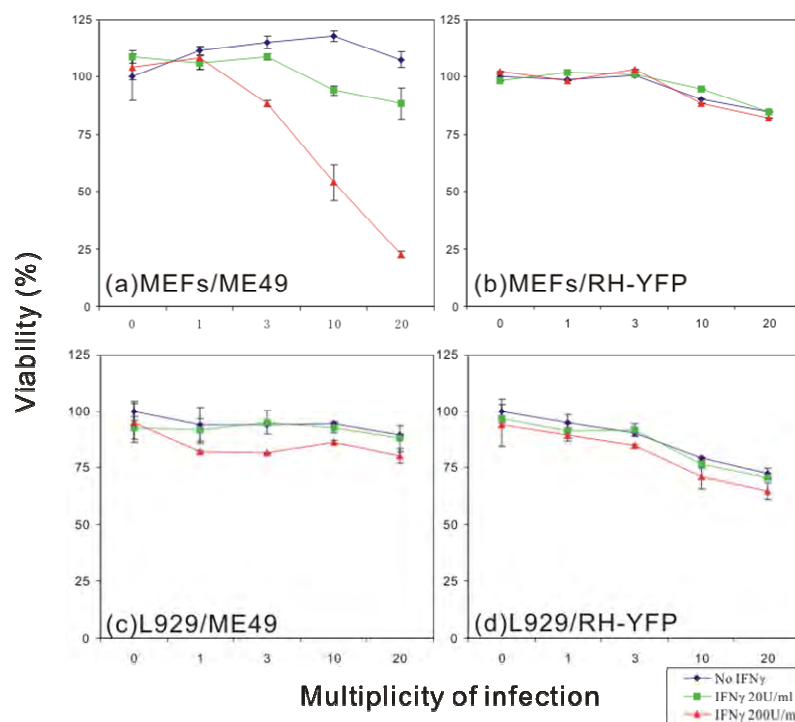


**Figure 4.9** Effects of IFN- $\gamma$  and *T. gondii* infection on host cell viability.

MEFs (a, b) and L929 cells (c, d) were seeded into 96 well plates ( $5 \times 10^3$ /well) and induced with indicated dose of IFN- $\gamma$  for 24 hours. Cells were then infected with *T. gondii* avirulent strain ME49 (a, c) or virulent strain RH-YFP (b, d) for 24 hours. Cell viability were measured and expressed as percentage of uninfected cells. ME49 infection cause significant decrease of cell viability in presence of IFN- $\gamma$  in MEFs while RH-YFP has no effect. Viability of L929 cells was not affected by IFN- $\gamma$  and/or *T. gondii* infection.

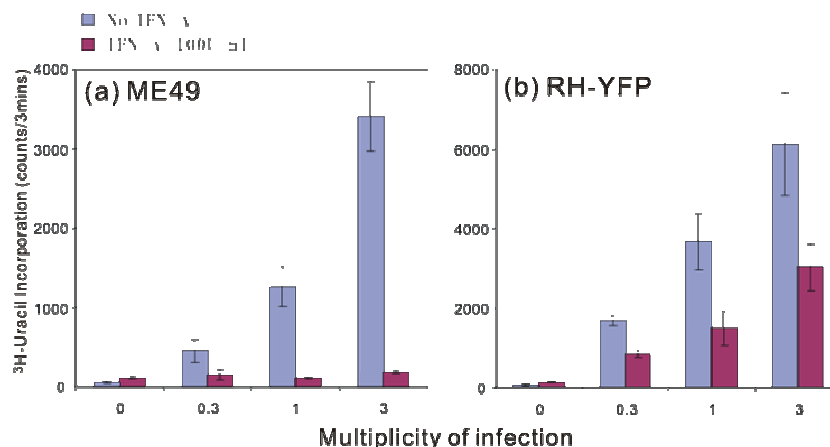


**Figure 4.10** IFN- $\gamma$  mediated cell-autonomous control of *T. gondii* avirulent (ME49) and virulent (RH-YFP) strains. (performed by Stephanie Könen-Waisman)

MEFs were treated with 100U/ml IFN- $\gamma$  or left untreated for 24 hours and infected with *T. gondii* avirulent ME49 strain or virulent RH-YFP strain by different multiplicities of infection. 48 hours later,  $1 \mu\text{Ci}/\text{well}$  [ $^3\text{H}$ ]-uracil were added to the culture and incubated for additional 24 hours. The *T. gondii* growth was determined by liquid scintillation counting. The growth of ME49 strain was completely inhibited in IFN- $\gamma$  treated cells, and almost no viable parasite could be detected. However, the RH-YFP strain can still grow in IFN- $\gamma$  treated cells, although to a less extent compared to the IFN- $\gamma$  untreated cells.

#### **4.6 The property of host cell death induced by IFN- $\gamma$ and *T. gondii* avirulent strain infection is rather necrosis than apoptosis.**

It is well established that intracellular *T. gondii* could extensively modify host cell signalling pathways resulting in an anti-apoptotic state in the host cell that presumably favours the intracellular growth of the parasites (Carmen 2007). *T. gondii* infected cells are resistant to numerous apoptotic stimuli (Carmen 2006). As shown above, IFN- $\gamma$  treated murine fibroblasts can apparently override the anti-apoptotic effect of *T. gondii* infection and initiate host cell death, but only on condition that the PVM can first be disrupted, which is supposed to be the responsibility of the IRG proteins. However, the nature of this IFN- $\gamma$ -dependent host cell death was unknown, and was therefore investigated.

Cytochrome C is a key molecule in apoptosis. It is released by the mitochondria in response to pro-apoptotic stimuli and facilitates the formation of the apoptosome, which further leads to the activation of caspases cascades, and finally apoptotic death of the cell (Goldstein 2000). Therefore, indirect immunofluorescence staining was performed to analyze whether cytochrome C is released during the process of ME49 infected IFN- $\gamma$  treated host cell death. As positive control, cells were treated with TNF- $\alpha$  and cycloheximide to induce apoptosis. Figure 4.11 shows that in normal cells, cytochrome c is localized to mitochondria while during apoptosis it is released into cytosol and showed diffused staining pattern (Figure 4.11 b). No cytochrome c release was detected during cell death caused by *T. gondii* infection at any time point (Figure 4.11 c, d). This result does not exclude the possibility that cytochrome c may be released right before the cell death. However, it suggests that the *T. gondii* infection induced cell death is non-apoptotic since during apoptosis the release of cytochrome c normally happens several hours before cell death (Goldstein 2000).

In normal viable cells, phosphatidylserine (PS) is located on the cytoplasmic face of the cell membrane. However, in apoptotic cells, PS is translocated from the inner to the outer leaflet of the plasma membrane, and is exposed to the external environment. Annexin V, a Ca<sup>2+</sup>-dependent PS binding protein, is used as an early marker for apoptosis (Koopman 1994). We investigated in live cell imaging system whether and when PS was externalized during *T. gondii* infection induced cell death by adding Alexa-555 labelled Annexin V to the medium. To identify the timing of the host cell death, EGFP was expressed in the cells and released

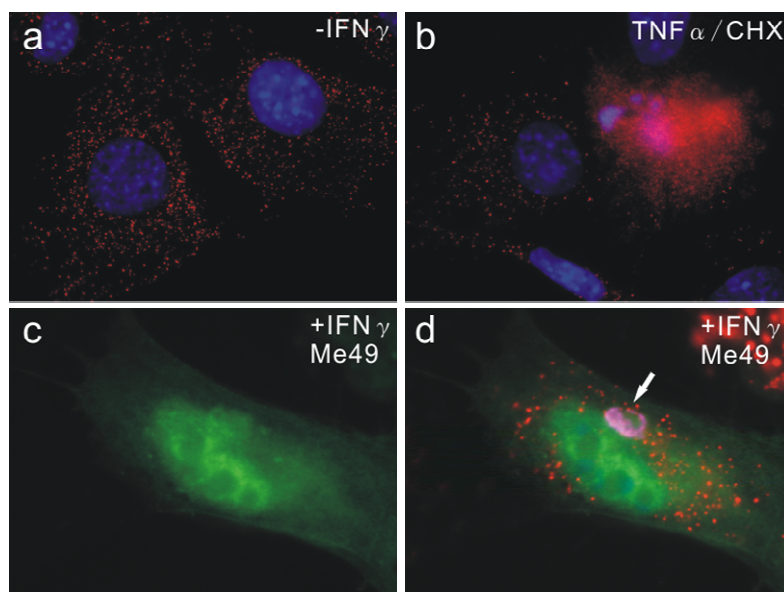


**Figure 4.11 Cytochrome C is not released during the process of ME49-infected IFN- $\gamma$ -treated host cell death.**

MEFs were treated with 200U/ml IFN- $\gamma$  for 24 hours (c, d), and infected with ME49 for 3 hours. As control, MEFs were treated with 40ng/ml TNF $\alpha$  combined with 10 cycloheximide  $\mu$ g/ml for 4 hours. Construct coding for EGFP was transiently transfected into cells (c,d). Cells were fixed with 3% PFA in PBS and stained for Cytochrome C (red, a-d) and Gra7 (magenta, c-d). Arrow indicates one permeabilized parasite and EGFP protein is diffused into it. No Cytochrome C was found to be released from mitochondria in ME49 infected IFN- $\gamma$  treated cells. Magnification: 630x. Nuclei were labelled with DAPI

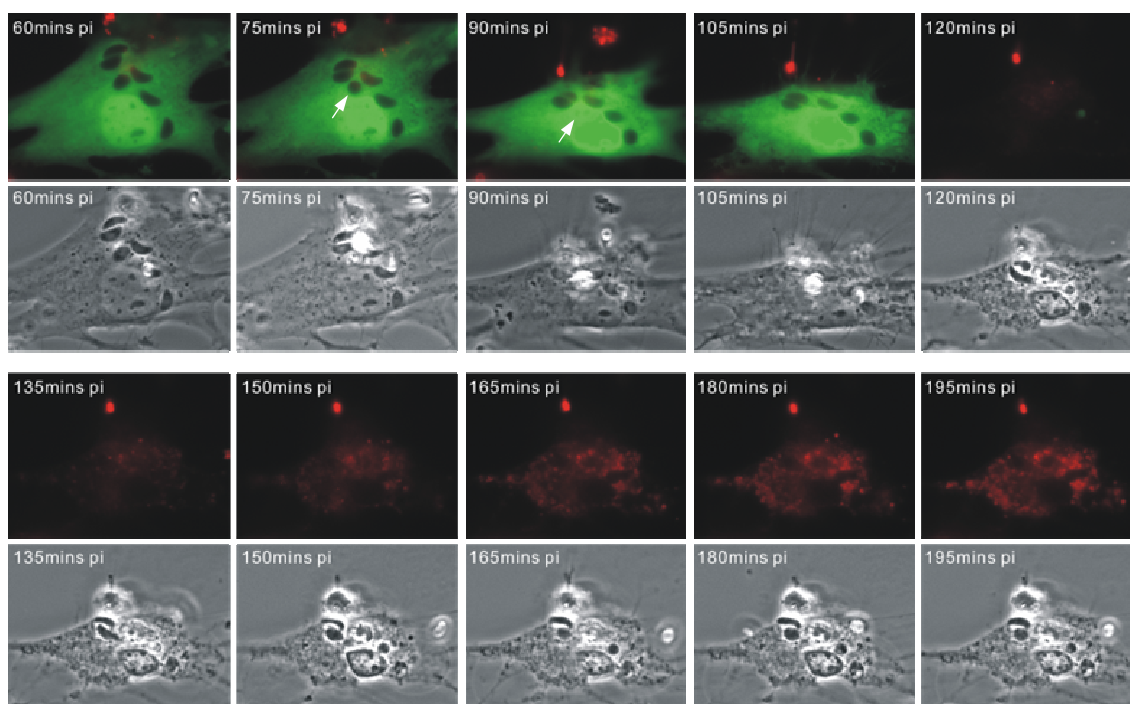


**Figure 4.12 Phosphatidylserine is not externalized before host cell death.**

MEFs were treated 200U/ml IFN- $\gamma$  and transiently transfected with pEGFP-C3 construct. After 24 hours, cells were infected with ME49 for 60 minutes and images were taken by time elapse microscopy. Alexa Fluor 555 labelled annexin V (1:100) and 2.5mM CaCl<sub>2</sub> were added to the medium. No annexin V signal was seen before the infected cell died and accumulated to overall cell membrane debris after the EGFP was released from the dead cell. Arrow shows the permeabilization of one parasite. Magnification: 400x

into the medium when the cell plasma membrane was permeabilized. As showed in Figure 4.12, Annexin V signals remained negative at the cell plasma membrane for a long time and only started to accumulate on the overall cellular membrane debris after the EGFP signal disappeared from the cell. This result further confirmed that the IFN- $\gamma$  treated host cell death by *T. gondii* infection is non-apoptotic.

High-mobility group box 1 (HMGB1), normally functioning as an intranuclear architectural protein within the healthy cells, is emerging as an important proinflammatory mediator which is released from cells undergoing necrosis (Scaffidi 2002; Chen 2004). This prompted us to examine whether HMGB1 was released during *T. gondii* infected host cell death. TNF- $\alpha$  plus cycloheximide was used to induce apoptosis as control. During apoptosis, caspase-3 is a pivotal executor proteinase which undergoes activating cleavage. In turn, caspase-3 cleaves PARP and other downstream substrates. Caspase-3 and PARP cleavage were also examined by western blot analysis. Figure 4.13 showed that in the presence of IFN- $\gamma$ , *T. gondii* avirulent ME49 strain infection induced HMGB1 release from host cells. Neither caspases-3 nor PARP was cleaved in this process, though both were cleaved during TNF- $\alpha$ -CHX induced apoptosis. In the absence of IFN- $\gamma$ , *T. gondii* infection did not induce HMGB-1 release or caspases-3 activation (Figure 4.13).

In conclusion, a further mechanism of IFN- $\gamma$  dependent cell autonomous resistance against *Toxoplasma gondii* appears to be induced host cell necrosis.

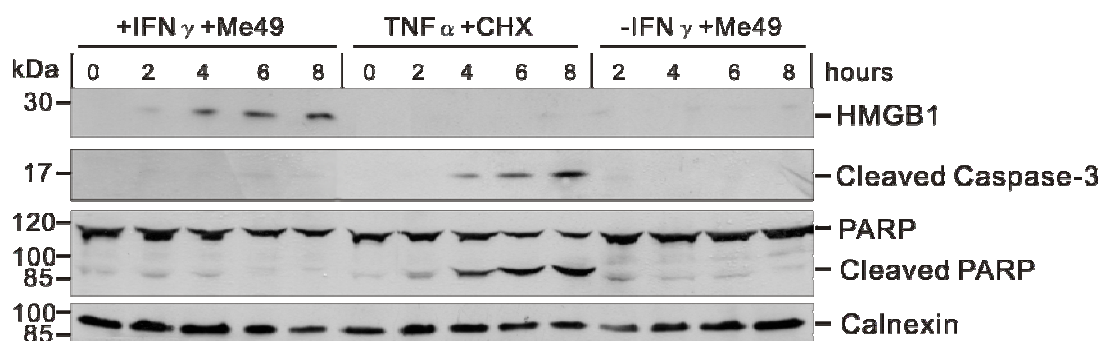


**Figure 4.13 HMGB1 is released, but caspase-3 is not activated, during IFN- $\gamma$ -treated ME49-infected host cell death.**

MEFs treated with 200U/ml IFN- $\gamma$  for 24 hours or untreated were infected with ME49 for indicated time. As control, cells were treated with 40ng/ml TNF $\alpha$  and 10 cycloheximide  $\mu$ g/ml to induce apoptosis. Cell culture supernatant (for HMGB1) or cell lysate (for caspases-3 and PARP) were collected at indicated time and subjected to western blot analysis. Calnexin was detected as loading control. HMGB1 was found to be released from ME49 infected IFN- $\gamma$  treated cells, but not from cells infected with ME49 without IFN- $\gamma$  treatment, also not from apoptotic cells. Neither caspase-3 nor PARP cleavage was found in *T. gondii* infected cell, whereas in apoptotic cells, both caspases-3 and PARP were cleaved

#### 4.7 Cathepsin B is not necessary for the IFN- $\gamma$ -dependent *T. gondii* avirulent strain elicited host cell necrosis.

Cathepsins are a family of lysosomal proteases which function normally inside lysosomes and have vital roles in cellular protein turnover. Among these, cysteine protease Cathepsin B and aspartic protease Cathepsin D are the most abundant and have mostly often been linked to cell death (Broker 2005; Golstein 2007; Willingham 2007).

To analyze the possible role of Cathepsin B in *T. gondii* induced host cell necrosis, Cathepsin B deficient embryonic fibroblasts were tested for their viability during *T. gondii* avirulent ME49 strain infection. As Figure 4.14 (a, b) shows, Cathepsin B deficient MEFs showed IFN- $\gamma$  dependent ME49 induced cell death, which were also seen in wild type cells. Western blots (Figure 4.14, c) showed that during cell death, HMGB-1 was released to the same extent in Cathepsin B deficient cells as in the wild type cells. Furthermore, Cathepsin B deficient MEFs can control ME49 strain growth upon IFN- $\gamma$  treatment as efficiently as wild type cells (data not shown). Therefore, we conclude that Cathepsin B is dispensable in the IFN- $\gamma$ -dependent *T. gondii* avirulent strain induced host cell necrosis.

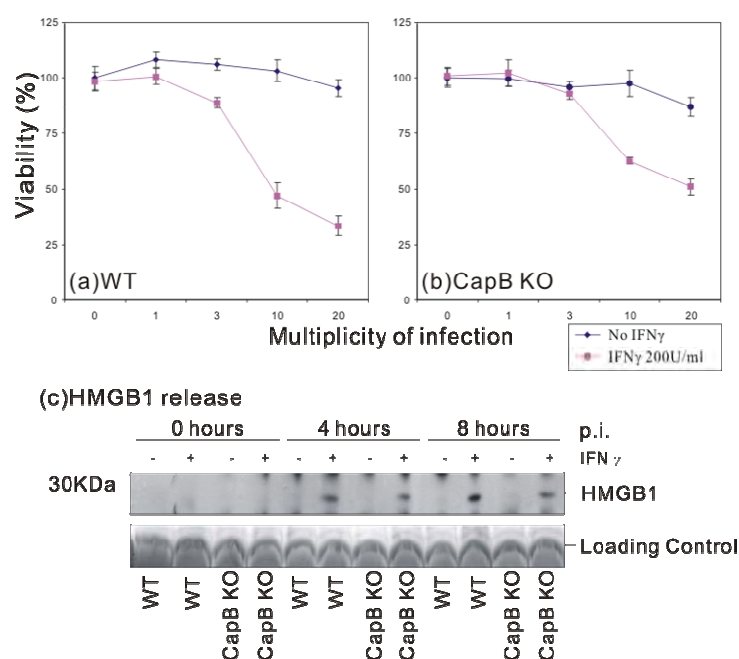


**Figure 4.14 Cathepsin B is not necessary for the IFN- $\gamma$ -dependent *T. gondii* ME49 strain elicited host cell necrosis.**

Wild type (a) and Cathepsin B deficient (b) MEFs were seeded into 96 well plates ( $7.5 \times 10^3$ /well) in the presence of 200U/ml IFN- $\gamma$  or without IFN- $\gamma$  for 24 hours and infected with ME49 for 8 hours. Cell viability were measured and expressed as percentage of uninfected cells. Western blot analysis was performed on cell culture supernatant for HMGB1(c). Nitrocellulose membrane was stained with Ponceau Red as loading control. Cathepsin B is not necessary for *T. gondii* ME49 induced IFN- $\gamma$  dependent host cell necrosis.

#### **4.8 *T. gondii* avirulent strain induced IFN- $\gamma$ -dependent necrosis dominates over the virulent strain resistance mechanisms against IFN- $\gamma$ protection.**

The IFN- $\gamma$ -induced cells infected with *T. gondii* virulent strain (RH-YFP) do not undergo necrotic death, as showed in Figure 4.9b. It has been also shown that IFN- $\gamma$  treatment failed to efficiently control the proliferation of *T. gondii* virulent strains in MEFs (Figure 4.10). Furthermore, the accumulation of IRG proteins onto the PVM of *T. gondii* virulent strain is largely blocked, and the vacuoles are not disrupted (Khaminets, manuscripts in preparation). Therefore, *T. gondii* virulent strains have a resistance mechanism against IFN- $\gamma$  mediated protection of host cells, while *T. gondii* avirulent strain was killed in the IFN- $\gamma$ -treated cell cytosol after vacuolar disruption, and followed by host cell necrosis. Taken together, it was therefore of interest to know whether in cells doubly infected with virulent and avirulent strain of *T. gondii*, the virulent or avirulent phenotype would be dominant. To answer this question, co-infection of avirulent strain ME49 and virulent strain RH-YFP was performed and host cell viability was measure 8 hours after infection. Figure 4.15 shows that the viability of host cells co-infected with both ME49 and RH-YFP strains was decreased in the same manner as ME49 infection alone in the presence of IFN- $\gamma$ . The resistance effect against IFN- $\gamma$  from RH-YFP strain was overcome. This must illustrate that the IFN- $\gamma$ -dependent host cell necrosis induced by the avirulent ME49 strain overcomes the resistance to IFN- $\gamma$  induction typical of the virulent RH-YFP strain. This is, at least partially, due to the fact that it fails to induce necrosis, but has no resistance to necrosis once induced (in our case by co-infecting of ME49 strain). This in turn suggests that the necrotic event is triggered by vacuolar disruption, which fails to occur for the virulent strains. It is therefore plausible that this failure of disruption is in turn due to the defective loading of IRG proteins onto the *T. gondii* virulent strain vacuoles.

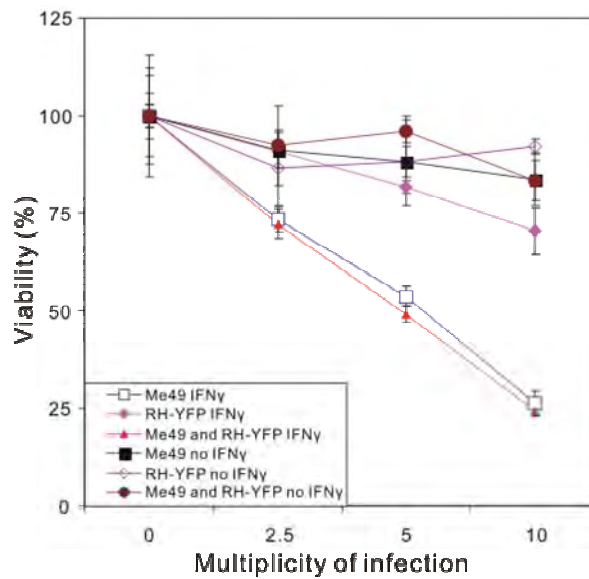


**Figure 4.15 IFN- $\gamma$ -dependent host cell necrosis elicited by *T. gondii* avirulent strain dominates over the IFN- $\gamma$  resistance mechanisms of *T. gondii* virulent strain.**

MEFs were seeded into 96 well plates ( $7.5 \times 10^3$ /well) and treated with 200U/ml IFN- $\gamma$  or left untreated for 24 hours. *T. gondii* avirulent strain ME49 and/or virulent strain RH-YFP were infected for 8 hours. Cell viability were measured and expressed as percentage of uninfected cells. ME49 infection caused IFN- $\gamma$  dependent host cell death while RH-YFP did not, even in the present of IFN- $\gamma$ . However, when ME49 and RH-YFP were coinfecting in the presence of IFN- $\gamma$ , host cell viability was decreased to the same level caused by ME49 infection alone.

## 5. Discussion

IRGs family members are indispensable resistance factors against intracellular pathogens in mice. Cellular membrane system is the frontier where intracellular pathogens are confronted with host resistance factors. Studies on the subcellular localization provide important information for the functions of the IRG proteins. In the present study, subcellular localization of endogenous Irgm1 and Irgm1 tagged by EGFP were investigated in depth. Furthermore, the cell-autonomous resistance mechanisms were extensively analyzed in the *T. gondii* infection model by live cell imaging and the possible role of Irgm1 in *T. gondii* resistance was examined.

### 5.1 Irgm1 localizes mainly to the Golgi apparatus and lysosomes, and mislocalizes as a result of EGFP-tagging at the N or C terminus.

Different members of IRG proteins showed different affinities to cellular membranes. Irgm1 has been found exclusively in membrane-bound form in cells and behaves like a transmembrane protein in biochemical assays even though no transmembrane domain has been identified within the protein sequences. In L929 fibroblasts, TIB-75 hepatocytes and Raw 264.7 macrophages, Irgm1 localizes to *cis*- and *medial*-Golgi apparatus with additional distributed granular signal (Martens 2004b). In the present study, by using TGN38 as a *trans*-Golgi and *trans*-Golgi network (TGN) marker, Irgm1 is further identified to be localized in these compartments as well. In addition, the distributed granular signals of Irgm1 overlap with those of LAMP1, which marks late endosomes and lysosomes. This observation is confirmed since Irgm1 has also been found to accumulate on the compartments enriched in the acidotropic dye LysoTracker. In addition, immunofluorescent staining shows that CI-M6PR and Irgm1 localize to adjacent compartments or partially colocalize. The steady state distribution of CI-M6PR is predominantly within late endosomes, less in the TGN and ~10% at plasma membrane, but not in lysosomes. It is therefore likely that in addition to Golgi state, Irgm1 is mostly distributed in the lysosomes, rather than in the late endosomes. Compared to the universal Golgi localization of Irgm1, the signal intensities of Irgm1 in the LAMP1-

**Table 5.1 Summary of the localization of Irgm1, EGFP-tagged Irgm1 and EGFP-Irgm1  $\alpha$ K**

	IFN- $\gamma$ induced Irgm1	Transfected Irgm1	Irgm1 S90N	EGFP-Irgm1	Irgm1-EGFP	EGFP-Irgm1 S90N	Irgm1-EGFP S90N	EGFP-Irgm1 $\alpha$ K
<b>Golgi</b>	+	+	+	–	–	+	+	+
<b>LE/LY</b>	+	+	–	–	+	–	–	+
<b>EE/RE</b>	–	ND	ND	+	+	–	–	–
<b>PG</b>	+	+	–	–	+	–	–	–

Abbreviations: LE/LY: late endosome/lysosome; EE/RE: early/recycling endosome; PG: latex bead containing phagosome; ND: not determined. See detailed descriptions in the text.

positive compartments vary in different individual cells, from obviously visible to hardly detectable. Since the MEFs are isolated from mouse embryos and composed of heterogeneous groups of cells, the variable degrees of lysosomal association of Irgm1 could correlate with the different states of individual cells controlled by cell cycles or other undefined factors. Finally, scarcely detectable amount of IFN- $\gamma$  induced endogenous Irgm1 is found associated with early and recycling endosomes by comparing fluorochrome-labelled transferrin with Irgm1 localization. To conclude, the IFN- $\gamma$  induced endogenous Irgm1 localizes to the whole Golgi apparatus and late endocytic/lysosomal compartments.

Both N and C terminally EGFP-tagged Irgm1 mislocalize in MEFs (Results-I) and Raw264.7 macrophages (Können-Waisman, unpublished). Both of them do not localize to the Golgi apparatus anymore. Irgm1-EGFP shows significant association with LAMP1-positive compartments in all transfected cells, in contrast to the variable lysosomal association of IFN- $\gamma$ -induced endogenous Irgm1. It also mislocalizes to the early/recycling endosomes defined by the uptaken transferrin, since endogenous Irgm1 shows scarcely, if at all, early/recycling endosomal distribution. EGFP-Irgm1 associates with LAMP1-positive compartments very weakly, if at all. It is distributed mainly in the early/recycling endosomes as well as some other undefined, non-Golgi, non-LAMP1-positive, vesicular structures. However, both N and C terminally EGFP-tagged nucleotide-binding deficient Irgm1 (S90N) restore the correct Golgi localization with almost diminished mislocalization. This indicates that the localization/mislocalization of Irgm1 are controlled by the nucleotide binding, and accordingly may reflect the inactive/active state of the protein. One member of the IRG proteins, Irga6, shows GTP-dependent oligomerization and self-activation (Uthaiyah 2003). In

addition, Irgm1 has been shown to interact with itself in yeast 2-hybrid system, and this self-interaction is abolished by destroying the nucleotide-binding motif (S90N) (Hunn 2007). Considering that the transfected EGFP proteins form dimer in cells, one possibility for the mislocalization of Irgm1 by an EGFP-tag could be that the interaction of two Irgm1 molecules is promoted by the EGFP dimer, thus stimulate the GTP-dependent activation of Irgm1.

Golgi localization may indeed reflect the inactive form of Irgm1 since nucleotide-binding deficient Irgm1 (S90N), no matter tagged with EGFP or not, localizes to Golgi. However, more cytoplasmic vesicular signals have been noticed in addition to Golgi localization when Irgm1 (S90N) and EGFP-tagged Irgm1 (S90N) were expressed. Those signals showed partial and weak overlapping with LAMP1/Transferrin positive compartments in some transfected cells (data not shown). This may reflect the weak capability of Irgm1 to associate passively with early/recycling/late endocytic/lysosomal compartments, but active accumulation on those organelles may be under strict control by nucleotide binding.

Accordingly, the early/recycling/late endosomal and lysosomal localization of EGFP-tagged Irgm1 could reflect the activated form of Irgm1. Activated Irgm1 may target to the lysosomes by interaction through N-terminus, since the lysosomal association for EGFP-Irgm1 is largely abolished. As discussed later, a helical fragment near C-terminus of Irgm1 ( $\alpha$ K) is responsible for its lysosomal targeting. However, based on the crystal structure of Irga6, a prototypic structure for all IRG proteins (Ghosh 2004), the N-terminus of the protein is close to the  $\alpha$ K helix. In contrast, the C-terminus of the protein is far from  $\alpha$ K helix and locates in another side of the molecule. Therefore, it is reasonable that the EGFP tagged at N-terminus, but not at C-terminus, may interfere with the interaction of  $\alpha$ K helix with its lysosomal target when Irgm1 is in its activated form. On the other hand, the early/recycling endosomal targeting of Irgm1 is probably independent of  $\alpha$ K helix, because both N and C terminally EGFP-tag does not interfere with the early/recycling endosomal mislocalization of tagged Irgm1. Furthermore, EGFP- $\alpha$ K targeting construct does not target to the early/recycling endosomes (data not shown). Endogenous Irgm1 has been shown to be rapidly recruited to active plasma membrane and phagocytic cups, probably mediated by its activated G-domain (Martens 2004b). Subsequently, Irgm1 remained association with phagosomes as they mature (through

early endocytic pathways) into LAMP1-positive phagolysosomes. Over-expressed Irgm1 and its isolated G-domain localize to the plasma membrane in L929 cells, and this is also abolished when Irgm1 (S90N) is over-expressed. Therefore, it is not implausible that a proportion of EGFP-Irgm1 and Irgm1-EGFP are recycling between plasma membrane and early/recycling compartments mediated by the activated G-domain. One hint in favour of this hypothesis is that, in the proposed molecular structure, in contrast to the  $\alpha$ K helix, the G-domain of the protein is distant from both N and C terminus, and therefore should not be directly influenced by EGFP-tag.

Nevertheless, the activation mechanism of Irgm1 controlled by the nucleotide binding and hydrolysis is obscured by the fact that Irgm1 has an unusual methionine in G1-motif in place of the otherwise universally conserved lysine, a property shared by the two other members in the IRGM subfamily. The well-conserved lysine in G-1 motif is responsible for binding the phosphates of the nucleotide and is important for hydrolysis activity of the GTPase. Several studies on other GTPases have shown that mutation of this conserved lysine interferes with nucleotide binding and hydrolysis (Bourne 1990; Bourne 1991). Especially in Mx proteins, substitution of a methionine for the lysine in G1 motif, same substitution in Irgm1, resulted in a loss of GTPase activity (Pitossi 1993). Little has been reported about the biochemical properties of Irgm1, except that the protein binds to GDP cross-linked to agarose beads, but not GTP and GMP (Martens 2004a). Taylor and colleagues reported that more than 90% of the nucleotide bound to immunoprecipitated Irgm3 is GTP (Taylor 1997). In addition, partially purified GST-Irgm3 has been shown to hydrolyze GTP to GDP, although GTP-binding deficient control (S98N) was missing in these experiments (Taylor 1996). It is also interesting to note that N-terminally EGFP-tagged Irgm2 and Irgm3 have the same localization as endogenous Irgm2 and Irgm3 in cells (Golgi and ER, respectively)(Martens 2004a). Taken together, Irgm1 may have dramatic different nucleotide binding and/or hydrolysis properties from classical GTPases as well as other IRGM proteins and biochemical studies on recombinant proteins are essential for further investigations.

Irga6 and Irgb6 form GTP-dependent aggregates and mislocalize when expressed alone in cells. However, this mislocalization can be reversed by treating cells simultaneously with IFN- $\gamma$ . It has been established that the IRGM proteins are the IFN- $\gamma$  induced factors

responsible for proper localization of Irga6 and Irgb6. The current model is that IRGM proteins interact with Irga6 and Irgb6, prevent GTP binding by those proteins, and keep them in GDP-bound inactive form (Hunn 2007). In contrast, the mislocalization of Irgm1 by EGFP-tag is not influenced by IFN- $\gamma$  co-treatment. The explanation again awaits the biochemical studies on recombinant Irgm1 proteins, as the mislocalization is indeed nucleotide-binding dependent.

The accumulation of Irgm1 on the phagosomes may largely reflect the critical biological function of this protein. Irgm1 deficient mice lose resistance to a broad range of intracellular pathogens, such as *T. gondii*, *T. cruzi*, *M. tuberculosis*, *S. typhimurium* and *L. monocytogenes* (Collazo 2001; MacMicking 2003; Santiago 2005; Henry 2007). Although those pathogens have diverse intracellular life styles, they share one common property: they can establish and reside in non-fusogenic pathogen-containing vacuoles after invasion into (or being taken up by) the host cells. However, the signal for Irgm1 to accumulate on phagosomes is probably pathogen-irrelevant, as phagocytosed latex beads is enough to recruit Irgm1. The accumulation of Irgm1 on phagosomes is strictly nucleotide-binding dependent. IFN- $\gamma$  induced endogenous Irgm1, transfected Irgm1 and Irgm1-EGFP fusion protein strongly associate with latex beads-containing phagosomes, but this accumulation is completely abolished when the nucleotide binding G1-motif is destroyed. Considering that IFN- $\gamma$ -induced endogenous Irgm1 has variable degrees of lysosomal associations, this could imply that Irgm1 may actively recycle and patrol in the endocytic compartments, because the lysosomal fraction of Irgm1 could be the spontaneously activated form of the protein. Macmicking *et al* have shown that Irgm1 could function by accelerating the acidification of *M. tuberculosis*-containing phagosomes, and Irgm1-deficient macrophages could not efficiently kill intracellular *M. tuberculosis* upon IFN- $\gamma$  treatment (MacMicking 2003). Nevertheless, the resistance mechanisms of Irgm1 for other pathogens remain to be examined. For example, *L. monocytogenes* escapes from the phagosome within 30 minutes after uptake to replicate within the cytosol while *T. gondii* actively invade all nucleated cells independent of the phagocytosis pathway (Tilney 1989; Portnoy 2002; Sibley 2004). The single phagosomal acidification mechanism may not explain the central role of Irgm1 for resistance against all those pathogens. Recently Macmicking *et al* have produced evidence that Irgm1 could also

accumulate on the *L. monocytogenes*-containing phagosomes (Shenoy 2008). Indeed, the escape from phagosomes by *L. monocytogenes* is efficiently blocked in the IFN- $\gamma$ -treated macrophages (Portnoy 1989). It is therefore possible that Irgm1 could execute different mechanisms against different pathogens.

Deretic and colleagues reported that Irgm1-EGFP (pF25) colocalized with MDC and LC3 positive compartments, suggesting that Irgm1 associates with autophagosomes and therefore has a pro-autophagy function in macrophages (Gutierrez 2004; Singh 2006). However, whether this association of Irgm1 with autophagosomes is actively autophagy-promoting or is only a secondary association remains to be further examined, since Irgm1-EGFP is shown in the present study to associate constitutively with lysosomes. More importantly, Irgm1-EGFP behaves differently from endogenous IFN- $\gamma$  induced proteins and IRGs proteins also cooperate with each other (Hunn 2007). Thus the transfection of Irgm1-EGFP alone is a highly artificial situation and the conclusion of Gutierrez and Singh *et al* remains to be confirmed.

Irgm1 is the only member in IRG family which has been found so far to associate with endocytic compartments. Irgm2 and Irgm3 are exclusively associated with Golgi apparatus and endoplasmic reticulum, respectively. Irga6 and Irgb6 are partially ER-residing proteins and partially cytosolic. And Irgd is largely cytosolic in cells (Taylor 1997; Martens 2004b; Butcher 2005; Martens 2006). In addition, Irgm2 is not recruited to latex bead-containing phagosomes (data not shown). Due to ER-localization of Irgm3 and Irga6, it was technically difficult to distinguish between accidental proximity and active association with the phagosomes of these proteins. However, it is clear that Irgm3 and Irga6 do not accumulate in significant amounts on latex bead-containing phagosomes as Irgm1 does (Martens 2004a). Preliminary data also indicate that Irgb6, Irgb10 and Irgd are also not accumulated on latex-beads phagosomes (data not shown). Interestingly, those who are not associated with latex beads phagosomes have been found to extensively accumulate on *T. gondii* avirulent strains PVM, from where Irgm1 is absent. Currently we consider the free diffusion from cytosolic pool to the *T. gondii* PVM as the re-localization mechanism. Irgm1 has been identified so far to be the only member of the IRG family that exclusively associates with membrane with no

free cytosolic pool. This may provide additional support for the diffusion model of the recruiting of other IRG proteins to the *T. gondii* parasitophorous vacuole.

## **5.2 Both Golgi and lysosomal localization of Irgm1 is dependent on a predicted amphipathic helix near the C-terminus.**

Golgi localization of Irgm1 has been shown to be mediated by the  $\alpha$ K helix near the C-terminus. This helix is predicted to be amphipathic and is sufficient to target EGFP protein to the Golgi apparatus when tagged at the C-terminus. Disruption of amphipathicity by insertion one or two glutamate residues into helical region abolishes the Golgi localization of the EGFP- $\alpha$ K construct as well as of the Irgm1 full-length protein (Martens 2004a). In the present study, Irgm1 has been further identified to localize in lysosomes defined by LAMP1, in addition to the Golgi apparatus. EGFP- $\alpha$ K was therefore examined in more detail for its localization in MEFs. Nearly half of EGFP- $\alpha$ K expressing cells show Golgi localization defined by GM130 and another half show punctate structures throughout the cytoplasm. Many of those punctate structures overlap with LAMP-positive compartments, indicating that EGFP- $\alpha$ K, like native Irgm1, localizes to lysosomes as well. Interestingly, Golgi and lysosomal localization of EGFP- $\alpha$ K has been observed simultaneously only in a small proportion of transfected cells (14%). This may correlate with the observation that IFN- $\gamma$  induced endogenous Irgm1 shows different levels of lysosomal association, with strong lysosomal signals in some cells while with hardly detectable signals in other cells. The mechanism is unclear. It could be that the lysosomal association is regulated by cell cycling, for instance. The Golgi/lysosomal localization of EGFP- $\alpha$ K has been observed in L929 fibroblasts as well as Raw 264.7 macrophages, indicating that the targeting mechanism is not cell type specific. Some of the punctate signals from EGFP- $\alpha$ K expressing cells show overlap neither with GM130/LAMP1 nor with early/recycling endosomes, suggesting the additional membrane associations of EGFP- $\alpha$ K, whose identity remains to be defined.

The Irgm1  $\alpha$ K helix is not only sufficient for targeting EGFP protein to Golgi/lysosomes, but also required for the localization of full-length protein. A mutant with glutamate insertions to disrupt the amphipathicity of  $\alpha$ K helix in full-length Irgm1 distributes as uncharacteristic dotted structures throughout the cytoplasm, which show no overlap with GM130 or LAMP1.

This observation has at least two implications: first, Golgi and lysosomal localization of full-length Irgm1 depends on the amphipathicity of the  $\alpha$ K helix; secondly, Irgm1 protein has additional membrane binding motif(s) since the glutamate insertion mutant does not distribute as a free cytosolic protein. For instance, the isolated G-domain of Irgm1 localizes to the plasma membrane, indicating that the G-domain of the protein also has a membrane association property (Martens 2004b). However, although Irgm1  $\alpha$ K helix is sufficient to target EGFP protein to Golgi and lysosomes, it is not sufficient to target EGFP to the latex beads-containing phagosomes. Full-length Irgm1 is accumulated on phagosomes depending on the integrity of nucleotide-binding motif. It is therefore plausible that nucleotide-binding dependent conformational change of full-length Irgm1 regulates the exposure of  $\alpha$ K helix to its binding partners on lysosome/phagosome. However, this hypothesis does not exclude the possibility that other region in the Irgm1 protein could contribute to the phagosomal accumulation of this protein.

An alanine scan was performed to investigate the possible mechanism of Golgi/lysosomal localization of EGFP- $\alpha$ K construct. Single mutations for each individual residue in  $\alpha$ K helical region and double/quadruple mutations for hydrophobic residues do not change the Golgi/lysosomal localization of EGFP- $\alpha$ K. When more than two non-hydrophobic residues are substituted to alanines, the mutants distribute in an uncharacteristic reticular structure throughout the cytoplasm, which displays neither overlapping with GM130 nor with LAMP1. These results suggest that both the overall amphipathicity of the  $\alpha$ K helix and the identity of the non-hydrophobic residues contribute together to the membrane and Golgi/lysosome localization of the  $\alpha$ K helix. The contribution of the non-hydrophobic residues needs further analysis as it is unclear whether the effect observed from the double/triple non-hydrophobic-residue to alanine mutations is primarily due to an increase in overall hydrophobicity or to the loss of the specific polar side-chains. In addition, there are two basic residues (K349, R351) and three large hydrophobic residues (L350, L352, M353) preceding the predicted amphipathic helix which were not analyzed in the present study. Altogether there is a high frequency of basic residues in this targeting sequence. Therefore, it is possible that those basic residues can interact with phosphate groups of the lipid bilayers. Recently Macmicking *et al* have suggested that Irgm1 interact with specific phosphoinositides generated on internal

membranes and the glutamate insertion mutants also interfere with this specific binding (Shenoy 2008). This may provide new insight into the targeting mechanism of Irgm1, in which  $\alpha$ K helix definitely plays a important role.

Not only Irgm1, but all IRGM proteins have a membrane-targeting signal which corresponds to the  $\alpha$ K helix in the Irga6 crystal structure (Martens 2006). The  $\alpha$ K helix from Irgm2 targets EGFP to the Golgi apparatus and the  $\alpha$ K helix from Irgm3 targets EGFP to a reticular endomembrane system, which largely overlaps with the localizations of respective full-length proteins. Although  $\alpha$ K from Irgm1 is predicted to be amphipathic, neither of the equivalent  $\alpha$ K from Irgm2 and Irgm3 has a predictable pronounced amphipathic character and that of Irgm2 is not even noticeably hydrophobic. Efforts to purify IRGM proteins for biochemical analysis have not been successful so far. Therefore it could be possible to take advantages of those small targeting peptide to study the subcellular localization of IRGM proteins. Initial trials to purify recombinant EGFP- $\alpha$ K of all three IRGM proteins from *E.coli* failed due to extensive proteins degradation in the bacteria (data not shown). Therefore the  $\alpha$ K peptides from IRGM proteins were synthesized and covalently labelled with biotin so that they could be later loaded onto the tetrameric streptavidin protein, which has four biotin binding sites. In addition, there are at least three advantages to use peptide-streptavidin tetramer system. First, since peptide from Irgm1 and Irgm3 were not soluble in neutral pH buffers, they had to be first dissolved in 10mM NaAc pH4.5 buffer with 10mM TCEP as reducing agent. However streptavidin is a 60kDa tetrameric protein that is extremely soluble in neutral solution. Furthermore the dissociation constant (Kd) of the biotin-streptavidin complex is on the order of  $\sim 10^{-15}$ M, ranking among one of the strongest known non-covalent interactions that is essentially irreversible (Weber 1989). Therefore when peptides were loaded onto streptavidin protein, the solubility of peptides was significantly increased. Secondly, EGFP forms a weak dimer when expressed in the cell. The streptavidin is a natural tetrameric protein and each molecule has the capacity to bind four biotinylated peptides, resulting in enhanced affinity of targeting peptides to their binding partners. Thirdly, streptavidin can be covalently labelled with fluorochromes and used directly in the fluoro-cytochemistry staining. Irgm1  $\alpha$ K peptide has been tested to successfully mimic the localization of endogenous full-length Irgm1 in both Golgi apparatus and lysosomal compartments in MEFs (Figure 3.18) and L929 cells (not

shown). Similar results were obtained using streptavidin- $\alpha$ K peptide from Irgm3, which displayed reticular staining pattern mimicking full-length Irgm3 in L929 fibroblasts (not shown). The streptavidin- $\alpha$ K peptide from Irgm2 stains the overall, unspecific cellular structures by the same experimental method, which does not mimic the localization of the endogenous protein. This indicates that the Irgm2  $\alpha$ K could have different targeting mechanisms.

Further experiments would become feasible using the artificial targeting-peptide-streptavidin complex. For instance, as suggested by a recently publication (Shenoy 2008), Irgm1 could bind to specific phosphoinositides generated on cellular membranes. Therefore, *in vitro* lipid vesicle binding experiments could be performed to test specific lipid binding affinities using the targeting peptides.

### **5.3 Irgm1 is not absolutely necessary for IFN- $\gamma$ -dependent cell-autonomous resistance against *T. gondii*.**

At least 5 members have been observed to accumulate massively onto the PVM of avirulent *T. gondii* in primary astrocytes, primary embryonic fibroblast and 3T3 fibroblast lines (Martens 2006 and unpublished). However, we could never detect Irgm1 on the PVM although this observation was obscured by the fact that the Irgm1 antiserum A19 cross-reacts to some extent with the *T. gondii* itself. In the present study, the absence of Irgm1 from avirulent *T. gondii* vacuoles has been confirmed in MEFs by using non-cross-reacting goat antiserum P20 and monoclonal antibody 1B2. In addition, an independent group also reported that they could not observe Irgm1 on *T. gondii* vacuoles in macrophages (Butcher 2005). It is a striking observation considering that Irgm1 is indispensable for mice to survive the acute phase of *T. gondii* infection and suggests that Irgm1 may function distantly from the parasitophorous vacuole. It is even more striking that the Irgm1-deficient MEFs could restrain intracellular *T. gondii* growth upon IFN- $\gamma$  induction, essentially as efficiently as the wild type cells.

As discussed above, other IRG proteins may relocate to *T. gondii* vacuoles by free diffusion from the cytosolic pool. Irgm1 has no cytosolic fraction and exclusively binds to cellular membranes (Marten 2004b). This may be the reason for the absence of Irgm1 from parasite vacuoles. Additionally we showed that IRGM proteins, including Irgm1, exercise regulatory,

non-redundant roles on other IRG proteins. They could interact directly with GKS subfamily members and keep them in inactive GDP-bound forms in their resting subcellular residences (Hunn 2007). This hypothesis was consolidated by the observation that in *Irgm1*-deficient cells, *Irga6* and *Irgb6* form aggregates in the cytosol (Figure 3.19, and Taylor, manuscript in preparation). This suggests that in the absence of *Irgm1*, GKS subfamily members could undergo spontaneous self-interaction and self-activation, whereas this activation process happens, in physiological situation, only when the *T. gondii* invades the cells and triggers the re-localization of IRG proteins onto the parasitophorous membrane. A reasonable conclusion may be that the GKS members are responsible for the vesiculation and disruption processes of *T. gondii* vacuoles while the GMS members prevent them from premature activation in the resting localization. In *Irgm1*-deficient MEFs, the amount of *Irga6* and *Irgb6* accumulated on the *T. gondii* vacuoles was decreased by about 30%, perhaps because spontaneous aggregations consumed a certain amount of those proteins. The decreased amount of GKS proteins on *T. gondii* vacuoles may have significance *in vivo* for the disruption process of *T. gondii* vacuoles. In the *in vitro* experiments, effectively saturating doses of IFN- $\gamma$  were used. These doses of IFN- $\gamma$  may induce huge amount of IRG proteins which allows the disruption process to proceed despite spontaneous activation and consumption due to *Irgm1* deficiency. However this may not reflect the real situation *in vivo* with limited IFN- $\gamma$  concentrations.

The elimination mechanism for denuded *T. gondii* after disruption of the vacuoles remains unknown. In primary astrocytes, *T. gondii* fusion with lysosomes has not been observed at any time point after infection (Martens 2005). The same result was obtained in present study in primary embryonic fibroblasts. However, Ling *et al* reported the lysosomal fusion with *T. gondii* in macrophages (Ling 2006). Perhaps this means that the cell-autonomous resistance mechanisms for *T. gondii* are cell-type specific. It is interesting to notice that in that study, primed macrophages were used. Therefore, this lysosomal fusion process may need participation of adaptive immunity. The authors suggested in their study that *Irgm3* is necessary for the formation of autophagolysosome around the denuded parasites and for the final degradation of the *T. gondii*. It is interesting to investigate whether *Irgm1* may function similarly in *T. gondii* resistance as, indeed, a pro-autophagy function has been suggested for *Irgm1* in resistance to *Mycobacterium* infection in macrophages (Gutierrez 2004). Such a role

might not necessarily involve the direct accumulation on the *T. gondii* PVM. Nevertheless, there is at the moment no evidence showing that native Irgm1 associates with autophagic structures.

#### **5.4 Loading of Irga6 onto the intracellular *T. gondii* vacuoles in real time**

We previously reported that at least 5 members of IRG family are accumulated massively onto the *T. gondii* parasitophorous vacuolar membrane by immunocytochemistry staining in fluorescence-microscopy and immuno-gold labeling in electro-microscopy (Martens 2005). This experimental method provides fundamental information for the function of IRG proteins, but could only observe the events in a “fixed” moment. In the present study, a live cell imaging system was established and this could allow us to observe the dynamic behaviours of IRG proteins (EGFP-tagged Irga6 in this study) as well as intracellular *T. gondii* in real time.

As exemplified in figure 4.1, the accumulation of Irga6 onto the *T. gondii* vacuoles is rather variable. First of all, there is a variable lag phase between the entry of the *T. gondii* and the beginning of the detectable accumulation of Irga6. This lag phase ranges from less than 6 minutes to 26 minutes in the two examples shown in Figure 4.1, and can extend for more than 12 hours. Indeed, some vacuoles acquire no detectable Irga6 signal as long as the culture conditions allowed. This observation may reflect two processes that are confronting each other on the parasitophorous vacuolar membrane: namely, the effort of host resistance factors to access the PVM and the maturation process of parasite-modified vacuoles tending to become less accessible to the host resistance factors and establish a replication-permissive niche. Indeed, the vacuole maturation process probably already starts during the invasion of *T. gondii* and PVM formation. In this process most of the host cell proteins are excluded from PVM and numerous parasite proteins are inserted into the PVM (Mordue 1999). Therefore the lag phase between the invasion of *T. gondii* and beginning of the loading of IRG proteins could reflect a race of IRG proteins (representing host resistance factors) against the maturation process of parasite vacuoles. In case of the avirulent *T. gondii* strain ME49, most of the vacuoles are overrun by IRG system within 30 minutes after invasion, while in virulence *T. gondii* strain, like RH, the vacuole maturation process seems to dominate against the host resistance factors. Only a few (less than 10%) RH vacuoles are coated with Irgb6

(Khaminets, manuscript in preparation). The remaining RH vacuoles are almost free of IRG proteins and IFN- $\gamma$ -dependent cell-autonomous resistance against RH strain is inefficient. This argument also suggested, once one *T. gondii* vacuole can escape the access of IRG protein accumulation in the initial phase after invasion, it would become progressively less accessible later. This is in turn consistent with the observation that most of ME49 vacuoles are coated within 30 minutes after infection.

Secondly, the progressive accumulation of Irga6, once started, also shows different dynamics. In Figure 4.1a the Irga6 signal on the vacuole rapidly reach the maximum capacity of the camera in 15 minutes whereas for the second vacuole in Figure 4.1b, it took 50 minutes for Irga6 signal to reach the plateau. Currently we assume that the re-localization of IRG proteins from their resting residences onto the *T. gondii* vacuoles is not accomplished by active transportation, but rather by free diffusion from cytosolic fraction. The progressive accumulation of IRG proteins on the PVM is due to an accelerated GTP-dependent activation and homo-/hetero-oligomerization of GKS IRG proteins. According to this hypothesis, we could easily conclude that the pace of the accumulation, as well as the final intensity, of Irga6 on the vacuoles is dependent on the cytosolic concentration of Irga6 protein. This could therefore explain the slower accumulation of Irga6 in Figure 4.1b since a previously invaded *T. gondii* has already been coated with and consumed a significant amount of Irga6 proteins. The absence of IRG proteins from some vacuoles could also be due to inadequate amount of available IRG proteins that results from the protein consumption by the previously invaded and IRG-coated vacuoles. In addition, there is a huge variation in IRG intensities on *T. gondii* vacuoles by immunofluorescence staining in fixed samples (Khaminets, manuscript in preparation). Accordingly, this huge variation could be partially due to the vacuolar maturation process, as mentioned above, and could be also partially due to the asynchrony, as well as different multiplicity of infection, which result in the ever-changing cytosolic IRG protein concentrations. The latter could be exemplified in the time-lapse images showing the evolving Irga6 signal intensities on two vacuoles in a single host cell in Figure 4.1b.

### 5.5 Intracellular *T. gondii* is killed after the disruption of the parasitophorous vacuole

Vesiculation and disruption of *T. gondii* parasitophorous vacuoles during IFN- $\gamma$ -dependent resistance have been observed in primary astrocytes by immunofluorescence staining and immuno-gold labeling in electro-microscopy, as well as in primed effector macrophages by electro-microscopy (Martens 2005; Ling 2006). In the present study, the disruption of *T. gondii* vacuoles has been observed in real time by using EGFP-labelled Irga6 in live cell imaging experiments. The visible disruption itself takes place in a short interval, normally in a space of 3 minutes (Figure 4.2). The Irga6-positive vacuoles are suddenly broken at one point. Frequently we could observe that during the disruption process, the *T. gondii* vacuoles, as well as the parasite itself observed in phase-contrast illumination (Figure 4.3b), were rounded up suggesting that the vacuolar membrane could be under tension before and during the disruption. After disruption, the broken vacuoles seem to slip away and the stripped parasites seem to recover the original bow-shape (Figure 4.3c).

The disruption of *T. gondii* vacuoles is accomplished, at least partially, by IRG proteins. Over-expression of Irga6 or Irgb6 could accelerate the vacuolar disruption process while expression of dominant-negative Irga6-K89A or Irgb6-K69A results in the impaired control of the *T. gondii* replication in IFN- $\gamma$  treated primary astrocytes (Martens 2005). Recently, members of another family of IFN- $\gamma$ -inducible GTPases, the p65 guanylate-binding proteins (GBPs), have been found to accumulate on *T. gondii* vacuoles as well (Degrandi 2007). Preliminary results showed that mouse GBPs contribute to the resistance to *T. gondii*. IRG and GBP protein families, together with the type I IFN-inducible antiviral GTPases, the Mx proteins, share the properties of forming GTP-dependent oligomers and co-operative GTP hydrolysis (Martens 2006). These properties relate them to the dynamin family of GTPases, which have an established function in membrane fission and deformation (Hinshaw 2000; Praefcke 2004). Therefore it is plausible that IRG and GBP proteins could accumulate on and vesiculate the parasitophorous vacuolar membrane resulting in the disruption of the vacuoles. It remains to be investigated whether IRG and GBP proteins act cooperatively. In addition, Irga6 has been shown to interact directly with microtubule motor binding protein, HOOK3 (Kaiser 2004). Whether this specific interaction could participate in the vacuolar disruption process, and how if it does, are also not known. The stripped *T. gondii* in the cytosol

deteriorate after the disruption of vacuoles and become permeable to free cytosolic proteins like EGFP or mDsRed, giving a direct indication that the parasite is now dead. Consistently, the morphology of the *T. gondii* in phase-contrast illumination changes from high density to a phase transparent form after the disruption of the vacuole.

The permeabilization of *T. gondii* indicated by EGFP/mDsRed entry provides a new experimental method to define a clear time point of *T. gondii* death. This method has been successfully applied to immunocytochemistry analysis in the PFA-fixed samples as well. By using EGFP/mDsRed entry as a marker for *T. gondii* killing, we have shown that dominant-negative Irgb6 (K69A) expressing cells clearly have impaired *T. gondii* killing efficiency, therefore directly proving that IRG proteins contribute to the killing of *T. gondii* (Khaminets, unpublished).

### **5.6 IFN- $\gamma$ -treated host cell undergoes necrotic-like death, which could serve as an IFN- $\gamma$ -mediated cell-autonomous resistance mechanism against *T. gondii***

It is well-documented that intracellular *T. gondii* can extensively modify host cell signalling pathways, resulting an anti-apoptotic state of host cell (Carmen 2007). Accordingly, *T. gondii* infected cells are resistant to numerous apoptotic stimuli, such as UV-irradiation and TNF $\alpha$  (Carmen 2006). In the present study, we observed that IFN- $\gamma$ -treated murine fibroblasts infected with *T. gondii* died after the *T. gondii* parasitophorous vacuole had been disrupted. Although the stripped *T. gondii* in the cytosol is dead as indicated by the permeabilization of parasite plasma membrane, subsequent host cell death seems to be inevitable. Therefore, the host cell death could be an active process which serves as an IFN- $\gamma$ -dependent cell-autonomous resistance mechanism against *T. gondii*, including the remaining intracellular parasites that have not yet been killed by vacuolar stripping.

The characteristics of the IFN- $\gamma$ -dependent host cell death caused by avirulent *T. gondii* strain infection are consistent with necrosis rather than apoptosis. Morphologically, the cytoplasm and nucleus of the dying host cell suddenly collapses. Cytosolic proteins (for example transfected EGFP) are spilled out to the medium and propidium iodide quickly stains the dead cell nucleus, indicating a rapid loss of cell membrane integrity. After the cell membrane permeabilization, Annexin-V starts to accumulate on residual cellular membrane material

indicating access to internal phosphatidylserine. This is contrary to apoptotic cell death, where phosphatidylserine is externalized before the loss of the plasma membrane integrity and nuclei of apoptotic cells remain inaccessible to propidium iodide (Goldstein 2000). By immunofluorescence staining, cytochrome-c was not found to be released from the mitochondria during the vacuolar disruption and host cell death process in IFN- $\gamma$  treated and ME49 infected MEFs, although the possibility that cytochrome-c is released right before cell death is not excluded. In apoptosis, cytochrome-c is released from mitochondria about 2 hours before the externalization of phosphatidylserine and several more hours before the loss of plasma-membrane integrity (Goldstein 2000). Western blot analysis shows that the caspase-3 and one of its substrates PARP are not cleaved during *T. gondii* induced IFN- $\gamma$ -dependent host cell death suggesting that the executor caspases are not participating in this process. Instead, high mobility group box 1 (HMGB1) is released from cells treated with IFN- $\gamma$  and infected with *T. gondii*, but not from apoptotic cells. HMGB1, normally functioning within healthy cells as an intranuclear architectural protein, has been described as an important proinflammatory mediator that is released from cells undergoing necrosis. Once released, HMGB1 acts as a potent danger indicator, inducing several inflammatory cytokines to elicit a severe inflammatory response (Scaffidi 2002; Chen 2004). Taken together, these results suggest that IFN- $\gamma$ -induced factors cause host cell necrosis upon infection with avirulent *T. gondii*, which serves as a cell-autonomous resistance mechanism against *T. gondii*. In addition, the necrotic host cell death could further promote local immune responses *in vivo* contributing to the control of the *T. gondii* infection.

The mechanism(s) of killing the intracellular *T. gondii* as well as the host cells are unknown. The data strongly suggest that there is a functional linkage between disruption of the *T. gondii* vacuole and host cell death. In live cell imaging experiments, disruption of the vacuole, death of *T. gondii*, and then death of the host cell occur always in a definite sequence, though not with a definite timing (Table 4.1). Previously we showed that over-expression of Irga6 could accelerate the vacuolar disruption (Martens 2005). Therefore the variable timing between the infection and the vacuolar disruption in the live cell experiments could be due to the heterogeneous expression level of transfected Irga6-EGFP. However, the time intervals between the disruption of the vacuoles and the permeabilization of the stripped parasites were

rather constant, ranging about 15 to 45 minutes. One simple possibility is that once the *T. gondii* vacuoles have been disrupted, or even earlier when the disruption process starts happening, the contents of toxoplasma are released from parasitophorous membrane, intermediate space between toxoplasma and PVM, as well as plasma membrane of toxoplasma itself, into the host cell cytosol. Those contents could act as foreign danger molecules (proteins and/or lipids) which elicit toxic effects from the host cell. These toxic effects could in turn kill the denuded *T. gondii* as well as the host cell. One evidence for the release of *T. gondii* contents accompanied by the vacuolar disruption process has been reported (Martens 2005). In IFN- $\gamma$  induced primary astrocytes, the disruption of intracellular *T. gondii* vacuoles leads to cytoplasmic distribution of toxoplasma protein GRA7, which normally localizes on PVM and mediates the nutrient up-take from host cells to the toxoplasma (Coppens 2006). Therefore other Toxoplasma proteins/lipids could be released to the host cell cytosol in a similar manner.

The virulent *T. gondii* strain, RH-YFP, does not elicit significant host cell death in the presence of IFN- $\gamma$ . We have shown that the accumulation of IRG proteins onto the virulent *T. gondii* vacuoles in IFN- $\gamma$ -induced cells is largely blocked and the vacuoles are not disrupted (Khaminets, unpublished). This is consistent with the hypothesis that the disruption of the toxoplasma vacuoles causes the host cell necrosis, although it is not excluded that other virulence factors could contribute to the resistance of virulent toxoplasma preventing the IFN- $\gamma$  mediated host cell death.

L929 fibroblasts are unable to control *T. gondii* avirulent ME49 strain infection even induced with IFN- $\gamma$  (Konen-Waisman 2007). Consistent with this, IFN- $\gamma$ -treated L929 cells fail to undergo host cell death when infected with ME49 *T. gondii* (Figure 4.9c). This in turn proves that the host cell necrosis is indeed a cell-autonomous resistance mechanism against *T. gondii*. However why L929 cells can not execute IFN- $\gamma$  mediated autonomous resistance against *T. gondii* remains a mystery. Preliminary results indicate that in IFN- $\gamma$ -treated L929 cells, the disruption of *T. gondii* ME49 vacuoles is largely ineffective indicated by the morphology of IRG-positive PVM, and the parasites are not permeabilized demonstrated by EGFP-entry experiments (Konen-Waisman and Khaminets, unpublished). This would be in favor of the hypothesis that the disruption of the parasitophorous vacuoles is the prerequisite for the

killing of *T. gondii* and probably for the host cells as well. Although 6 members of the IRG family have been demonstrated to be expressed normally upon IFN- $\gamma$  induction in L929 cells, 21 genes (25 coding units) indeed exist in the C57BL/6 mouse genome (Bekpen 2005). Further investigation would be then justified to analyze the functions of the whole IRG family in L929 cells, and could possibly reveal an elusive component of IRG system as far, which would play an important role in cell-autonomous resistance.

If we assume that the disruption of the *T. gondii* vacuoles is the trigger for the subsequent permeabilization of stripped parasites and probably also the host cells, what would be the executors of those events? The participation of executor caspases has been excluded (Figure 4.13). Based on the morphological characteristics and the timing of the death of the host cells, one could daringly suppose that reactive oxygen species could play a role in this process. Cells under oxidative stress exhibit necrotic-like death with characteristics like rupture of the plasma membrane, spilling out the cell contents, intracellular vesicles swelling (frequently could also be observed in the *T. gondii* infected IFN- $\gamma$ -induced MEFs) (Fiers 1999; Kroemer 2005). Extensive oxidative stress (respiratory burst) is a landmark mechanism for the activated neutrophils and macrophages to kill the phagocytosed pathogens and finally themselves (Segal 2005), a similar process observed in the *T. gondii* infected IFN- $\gamma$ -induced MEFs. Another candidate for the killing mechanism would be the lysosomal proteases. Production of reactive oxygen species could cause lysosomal membrane permeabilization, therefore lysosomal proteases could be released and exaggerate the toxic effect (Fiers 1999; Guicciardi, 2004). Although Cathepsin B is dispensable for *T. gondii* elicited host cell necrosis (Figure 4.14), other proteases from lysosomes could compensate for the single protease defect. Indeed, complete breakdown of the lysosomes with release of high concentrations of lysosomal enzymes into the cytosol results in necrosis, whereas partial, selective permeabilization triggers cell apoptosis (Bursch 2001, Turk 2002, Guicciardi 2004). Furthermore, it has been extensively studied that cytosolic exposure of bacterial components could activate the inflammasomes which would subsequently elicit host cell necrotic cell death mediated by lysosomal proteases like cathepsins or calpains (Mariathasan 2007; Sutterwala 2007). No studies have been reported that *T. gondii* could activate the inflammasome in a similar manner. However, in the condition we observed in the present

study, it would not be surprising that some components of stripped *T. gondii* in the cytosol could activate the inflammasome through cytosolic NOD-like receptors. Although TLR/MyD88 has been identified as a major class of sensors for *T. gondii* infection, a role of non-TLR, non-MyD88-based recognition and response has been indicated by studies in MyD88-deficient mice (Scanga 2002; Kim 2006b). Finally, it is interesting to notice that IFN- $\gamma$  could potentially induce the expression of lysosomal protease like Cathepsin D, as well as enzymes for the production of reactive oxygen species (phox91 and phox67), which have potential microbicidal activities (Schroder 2004). Conclusively, the IFN- $\gamma$  dependent host cell necrosis caused by *T. gondii* avirulent strain infection could be a complex toxic response, probably triggered by IRG proteins and participated by several executor molecules. Whether the role of the IRG proteins is simply to disrupt the vacuolar membrane, or whether they play a further role in transducing the fatal signal will be an interesting issue. Further experiments have to be designed and those speculative hypotheses will be tested.

### **5.7 Autophagy in cell-autonomous resistance against *T. gondii* infection**

Autophagy describes the cellular degradative pathway that involves the delivery of cytoplasmic cargos to the lysosome (Levine 2008). It is an ancient, highly conserved and tightly-regulated process that is essential for cell growth, development, differentiation and homeostasis. Compared to the alternative degradation pathway via proteasomes that target the soluble short-lived proteins, autophagosomes degrade cell organelles and aggregates of long-lived proteins in the lysosomes. At least three forms of autophagy have been described: the chaperone-mediated autophagy, microautophagy and macroautophagy that differ in their physiological functions and the mode of cargo delivery to the lysosomes. Macroautophagy involves the *de novo* formation of isolated double-membrane around the targeted cytoplasmic materials and has been suggested recently to play a role in cell-autonomous resistance against intracellular pathogens such as viruses, bacteria and protozoa. The cup-shaped autophagosomal membrane finally closes and fuses with lysosomes leading to degradation of their contents, therefore could target intracellular pathogens as well for elimination in certain circumstances (Deretic 2006; Schmid 2007). In addition, it has been known for a long time that enhanced autophagy could be observed in dying cells under certain conditions, a

phenomenon termed “autophagic cell death”. This type of cell death has been described historically by morphological criteria, but whether the role of the autophagy in dying cells is cyto-toxic or cyto-protective (but obviously failed) is unclear and still under extensive investigations (Levine 2005; Maiuri 2007).

Several studies have suggested that autophagy could be a mechanism to eliminate intracellular *T. gondii* infection. Ling and his colleagues suggested that *T. gondii* vacuolar membranes were stripped and denuded parasites were eliminated through autophago-lysosome pathway in primed mouse macrophages (Ling 2006). Alternatively, but probably dispensable, CD40 ligation could trigger a similar autophagy-dependent lysosomal degradation mechanism against *T. gondii* intracellular infection in mouse and human macrophages (Andrade 2006; Zhao 2007). We previously also reported that EGFP-LC3, a marker for autophagosomal membrane, was accumulated in the vicinity of stripped *T. gondii* in mouse primary astrocytes, although lysosome fusion was not observed for either *T. gondii* vacuoles or denuded parasites themselves (Martens 2005). In the present study, we observed that host cell necrosis caused by *T. gondii* avirulent strain infection functions as an IFN- $\gamma$ -dependent cell-autonomous resistance mechanism in mouse fibroblasts. Considering the potential relevance of the autophagy in the resistance against *T. gondii* as well as in the cell death, we were prompted to investigate the possible role of autophagy in the host cell necrosis process. Transfected EGFP-LC3 could associate with *T. gondii* ME49 vacuoles with or without IFN- $\gamma$  treatment indicating that IFN- $\gamma$  induced factors, including IRG proteins, are not necessary for the initiation of autophagy on the *T. gondii* vacuoles. Autophagy occurs at low basal level in virtually all cells to perform homeostatic functions. Consistently, low level of EGFP-LC3 aggregation could be observed in uninfected cells. However autophagy is rapidly up-regulated when cells are under stress, such as nutrient shortage, oxidative stress, or infection (Levine 2008). Accordingly, upon *T. gondii* infection, *T. gondii* vacuoles could be a default target for autophagy as an alien stimulus for the infected cells. However, *T. gondii* has developed a sophisticated strategy to avoid lysosomal fusion inside of the infected cells (Sinai 1997). In mouse fibroblasts and astrocytes, this non-fusogenic property of *T. gondii* vacuoles is preserved even when the host cells are treated with IFN- $\gamma$ . Therefore, direct lysosomal degradation does not seem to be an IFN- $\gamma$  mediated elimination mechanism against *T. gondii*

in mouse astrocytes and fibroblasts. In live cell imaging experiment, no significant amount of enhanced EGFP-LC3 aggregation could be observed in the host cell necrosis process. By immunofluorescence analysis, enhanced autophagy could be occasionally observed in some IFN- $\gamma$ -treat infected cells at latter time points after infection (Figure 4.5). But considering that necrosis processes are uniformly taking place, it is therefore in favour of the hypothesis that the host cells are undergo necrosis “with autophagy” rather than “by autophagy”. Conclusively, autophagy does not seem to be a major component in either initiation or execution phase in IFN- $\gamma$ -dependent resistance in mouse fibroblasts. It rather seems to function as a conserved cyto-protective mechanism which tries to rescue the infected cell, but could not succeed.

It is therefore interesting to notice the discrepancy that the autophago-lysosomal pathway to eliminate the *T. gondii* vacuoles has been documented in the primed macrophages, which is clearly dependent on the IRG (Irgm3) proteins (Ling 2006). However, it seems that the IFN- $\gamma$  alone, therefore the IRG system alone, is not sufficient for this process since the unprimed macrophages pre-treated with IFN- $\gamma$  failed to eliminate the *T. gondii* in a similar lysosomal pathway (Ling 2006). Thus it suggests that the *in vivo* priming could provide additional undefined accessory signals for the macrophages to efficiently eliminate the *T. gondii* through the autophago-lysosomal pathway, and this undefined signal from *in vivo* priming process could well be to stimulate the effective autophagosome formation. As we discussed above, the disruption of the *T. gondii* vacuole and the subsequent release of the *T. gondii* contents probably trigger the toxic effect for the stripped toxoplasma as well as the host cell. Therefore the effective autophagosome formation and enclosure around the *T. gondii* vacuoles could prevent the toxic effect-inducing agents to be spilled out, which obviously does not happen in the primary IFN- $\gamma$ -induced fibroblasts and astrocytes. In addition, the bone marrow macrophages also undergo necrosis when treated with IFN- $\gamma$  and infected with *T. gondii* ME49 strain (Khaminets, unpublished), indicating that this mechanism is not cell-type specific, but is rather conserved in both hemopoietic and non-hemopoietic cells. Taken together, we could propose that, during the acute phase of *T. gondii* infection, the host cell necrosis could be an important innate immune response to kill most of the *T. gondii* and to further promote the local immune responses by releasing proinflammatory factors. The

autophago-lysosomal pathway could function in the repeated or latter stage of the *T. gondii* infection, which could eliminate the *T. gondii* without excessive tissue injury.

### **5.8 Virulent vs avirulent *T. gondii* strain infection**

It has long been realized that different strains of *T. gondii* produce radically different pathologies in mice (Sibley 1992; Saeij 2005). The virulent type I strain are universally lethal in mice, as a single viable parasite could cause the infected mice to die. In contrast, the avirulent strains, the type II and III strains are well tolerated in mice, normally causing a chronic latent infection. This difference could be due to the cellular events we described. The IFN- $\gamma$ -treated host cells can autonomously control the avirulent strain growth, but cannot efficiently control the infection of the virulent strains.

As IRG proteins are the major IFN- $\gamma$ -inducible effectors in cell-autonomous resistance against *T. gondii* infection, it is highly suggestive that the IRG proteins are the targets of the *T. gondii* virulence factors. We have already shown that the accumulation of IRG proteins and subsequent vacuolar disruptions are largely blocked by virulent *T. gondii* strains such as RH and BK, probably by targeting the IRG protein Irgb6, which pioneers the access to the PVM (Khaminets, manuscript in preparation). Interestingly, this blockade of IRG proteins is specific to the individual parasitophorous vacuole membrane since in cells co-infected with the virulent and avirulent *T. gondii*, the accumulation of IRG proteins onto the avirulent vacuoles is not blocked by the co-existence of virulent vacuoles in the same host cell. In the present study, we further demonstrate that host cell necrosis is an IFN- $\gamma$ -dependent cell-autonomous resistance mechanism against avirulent *T. gondii* strain, but the IFN- $\gamma$ -induced host cells could not efficiently control the virulent *T. gondii* strain RH-YFP because of its ability to avoid eliciting the necrotic reaction. This could in turn due to the blockade of IRG accumulation onto the virulent toxoplasma vacuoles, thus avoiding the disruption of the vacuoles that is probably the trigger for killing of the stripped parasites and the host cells. Finally, we showed that the avirulent strain elicited host cell death is dominant over the resistance effect against IFN- $\gamma$  from virulent strain by co-infection with both virulent and avirulent *T. gondii* strains. This result further demonstrates that the blockade of IRG system

by the virulent toxoplasma is mainly focused on the PVM, but it could not block the host cell death once the death process is initiated.

Recently, two polymorphic kinases ROP16 and ROP18 have been identified as the virulence factors between different *T. gondii* strains. ROP16 is secreted from *T. gondii* and translocates to the host cell nucleus, probably functioning by affecting the host STAT signalling pathways (Saeij 2006; Saeij 2007). In contrast, ROP18 is also secreted by *T. gondii* from rhoptries, but associated exclusively with the parasitophorous vacuolar membrane (El Hajj 2007). Therefore, ROP18 is a strong candidate to counteract the IRG system (and probably also GBPs (Degrandi 2007)) on PVM. ROP18 has been experimentally shown to be able to specifically phosphorylate one protein in *T. gondii* extract, but no protein in a HeLa cell extract. It is plausible that ROP18 could phosphorylate one or more of IRG and/or GBP proteins that is recruited to the PVM. By doing so, ROP18 could inactivate IRG/GBP proteins and perhaps interfere with their oligomerization, thereby preventing the vacuolar disruption. It is known that the ROP18 allele in avirulent strain yields a tiny fraction (~0.1%) of mRNA compared to the amount that is produced by the alleles in virulent strain (Saeij 2006; Taylor 2006). This could correlate with the strikingly different efficiency in blocking the accumulation of the IRG proteins onto the corresponding virulent and avirulent strain vacuoles. In addition, the over-expression of ROP18 could enhance the intracellular parasite growth. But this effect is again vacuole-specific, meaning only vacuoles over-expressing ROP18 could have an enhanced growth in the same cell doubly infected with *T. gondii* expressing normal amount of ROP18 (El Hajj 2007). This further suggests that ROP18 could be a virulence factor directly challenging the host resistance factors like IRGs and GBPs on the *T. gondii* PVM.

### **5.9 Manipulation of the host cell death: a common theme in the host-pathogen interaction**

Programmed cell death (PCD) is essential for development, morphogenesis and tissue remodelling, as well as for the immune responses in multicellular organisms. The infection-induced suicide of host cells following invasion by intracellular pathogens has long been realized to be an ancient defense mechanism observed in multicellular organisms of both the

animal and plant kingdoms (Gao 2000; Iriti 2007). It is therefore not surprising that persistent pathogens, including viruses, bacteria and protozoa, have evolved many different mechanisms to modify the host cell death pathways. Generally obligate intracellular pathogens suppress host cell apoptotic death. It is more complex for non-obligate pathogens as they could both promote and inhibit host cell death depending on the different stages of the infection as well as the different host cell types. In addition, the intracellular pathogens could stimulate the apoptosis of the uninfected bystander cells, probably to avoid the attack from the immune cells (Gao 2000; James 2004; Finlay 2006; Carmen 2007).

We demonstrate in the present study that the IFN- $\gamma$ -inducible factors, essentially the IRG proteins, could overcome the anti-apoptotic state of the *T. gondii*-infected cells by eliciting host cell necrosis. This result could provide new insight into the investigation of the host-pathogen interactions. Although large amount of publications have revealed how intracellular pathogens could modified the host cell death signalling pathways, little is known about how IFN- $\gamma$  could influence this pathogen-caused cell death modification. This has important implications because the resistance against the intracellular bacterial and protozoal pathogens is largely dependent on IFN- $\gamma$ . IRG family members have been shown to be involved in resistance against intracellular bacterial pathogens: *Mycobacterium*, *Salmonella*, *Listeria*, *Chlamydia*, as well as protozoan: *Toxoplasma*, *Trypanosoma* and *Leishmania*. All of them have been shown to be able to manipulate the host cell death signaling pathways (Gao 2000, Carmen 2007). Therefore, studies on the influence of IFN- $\gamma$ , and especially of the IRG proteins, on host cell death pathways manipulated by such pathogens could probably reveal new resistance mechanisms of the host innate immunity system.

## 6. References

- Aliberti, J. 2005. Host persistence: exploitation of anti-inflammatory pathways by *Toxoplasma gondii*. *Nat Rev Immunol.* **5**(2): 162-70.
- Aliberti, J., S. Hieny, C. Reis e Sousa, C. N. Serhan and A. Sher. 2002a. Lipoxin-mediated inhibition of IL-12 production by DCs: a mechanism for regulation of microbial immunity. *Nat Immunol.* **3**(1): 76-82.
- Aliberti, J., C. Reis e Sousa, M. Schito, S. Hieny, T. Wells, G. B. Huffnagle and A. Sher. 2000. CCR5 provides a signal for microbial induced production of IL-12 by CD8 alpha+ dendritic cells. *Nat Immunol.* **1**(1): 83-7.
- Aliberti, J., C. Serhan and A. Sher. 2002b. Parasite-induced lipoxin A4 is an endogenous regulator of IL-12 production and immunopathology in *Toxoplasma gondii* infection. *J Exp Med.* **196**(9): 1253-62.
- Aliberti, J., J. G. Valenzuela, V. B. Carruthers, S. Hieny, J. Andersen, H. Charest, C. Reis e Sousa, A. Fairlamb, J. M. Ribeiro and A. Sher. 2003. Molecular mimicry of a CCR5 binding-domain in the microbial activation of dendritic cells. *Nat Immunol.* **4**(5): 485-90.
- Anderson, S. L., J. M. Carton, J. Lou, L. Xing and B. Y. Rubin. 1999. Interferon-induced guanylate binding protein-1 (GBP-1) mediates an antiviral effect against vesicular stomatitis virus and encephalomyocarditis virus. *Virology.* **256**(1): 8-14.
- Andrade, R. M., M. Wessendarp, M. J. Gubbels, B. Striepen and C. S. Subauste. 2006. CD40 induces macrophage anti-*Toxoplasma gondii* activity by triggering autophagy-dependent fusion of pathogen-containing vacuoles and lysosomes. *J Clin Invest.* **116**(9): 2366-77.
- Bafica, A., C. G. Feng, H. C. Santiago, J. Aliberti, A. Cheever, K. E. Thomas, G. A. Taylor, S. N. Vogel and A. Sher. 2007. The IFN-inducible GTPase LRG47 (*Irgm1*) negatively regulates TLR4-triggered proinflammatory cytokine production and prevents endotoxemia. *J Immunol.* **179**(8): 5514-22.
- Bancroft, G. J. 1993. The role of natural killer cells in innate resistance to infection. *Curr Opin Immunol.* **5**(4): 503-10.
- Bazer, F. W., T. E. Spencer and T. L. Ott. 1997. Interferon tau: a novel pregnancy recognition signal. *Am J Reprod Immunol.* **37**(6): 412-20.
- Bekpen, C., J. P. Hunn, C. Rohde, I. Parvanova, L. Guethlein, D. M. Dunn, E. Glowalla, M. Leptin and J. C. Howard. 2005. The interferon-inducible p47 (IRG) GTPases in vertebrates:

- loss of the cell autonomous resistance mechanism in the human lineage. *Genome Biol.* **6**(11): R92.
- Bernstein-Hanley, I., J. Coers, Z. R. Balsara, G. A. Taylor, M. N. Starnbach and W. F. Dietrich. 2006. The p47 GTPases Igtg and Irgb10 map to the Chlamydia trachomatis susceptibility locus Ctrq-3 and mediate cellular resistance in mice. *Proc Natl Acad Sci U S A.* **103**(38): 14092-7.
- Blader, I. J., I. D. Manger and J. C. Boothroyd. 2001. Microarray analysis reveals previously unknown changes in Toxoplasma gondii-infected human cells. *J Biol Chem.* **276**(26): 24223-31.
- Boehm, U., L. Guethlein, T. Klamp, K. Ozbek, A. Schaub, A. Futterer, K. Pfeffer and J. C. Howard. 1998. Two families of GTPases dominate the complex cellular response to IFN-gamma. *J Immunol.* **161**(12): 6715-23.
- Boehm, U., T. Klamp, M. Groot and J. C. Howard. 1997. Cellular responses to interferon-gamma. *Annu Rev Immunol.* **15**: 749-95.
- Borden, E. C., G. C. Sen, G. Uze, R. H. Silverman, R. M. Ransohoff, G. R. Foster and G. R. Stark. 2007. Interferons at age 50: past, current and future impact on biomedicine. *Nat Rev Drug Discov.* **6**(12): 975-90.
- Bourne, H. R., D. A. Sanders and F. McCormick. 1990. The GTPase superfamily: a conserved switch for diverse cell functions. *Nature.* **348**(6297): 125-32.
- Bourne, H. R., D. A. Sanders and F. McCormick. 1991. The GTPase superfamily: conserved structure and molecular mechanism. *Nature.* **349**(6305): 117-27.
- Broker, L. E., F. A. Kruyt and G. Giaccone. 2005. Cell death independent of caspases: a review. *Clin Cancer Res.* **11**(9): 3155-62.
- Bursch, W. 2001. The autophagosomal-lysosomal compartment in programmed cell death. *Cell Death Differ.* **8**(6): 569-81.
- Butcher, B. A. and E. Y. Denkers. 2002. Mechanism of entry determines the ability of Toxoplasma gondii to inhibit macrophage proinflammatory cytokine production. *Infect Immun.* **70**(9): 5216-24.
- Butcher, B. A., R. I. Greene, S. C. Henry, K. L. Annecharico, J. B. Weinberg, E. Y. Denkers, A. Sher and G. A. Taylor. 2005. p47 GTPases regulate Toxoplasma gondii survival in activated macrophages. *Infect Immun.* **73**(6): 3278-86.
- Butcher, B. A., L. Kim, P. F. Johnson and E. Y. Denkers. 2001. Toxoplasma gondii tachyzoites inhibit proinflammatory cytokine induction in infected macrophages by

- preventing nuclear translocation of the transcription factor NF-kappa B. *J Immunol.* **167**(4): 2193-201.
- Carlow, D. A., S. J. Teh and H. S. Teh. 1998. Specific antiviral activity demonstrated by TGTP, a member of a new family of interferon-induced GTPases. *J Immunol.* **161**(5): 2348-55.
- Carmen, J. C., L. Hardi and A. P. Sinai. 2006. Toxoplasma gondii inhibits ultraviolet light-induced apoptosis through multiple interactions with the mitochondrion-dependent programmed cell death pathway. *Cell Microbiol.* **8**(2): 301-15.
- Carmen, J. C. and A. P. Sinai. 2007. Suicide prevention: disruption of apoptotic pathways by protozoan parasites. *Mol Microbiol.* **64**(4): 904-16.
- Carter, C. C., V. Y. Gorbacheva and D. J. Vestal. 2005. Inhibition of VSV and EMCV replication by the interferon-induced GTPase, mGBP-2: differential requirement for wild-type GTP binding domain. *Arch Virol.* **150**(6): 1213-20.
- Chen, G., M. F. Ward, A. E. Sama and H. Wang. 2004. Extracellular HMGB1 as a proinflammatory cytokine. *J Interferon Cytokine Res.* **24**(6): 329-33.
- Cheng, Y. S., C. E. Patterson and P. Staeheli. 1991. Interferon-induced guanylate-binding proteins lack an N(T)KXD consensus motif and bind GMP in addition to GDP and GTP. *Mol Cell Biol.* **11**(9): 4717-25.
- Coers, J. Manuscripts in preparation.
- Collazo, C. M., G. S. Yap, G. D. Sempowski, K. C. Lusby, L. Tessarollo, G. F. Woude, A. Sher and G. A. Taylor. 2001. Inactivation of LRG-47 and IRG-47 reveals a family of interferon gamma-inducible genes with essential, pathogen-specific roles in resistance to infection. *J Exp Med.* **194**(2): 181-8.
- Coppens, I., J. D. Dunn, J. D. Romano, M. Pypaert, H. Zhang, J. C. Boothroyd and K. A. Joiner. 2006. Toxoplasma gondii sequesters lysosomes from mammalian hosts in the vacuolar space. *Cell.* **125**(2): 261-74.
- DeFranco, A. L., R. M. Locksley and M. Robertson 2007. Immunity : the immune response in infectious and inflammatory disease. London  
Sunderland, MA, New Science Press ;  
Sinauer Associates.
- Deghmane, A. E., H. Soualhine, H. Bach, K. Sendide, S. Itoh, A. Tam, S. Noubir, A. Talal, R. Lo, S. Toyoshima, Y. Av-Gay and Z. Hmama. 2007. Lipoamide dehydrogenase mediates retention of coronin-1 on BCG vacuoles, leading to arrest in phagosome maturation. *J Cell Sci.* **120**(Pt 16): 2796-806.

- Degrandi, D., C. Konermann, C. Beuter-Gunia, A. Kresse, J. Wurthner, S. Kurig, S. Beer and K. Pfeffer. 2007. Extensive Characterization of IFN-Induced GTPases mGBP1 to mGBP10 Involved in Host Defense. *J Immunol.* **179**(11): 7729-40.
- Denkers, E. Y. 2003. From cells to signaling cascades: manipulation of innate immunity by *Toxoplasma gondii*. *FEMS Immunol Med Microbiol.* **39**(3): 193-203.
- Deretic, V. 2006. Autophagy as an immune defense mechanism. *Curr Opin Immunol.* **18**(4): 375-82.
- Durbin, J. E., R. Hackenmiller, M. C. Simon and D. E. Levy. 1996. Targeted disruption of the mouse Stat1 gene results in compromised innate immunity to viral disease. *Cell.* **84**(3): 443-50.
- El Hajj, H., M. Lebrun, S. T. Arold, H. Vial, G. Labesse and J. F. Dubremetz. 2007. ROP18 is a rhoptry kinase controlling the intracellular proliferation of *Toxoplasma gondii*. *PLoS Pathog.* **3**(2): e14.
- Feng, C. G., C. M. Collazo-Custodio, M. Eckhaus, S. Hieny, Y. Belkaid, K. Elkins, D. Jankovic, G. A. Taylor and A. Sher. 2004. Mice deficient in LRG-47 display increased susceptibility to mycobacterial infection associated with the induction of lymphopenia. *J Immunol.* **172**(2): 1163-8.
- Fiers, W., R. Beyaert, W. Declercq and P. Vandenabeele. 1999. More than one way to die: apoptosis, necrosis and reactive oxygen damage. *Oncogene.* **18**(54): 7719-30.
- Finlay, B. B. and G. McFadden. 2006. Anti-immunology: evasion of the host immune system by bacterial and viral pathogens. *Cell.* **124**(4): 767-82.
- Gao, L. Y. and Y. A. Kwak. 2000. The modulation of host cell apoptosis by intracellular bacterial pathogens. *Trends Microbiol.* **8**(7): 306-13.
- Gazzinelli, R. T., A. Sher, A. Cheever, S. Gerstberger, M. A. Martin and P. Dickie. 1996. Infection of human immunodeficiency virus 1 transgenic mice with *Toxoplasma gondii* stimulates proviral transcription in macrophages in vivo. *J Exp Med.* **183**(4): 1645-55.
- Ghosh, A., R. Uthaiyah, J. Howard, C. Herrmann and E. Wolf. 2004. Crystal structure of IIGP1: a paradigm for interferon-inducible p47 resistance GTPases. *Mol Cell.* **15**(5): 727-39.
- Goebel, S., U. Gross and C. G. Luder. 2001. Inhibition of host cell apoptosis by *Toxoplasma gondii* is accompanied by reduced activation of the caspase cascade and alterations of poly(ADP-ribose) polymerase expression. *J Cell Sci.* **114**(Pt 19): 3495-505.

- Goetschy, J. F., H. Zeller, J. Content and M. A. Horisberger. 1989. Regulation of the interferon-inducible IFI-78K gene, the human equivalent of the murine Mx gene, by interferons, double-stranded RNA, certain cytokines, and viruses. *J Virol.* **63**(6): 2616-22.
- Goldstein, J. C., N. J. Waterhouse, P. Juin, G. I. Evan and D. R. Green. 2000. The coordinate release of cytochrome c during apoptosis is rapid, complete and kinetically invariant. *Nat Cell Biol.* **2**(3): 156-62.
- Golstein, P. and G. Kroemer. 2007. Cell death by necrosis: towards a molecular definition. *Trends Biochem Sci.* **32**(1): 37-43.
- Gorbacheva, V. Y., D. Lindner, G. C. Sen and D. J. Vestal. 2002. The interferon (IFN)-induced GTPase, mGBP-2. Role in IFN-gamma-induced murine fibroblast proliferation. *J Biol Chem.* **277**(8): 6080-7.
- Guenzi, E., K. Topolt, E. Cornali, C. Lubeseder-Martellato, A. Jorg, K. Matzen, C. Zietz, E. Kremmer, F. Nappi, M. Schwemmler, C. Hohenadl, G. Barillari, E. Tschachler, P. Monini, B. Ensoli and M. Sturzl. 2001. The helical domain of GBP-1 mediates the inhibition of endothelial cell proliferation by inflammatory cytokines. *Embo J.* **20**(20): 5568-77.
- Guenzi, E., K. Topolt, C. Lubeseder-Martellato, A. Jorg, E. Naschberger, R. Benelli, A. Albin and M. Sturzl. 2003. The guanylate binding protein-1 GTPase controls the invasive and angiogenic capability of endothelial cells through inhibition of MMP-1 expression. *Embo J.* **22**(15): 3772-82.
- Guicciardi, M. E., M. Leist and G. J. Gores. 2004. Lysosomes in cell death. *Oncogene.* **23**(16): 2881-90.
- Gutierrez, M. G., S. S. Master, S. B. Singh, G. A. Taylor, M. I. Colombo and V. Deretic. 2004. Autophagy is a defense mechanism inhibiting BCG and Mycobacterium tuberculosis survival in infected macrophages. *Cell.* **119**(6): 753-66.
- Haller, O., P. Staeheli and G. Kochs. 2007. Interferon-induced Mx proteins in antiviral host defense. *Biochimie.* **89**(6-7): 812-8.
- Halonen, S. K., G. A. Taylor and L. M. Weiss. 2001. Gamma interferon-induced inhibition of *Toxoplasma gondii* in astrocytes is mediated by IGTP. *Infect Immun.* **69**(9): 5573-6.
- Hauptmann, R. and P. Swetly. 1985. A novel class of human type I interferons. *Nucleic Acids Res.* **13**(13): 4739-49.
- Hayden, M. S. and S. Ghosh. 2004. Signaling to NF-kappaB. *Genes Dev.* **18**(18): 2195-224.

- Henry, S. C., X. Daniell, M. Indaram, J. F. Whitesides, G. D. Sempowski, D. Howell, T. Oliver and G. A. Taylor. 2007. Impaired Macrophage Function Underscores Susceptibility to Salmonella in Mice Lacking Irgm1 (LRG-47). *J Immunol.* **179**(10): 6963-72.
- Hinshaw, J. E. 2000. Dynamin and its role in membrane fission. *Annu Rev Cell Dev Biol.* **16**: 483-519.
- Huang, S., W. Hendriks, A. Althage, S. Hemmi, H. Bluethmann, R. Kamijo, J. Vilcek, R. M. Zinkernagel and M. Aguet. 1993. Immune response in mice that lack the interferon-gamma receptor. *Science.* **259**(5102): 1742-5.
- Hunn, J. (2007). Evolution and Cellular Resistance Mechanisms of the Immunity-Related GTPases.
- Iriti, M. and F. Faoro. 2007. Review of innate and specific immunity in plants and animals. *Mycopathologia.* **164**(2): 57-64.
- Isaacs, A. and J. Lindenmann. 1957. Virus interference. I. The interferon. *Proc R Soc Lond B Biol Sci.* **147**(927): 258-67.
- James, E. R. and D. R. Green. 2004. Manipulation of apoptosis in the host-parasite interaction. *Trends Parasitol.* **20**(6): 280-7.
- Janeway, C. 2001. Immunobiology 5 : the immune system in health and disease. New York, Garland Pub.
- Janeway, C. A., Jr. and R. Medzhitov. 2002. Innate immune recognition. *Annu Rev Immunol.* **20**: 197-216.
- Kaiser, F., S. H. Kaufmann and J. Zerrahn. 2004. IIGP, a member of the IFN inducible and microbial defense mediating 47 kDa GTPase family, interacts with the microtubule binding protein hook3. *J Cell Sci.* **117**(Pt 9): 1747-56.
- Karin, M. and A. Lin. 2002. NF-kappaB at the crossroads of life and death. *Nat Immunol.* **3**(3): 221-7.
- Keller, P., F. Schaumburg, S. F. Fischer, G. Hacker, U. Gross and C. G. Luder. 2006. Direct inhibition of cytochrome c-induced caspase activation in vitro by Toxoplasma gondii reveals novel mechanisms of interference with host cell apoptosis. *FEMS Microbiol Lett.* **258**(2): 312-9.
- Kim, J. M., Y. K. Oh, Y. J. Kim, S. J. Cho, M. H. Ahn and Y. J. Cho. 2001. Nuclear factor-kappa B plays a major role in the regulation of chemokine expression of HeLa cells in response to Toxoplasma gondii infection. *Parasitol Res.* **87**(9): 758-63.

- Kim, L. and E. Y. Denkers. 2006a. *Toxoplasma gondii* triggers Gi-dependent PI 3-kinase signaling required for inhibition of host cell apoptosis. *J Cell Sci.* **119**(Pt 10): 2119-26.
- Kim, L., B. A. Butcher, C. W. Lee, S. Uematsu, S. Akira and E. Y. Denkers. 2006b. *Toxoplasma gondii* genotype determines MyD88-dependent signaling in infected macrophages. *J Immunol.* **177**(4): 2584-91.
- Klamp, T., U. Boehm, D. Schenk, K. Pfeffer and J. C. Howard. 2003. A giant GTPase, very large inducible GTPase-1, is inducible by IFNs. *J Immunol.* **171**(3): 1255-65.
- Kleinecke, J. and H. Soeling. 1979. Subcellular compartmentation of guanine nucleotides and functional relationships between the adenine and guanine nucleotide systems in isolated hepatocytes. *FEBS Lett.* **107**: 1255-65.
- Koga, R., S. Hamano, H. Kuwata, K. Atarashi, M. Ogawa, H. Hisaeda, M. Yamamoto, S. Akira, K. Himeno, M. Matsumoto and K. Takeda. 2006. TLR-dependent induction of IFN-beta mediates host defense against *Trypanosoma cruzi*. *J Immunol.* **177**(10): 7059-66.
- Konen-Waisman, S. and J. C. Howard. 2007. Cell-autonomous immunity to *Toxoplasma gondii* in mouse and man. *Microbes Infect.* **9**(14-15): 1652-61.
- Koopman, G., C. P. Reutelingsperger, G. A. Kuijten, R. M. Keehnen, S. T. Pals and M. H. van Oers. 1994. Annexin V for flow cytometric detection of phosphatidylserine expression on B cells undergoing apoptosis. *Blood.* **84**(5): 1415-20.
- Kotenko, S. V., G. Gallagher, V. V. Baurin, A. Lewis-Antes, M. Shen, N. K. Shah, J. A. Langer, F. Sheikh, H. Dickensheets and R. P. Donnelly. 2003. IFN-lambdas mediate antiviral protection through a distinct class II cytokine receptor complex. *Nat Immunol.* **4**(1): 69-77.
- Kroemer, G., W. S. El-Deiry, P. Golstein, M. E. Peter, D. Vaux, P. Vandenabeele, B. Zhivotovsky, M. V. Blagosklonny, W. Malorni, R. A. Knight, M. Piacentini, S. Nagata and G. Melino. 2005. Classification of cell death: recommendations of the Nomenclature Committee on Cell Death. *Cell Death Differ.* **12 Suppl 2**: 1463-7.
- LaFleur, D. W., B. Nardelli, T. Tsareva, D. Mather, P. Feng, M. Semenuk, K. Taylor, M. Buergin, D. Chinchilla, V. Roshke, G. Chen, S. M. Ruben, P. M. Pitha, T. A. Coleman and P. A. Moore. 2001. Interferon-kappa, a novel type I interferon expressed in human keratinocytes. *J Biol Chem.* **276**(43): 39765-71.
- Lapaque, N., O. Takeuchi, F. Corrales, S. Akira, I. Moriyon, J. C. Howard and J. P. Gorvel. 2006. Differential inductions of TNF-alpha and IGTP, IIGP by structurally diverse classic and non-classic lipopolysaccharides. *Cell Microbiol.* **8**(3): 401-13.
- Lasfar, A., A. Lewis-Antes, S. V. Smirnov, S. Anantha, W. Abushahba, B. Tian, K. Reuhl, H. Dickensheets, F. Sheikh, R. P. Donnelly, E. Raveche and S. V. Kotenko. 2006.

- Characterization of the mouse IFN-lambda ligand-receptor system: IFN-lambdas exhibit antitumor activity against B16 melanoma. *Cancer Res.* **66**(8): 4468-77.
- Lefevre, F., M. Guillomot, S. D'Andrea, S. Battegay and C. La Bonnardiere. 1998. Interferon-delta: the first member of a novel type I interferon family. *Biochimie.* **80**(8-9): 779-88.
- Leipe, D. D., Y. I. Wolf, E. V. Koonin and L. Aravind. 2002. Classification and evolution of P-loop GTPases and related ATPases. *J Mol Biol.* **317**(1): 41-72.
- Levine, B. and J. Yuan. 2005. Autophagy in cell death: an innocent convict? *J Clin Invest.* **115**(10): 2679-88.
- Levine, B. and G. Kroemer. 2008. Autophagy in the Pathogenesis of Disease. *Cell.* **132**(1): 27-42.
- Lindenmann, J. 1964. Inheritance Of Resistance To Influenza Virus In Mice. *Proc Soc Exp Biol Med.* **116**: 506-9.
- Lindenmann, J., E. Deuel, S. Fanconi and O. Haller. 1978. Inborn resistance of mice to myxoviruses: macrophages express phenotype in vitro. *J Exp Med.* **147**(2): 531-40.
- Lindenmann, J., C. A. Lane and D. Hobson. 1963. The Resistance Of A2g Mice To Myxoviruses. *J Immunol.* **90**: 942-51.
- Ling, Y. M., M. H. Shaw, C. Ayala, I. Coppens, G. A. Taylor, D. J. Ferguson and G. S. Yap. 2006. Vacuolar and plasma membrane stripping and autophagic elimination of *Toxoplasma gondii* in primed effector macrophages. *J Exp Med.* **203**(9): 2063-71.
- Luder, C. G., W. Walter, B. Beuerle, M. J. Maeurer and U. Gross. 2001. *Toxoplasma gondii* down-regulates MHC class II gene expression and antigen presentation by murine macrophages via interference with nuclear translocation of STAT1alpha. *Eur J Immunol.* **31**(5): 1475-84.
- Luft, B. J. and J. S. Remington. 1992. Toxoplasmic encephalitis in AIDS. *Clin Infect Dis.* **15**(2): 211-22.
- MacMicking, J. D., G. A. Taylor and J. D. McKinney. 2003. Immune control of tuberculosis by IFN-gamma-inducible LRG-47. *Science.* **302**(5645): 654-9.
- Maiuri, M. C., E. Zalckvar, A. Kimchi and G. Kroemer. 2007. Self-eating and self-killing: crosstalk between autophagy and apoptosis. *Nat Rev Mol Cell Biol.* **8**(9): 741-52.
- Margulis, L. 1975. Symbiotic theory of the origin of eukaryotic organelles; criteria for proof. *Symp Soc Exp Biol.* (29): 21-38.

- Mariathasan, S. and D. M. Monack. 2007. Inflammasome adaptors and sensors: intracellular regulators of infection and inflammation. *Nat Rev Immunol.* **7**(1): 31-40.
- Martens, S. (2004a). Cell-Biology of Interferon Inducible GTPases.
- Martens, S. and J. Howard. 2006. The interferon-inducible GTPases. *Annu Rev Cell Dev Biol.* **22**: 559-89.
- Martens, S., I. Parvanova, J. Zerrahn, G. Griffiths, G. Schell, G. Reichmann and J. C. Howard. 2005. Disruption of *Toxoplasma gondii* parasitophorous vacuoles by the mouse p47-resistance GTPases. *PLoS Pathog.* **1**(3): e24.
- Martens, S., K. Sabel, R. Lange, R. Uthaiyah, E. Wolf and J. C. Howard. 2004b. Mechanisms regulating the positioning of mouse p47 resistance GTPases LRG-47 and IIGP1 on cellular membranes: retargeting to plasma membrane induced by phagocytosis. *J Immunol.* **173**(4): 2594-606.
- Meraz, M. A., J. M. White, K. C. Sheehan, E. A. Bach, S. J. Rodig, A. S. Dighe, D. H. Kaplan, J. K. Riley, A. C. Greenlund, D. Campbell, K. Carver-Moore, R. N. DuBois, R. Clark, M. Aguet and R. D. Schreiber. 1996. Targeted disruption of the Stat1 gene in mice reveals unexpected physiologic specificity in the JAK-STAT signaling pathway. *Cell.* **84**(3): 431-42.
- Miyairi, I., V. R. Tatireddigari, O. S. Mahdi, L. A. Rose, R. J. Belland, L. Lu, R. W. Williams and G. I. Byrne. 2007. The p47 GTPases Iigp2 and Irgb10 regulate innate immunity and inflammation to murine *Chlamydia psittaci* infection. *J Immunol.* **179**(3): 1814-24.
- Mogensen, K. E., M. Lewerenz, J. Reboul, G. Lutfalla and G. Uze. 1999. The type I interferon receptor: structure, function, and evolution of a family business. *J Interferon Cytokine Res.* **19**(10): 1069-98.
- Molestina, R. E. and A. P. Sinai. 2005a. Detection of a novel parasite kinase activity at the *Toxoplasma gondii* parasitophorous vacuole membrane capable of phosphorylating host IkappaBalpha. *Cell Microbiol.* **7**(3): 351-62.
- Molestina, R. E. and A. P. Sinai. 2005b. Host and parasite-derived IKK activities direct distinct temporal phases of NF-kappaB activation and target gene expression following *Toxoplasma gondii* infection. *J Cell Sci.* **118**(Pt 24): 5785-96.
- Mordue, D. G., N. Desai, M. Dustin and L. D. Sibley. 1999. Invasion by *Toxoplasma gondii* establishes a moving junction that selectively excludes host cell plasma membrane proteins on the basis of their membrane anchoring. *J Exp Med.* **190**(12): 1783-92.
- Nantais, D. E., M. Schwemmler, J. T. Stickney, D. J. Vestal and J. E. Buss. 1996. Prenylation of an interferon-gamma-induced GTP-binding protein: the human guanylate binding protein, huGBP1. *J Leukoc Biol.* **60**(3): 423-31.

- Nelson, D. E., D. P. Virok, H. Wood, C. Roshick, R. M. Johnson, W. M. Whitmire, D. D. Crane, O. Steele-Mortimer, L. Kari, G. McClarty and H. D. Caldwell. 2005. Chlamydial IFN-gamma immune evasion is linked to host infection tropism. *Proc Natl Acad Sci U S A*. **102**(30): 10658-63.
- Olszewski, M. A., J. Gray and D. J. Vestal. 2006. In silico genomic analysis of the human and murine guanylate-binding protein (GBP) gene clusters. *J Interferon Cytokine Res*. **26**(5): 328-52.
- Papic, N. (2007). Biochemical Analysis of the Immunity-Related GTPase Irga6 *In Vivo* and *In Vitro*; The Role of the Myristoyl Group.
- Pestka, S., C. D. Krause and M. R. Walter. 2004. Interferons, interferon-like cytokines, and their receptors. *Immunol Rev*. **202**: 8-32.
- Pitossi, F., A. Blank, A. Schroder, A. Schwarz, P. Hussi, M. Schwemmler, J. Pavlovic and P. Staeheli. 1993. A functional GTP-binding motif is necessary for antiviral activity of Mx proteins. *J Virol*. **67**(11): 6726-32.
- Portnoy, D. A., V. Auerbuch and I. J. Glomski. 2002. The cell biology of *Listeria monocytogenes* infection: the intersection of bacterial pathogenesis and cell-mediated immunity. *J Cell Biol*. **158**(3): 409-14.
- Portnoy, D. A., R. D. Schreiber, P. Connelly and L. G. Tilney. 1989. Gamma interferon limits access of *Listeria monocytogenes* to the macrophage cytoplasm. *J Exp Med*. **170**(6): 2141-6.
- Praefcke, G. J. and H. T. McMahon. 2004. The dynamin superfamily: universal membrane tubulation and fission molecules? *Nat Rev Mol Cell Biol*. **5**(2): 133-47.
- Robertson, B., J. Zou, C. Secombes and J. A. Leong. 2006. Molecular and expression analysis of an interferon-gamma-inducible guanylate-binding protein from rainbow trout (*Oncorhynchus mykiss*). *Dev Comp Immunol*. **30**(11): 1023-33.
- Rohde, C. (2007). Genetic and Functional Studies on the Conserved IRG (Immunity-related GTPase) Protein IRGC (CINEMA).
- Rothenberger, S., B. J. Iacopetta and L. C. Kuhn. 1987. Endocytosis of the transferrin receptor requires the cytoplasmic domain but not its phosphorylation site. *Cell*. **49**(3): 423-31.
- Saeij, J. P., J. P. Boyle and J. C. Boothroyd. 2005. Differences among the three major strains of *Toxoplasma gondii* and their specific interactions with the infected host. *Trends Parasitol*. **21**(10): 476-81.
- Saeij, J. P., J. P. Boyle, S. Collier, S. Taylor, L. D. Sibley, E. T. Brooke-Powell, J. W. Ajioka

- and J. C. Boothroyd. 2006. Polymorphic secreted kinases are key virulence factors in toxoplasmosis. *Science*. **314**(5806): 1780-3.
- Saeij, J. P., S. Coller, J. P. Boyle, M. E. Jerome, M. W. White and J. C. Boothroyd. 2007. Toxoplasma co-opts host gene expression by injection of a polymorphic kinase homologue. *Nature*. **445**(7125): 324-7.
- Sagan, L. 1993. On the origin of mitosing cells. 1967. *J NIH Res*. **5**(3): 65-72.
- Santiago, H. C., C. G. Feng, A. Bafica, E. Roffe, R. M. Arantes, A. Cheever, G. Taylor, L. Q. Vieira, J. Aliberti, R. T. Gazzinelli and A. Sher. 2005. Mice deficient in LRG-47 display enhanced susceptibility to *Trypanosoma cruzi* infection associated with defective hemopoiesis and intracellular control of parasite growth. *J Immunol*. **175**(12): 8165-72.
- Scaffidi, P., T. Misteli and M. E. Bianchi. 2002. Release of chromatin protein HMGB1 by necrotic cells triggers inflammation. *Nature*. **418**(6894): 191-5.
- Scanga, C. A., J. Aliberti, D. Jankovic, F. Tilloy, S. Bennouna, E. Y. Denkers, R. Medzhitov and A. Sher. 2002. Cutting edge: MyD88 is required for resistance to *Toxoplasma gondii* infection and regulates parasite-induced IL-12 production by dendritic cells. *J Immunol*. **168**(12): 5997-6001.
- Scharton-Kersten, T. M., T. A. Wynn, E. Y. Denkers, S. Bala, E. Grunvald, S. Hieny, R. T. Gazzinelli and A. Sher. 1996. In the absence of endogenous IFN-gamma, mice develop unimpaired IL-12 responses to *Toxoplasma gondii* while failing to control acute infection. *J Immunol*. **157**(9): 4045-54.
- Schmid, D. and C. Munz. 2007. Innate and adaptive immunity through autophagy. *Immunity*. **27**(1): 11-21.
- Schroder, K., P. J. Hertzog, T. Ravasi and D. A. Hume. 2004. Interferon-gamma: an overview of signals, mechanisms and functions. *J Leukoc Biol*. **75**(2): 163-89.
- Segal, A. W. 2005. How neutrophils kill microbes. *Annu Rev Immunol*. **23**: 197-223.
- Shapira, S., O. S. Harb, J. Margarit, M. Matrajt, J. Han, A. Hoffmann, B. Freedman, M. J. May, D. S. Roos and C. A. Hunter. 2005. Initiation and termination of NF-kappaB signaling by the intracellular protozoan parasite *Toxoplasma gondii*. *J Cell Sci*. **118**(Pt 15): 3501-8.
- Shenoy, A. R., B. H. Kim, H. P. Choi, T. Matsuzawa, S. Tiwari and J. D. Macmicking. 2008. Emerging themes in IFN-gamma-induced macrophage immunity by the p47 and p65 GTPase families. *Immunobiology*. **212**(9-10): 771-84.
- Sibley, L. D. and J. C. Boothroyd. 1992. Virulent strains of *Toxoplasma gondii* comprise a single clonal lineage. *Nature*. **359**(6390): 82-5.

- Sibley, L. D. 2004. Intracellular parasite invasion strategies. *Science*. **304**(5668): 248-53.
- Simon, A., J. Fah, O. Haller and P. Staeheli. 1991. Interferon-regulated Mx genes are not responsive to interleukin-1, tumor necrosis factor, and other cytokines. *J Virol*. **65**(2): 968-71.
- Sinai, A. P. and K. A. Joiner. 1997. Safe haven: the cell biology of nonfusogenic pathogen vacuoles. *Annu Rev Microbiol*. **51**: 415-62.
- Singh, S. B., A. S. Davis, G. A. Taylor and V. Deretic. 2006. Human IRGM induces autophagy to eliminate intracellular mycobacteria. *Science*. **313**(5792): 1438-41.
- Staeheli, P. and O. Haller. 1985. Interferon-induced human protein with homology to protein Mx of influenza virus-resistant mice. *Mol Cell Biol*. **5**(8): 2150-3.
- Sutterwala, F. S., Y. Ogura and R. A. Flavell. 2007. The inflammasome in pathogen recognition and inflammation. *J Leukoc Biol*. **82**(2): 259-64.
- Suzuki, Y., M. A. Orellana, R. D. Schreiber and J. S. Remington. 1988. Interferon-gamma: the major mediator of resistance against *Toxoplasma gondii*. *Science*. **240**(4851): 516-8.
- Taylor, G. A. 2007. IRG proteins: key mediators of interferon-regulated host resistance to intracellular pathogens. *Cell Microbiol*. **9**(5): 1099-107.
- Taylor, G. A., C. M. Collazo, G. S. Yap, K. Nguyen, T. A. Gregorio, L. S. Taylor, B. Eagleson, L. Secret, E. A. Southon, S. W. Reid, L. Tessarollo, M. Bray, D. W. McVicar, K. L. Komschlies, H. A. Young, C. A. Biron, A. Sher and G. F. Vande Woude. 2000. Pathogen-specific loss of host resistance in mice lacking the IFN-gamma-inducible gene IGTP. *Proc Natl Acad Sci U S A*. **97**(2): 751-5.
- Taylor, G. A., M. Jeffers, D. A. Largaespada, N. A. Jenkins, N. G. Copeland and G. F. Woude. 1996. Identification of a novel GTPase, the inducibly expressed GTPase, that accumulates in response to interferon gamma. *J Biol Chem*. **271**(34): 20399-405.
- Taylor, G. A., R. Stauber, S. Rulong, E. Hudson, V. Pei, G. N. Pavlakis, J. H. Resau and G. F. Vande Woude. 1997. The inducibly expressed GTPase localizes to the endoplasmic reticulum, independently of GTP binding. *J Biol Chem*. **272**(16): 10639-45.
- Taylor, S., A. Barragan, C. Su, B. Fux, S. J. Fentress, K. Tang, W. L. Beatty, H. E. Hajj, M. Jerome, M. S. Behnke, M. White, J. C. Wootton and L. D. Sibley. 2006. A secreted serine-threonine kinase determines virulence in the eukaryotic pathogen *Toxoplasma gondii*. *Science*. **314**(5806): 1776-80.

- Tilney, L. G. and D. A. Portnoy. 1989. Actin filaments and the growth, movement, and spread of the intracellular bacterial parasite, *Listeria monocytogenes*. *J Cell Biol.* **109**(4 Pt 1): 1597-608.
- Turk, B., V. Stoka, J. Rozman-Pungercar, T. Cirman, G. Droga-Mazovec, K. Oresic and V. Turk. 2002. Apoptotic pathways: involvement of lysosomal proteases. *Biol Chem.* **383**(7-8): 1035-44.
- Uthaiyah, R. C., G. J. Praefcke, J. C. Howard and C. Herrmann. 2003. IIGP1, an interferon-gamma-inducible 47-kDa GTPase of the mouse, showing cooperative enzymatic activity and GTP-dependent multimerization. *J Biol Chem.* **278**(31): 29336-43.
- van Pesch, V., H. Lanaya, J. C. Renauld and T. Michiels. 2004. Characterization of the murine alpha interferon gene family. *J Virol.* **78**(15): 8219-28.
- Vetter, I. R. and A. Wittinghofer. 2001. The guanine nucleotide-binding switch in three dimensions. *Science.* **294**(5545): 1299-304.
- Weber, P. C., D. H. Ohlendorf, J. J. Wendoloski and F. R. Salemme. 1989. Structural origins of high-affinity biotin binding to streptavidin. *Science.* **243**(4887): 85-8.
- Willingham, S. B., D. T. Bergstralh, W. O'Connor, A. C. Morrison, D. J. Taxman, J. A. Duncan, S. Barnoy, M. M. Venkatesan, R. A. Flavell, M. Deshmukh, H. M. Hoffman and J. P. Ting. 2007. Microbial pathogen-induced necrotic cell death mediated by the inflammasome components CIAS1/cryopyrin/NLRP3 and ASC. *Cell Host Microbe.* **2**(3): 147-59.
- Zerrahn, J., U. E. Schaible, V. Brinkmann, U. Guehlich and S. H. Kaufmann. 2002. The IFN-inducible Golgi- and endoplasmic reticulum-associated 47-kDa GTPase IIGP is transiently expressed during listeriosis. *J Immunol.* **168**(7): 3428-36.
- Zhang, H. M., J. Yuan, P. Cheung, H. Luo, B. Yanagawa, D. Chau, N. Stephan-Tozy, B. W. Wong, J. Zhang, J. E. Wilson, B. M. McManus and D. Yang. 2003. Overexpression of interferon-gamma-inducible GTPase inhibits coxsackievirus B3-induced apoptosis through the activation of the phosphatidylinositol 3-kinase/Akt pathway and inhibition of viral replication. *J Biol Chem.* **278**(35): 33011-9.
- Zhao, Y., D. Wilson, S. Matthews and G. S. Yap. 2007. Rapid Elimination of *Toxoplasma gondii* by Gamma Interferon-Primed Mouse Macrophages Is Independent of CD40 Signaling. *Infect Immun.* **75**(10): 4799-803.

## 7. Summary

Immunity-related GTPases are interferon-inducible, indispensable resistance factors against a variety of intracellular bacterial and protozoal pathogens in mice. *Irgm1* is the most powerful member of the IRG family. Previous studies showed that *Irgm1* localizes mainly to the Golgi apparatus, and relocalizes to phagocytic cups during phagocytosis. Macrophages deficient in *Irgm1* have impaired acidification of *M. tuberculosis*-containing phagosomes. In addition, a role of *Irgm1* in promoting autophagy has been proposed based on EGFP-tagged *Irgm1* over-expression experiments. During *T. gondii* infection, at least 6 IRG family members translocate from their resting localization onto the *T. gondii* parasitophorous vacuolar membrane and contribute to disruption of the *T. gondii* vacuoles.

In the present study, *Irgm1* has been shown to be associated with late endocytic/lysosomal compartments in addition to Golgi apparatus. N or C terminally EGFP-tagged *Irgm1* is not localized to the Golgi and mislocalizes to the early/recycling endosomes as well as other unknown vesicular structures. Both Golgi and lysosomal localization of *Irgm1* are mediated by a C-terminal amphipathic helix. Although *Irgm1* is indispensable for mice to survive *T. gondii* infection, *Irgm1* is not recruited to the *T. gondii* vacuole and is not absolutely necessary for the IFN- $\gamma$ -dependent cell-autonomous control of *T. gondii*.

Using live cell imaging, the present experiments show the sequence of events by which IFN- $\gamma$  treated cells eliminate *T. gondii*. After the invasion of *T. gondii*, the vacuoles are coated with IRG proteins and subsequently disrupted. The stripped *T. gondii* are released to the cytosol and killed. The host cells finally undergo necrosis, and this presumably serves as a cell-autonomous resistance mechanism. The necrotic host cells release the proinflammatory mediator, HMGB1, to further enhance the host immune responses. Virulent *T. gondii* strains do not elicit IFN- $\gamma$ -dependent host cell death, but could not inhibit the death process once it is initiated by co-infection with an avirulent strain. The presented results show that in *T. gondii* infection, the IRG proteins contribute to the disruption of the *T. gondii* vacuole and this could be a trigger for the subsequent parasite killing as well as host cell death.

## 8. Zusammenfassung

Die Immunity-related GTPasen sind Interferon induzierbare, essentielle Resistenzfaktoren gegen ein breites Spektrum intrazellulärer bakterieller und protozoischer Pathogene in der Maus. Das stärkste Mitglied der IRG Familie ist Irgm1. In vorherigen Studien wurde gezeigt, dass Irgm1 hauptsächlich am Golgi Apparat lokalisiert ist und während der Phagozytose zu den sogenannten „phagocytic cups“ relokalisiert wird. Irgm1 defiziente Makrophagen zeigen eine verminderte Ansäuerung von Phagosomen die *M. tuberculosis* enthalten. Basierend auf Experimenten in den an EGFP gekoppeltes Irgm1 überexprimiert wurde, wurde eine Funktion von Irgm1 in der Stimulierung von Autophagie vorgeschlagen. Während der Infektion mit *T. gondii* verlagern mindestens sechs IRG Proteine ihre Lokalisation an die Membran der *T. gondii* enthaltenden parasitophoren Vakuole und tragen zur Zerstörung der *T. gondii* Vakuolen bei.

In dieser Studie wurde gezeigt, dass Irgm1 neben dem Golgi Apparat auch mit dem späten endozytischen/lysosomalen Kompartiment assoziiert ist. N- oder C-terminal EGFP-gekoppeltes Irgm1 lokalisiert nicht am Golgi sondern mislokalisiert an den frühen/recycling Endosomen und unbekanntes vesikulären Strukturen. Die richtige Lokalisation von Irgm1 am Golgi und Lysosomen wird durch eine C-terminale amphipatische Helix vermittelt. Obwohl Irgm1 essentiell für Mäuse ist um eine Infektion mit *T. gondii* zu überleben, wird Irgm1 nicht zur *T. gondii* Vakuole rekrutiert und ist nur bedingt essentiell für die IFN- $\gamma$ -abhängige zellautonome Kontrolle von *T. gondii*.

Durch den Einsatz von „live cell imaging“ wurde die zeitliche Abfolge von Ereignissen aufgeklärt durch die IFN- $\gamma$ -stimulierte Zellen *T. gondii* eliminieren. Nach der Invasion von *T. gondii* wird die Vakuole mit IRG Proteinen bedeckt und anschließend zerstört. Die freien *T. gondii* werden ins Cytosol freigesetzt und getötet. Abschließend sterben die Wirtszellen durch Nekrose. Diese Nekrose dient wahrscheinlich als zellautonomer Resistenzmechanismus. Die nekrotischen Wirtszellen setzen den proinflammatorischen Mediator HMGB1 frei um die Immunantwort des Wirts weiter zu stärken. Virulente *T. gondii* Stämme führen nicht zum IFN- $\gamma$ -abhängigen Tod der Wirtszelle, aber sie können die Einleitung des Todes der Zelle

durch Nekrose, hervorgerufen durch Koinfektion mit avirulenten Stämmen, nicht unterbinden. Die hier gezeigten Ergebnisse zeigen, dass IRG Proteine während der Infektion mit *T. gondii* zur Zerstörung der *T. gondii* Vakuole beitragen und dass dies der Auslöser für die anschließende Eliminierung des Parasiten und den Tod der Wirtszelle sein könnte.

## 9. Acknowledgement

First of all, I would like to thank Prof. Jonathan Howard, for giving me a great opportunity to work in his lab, showing me what real science is and how much fun we can make out of it, and making me really understand that being a good scientist is a process of “learning everything about something, and something about everything”.

Thank Prof. Thomas Langer for reviewing my work and being in my examination committee.

Thank Prof. Siegfried Roth for taking over the chairmanship in my examination committee.

Dr. Matthias Cramer for his great help in all bureaucratic matters and his kindness.

Dr. Sascha Martens for his guidance in the beginning of my PhD.

Christoph and Jia for their interesting discussion with me outside of science, and Sasha for his also interesting discussion in science.

Rita and Gaby for their great help from the very beginning of my lab life.

Special thanks to Natasa Papic for her help from the beginning during my rotation in the lab, through my PhD, until the final proof-reading of my thesis.

Thanks to Steffi, Julia, Niko, Tobi, Stefan, Bettina, Claudia, Caroline, Tao and all former and present members of the lab for their help and friendship.

Thanks to Sascha Dargazanli for his discussion and help in the field of Apoptosis.

Finally I would like thank “International graduate Graduate School in Genetics and Functional Genomics” for funding me, and especially Brigitte for her tremendous help.

## **10. Erklärung**

Ich versichere, dass ich die von mir vorgelegte Dissertation selbständig angefertigt, die benutzten Quellen und Hilfsmittel vollständig angegeben und die Stellen der Arbeit – einschließlich Tabellen, Karten und Abbildungen-, die anderen Werken im Wortlaut oder dem Sinn nach entnommen sind, in jedem Einzelfall als Entlehnung kenntlich gemacht habe; dass diese Dissertation noch keiner anderen Fakultät oder Universität zur Prüfung vorgelegen hat; dass sie abgesehen von den unten angegebenen Teilpublikationen noch nicht veröffentlicht worden ist, sowie, dass ich eine solche Veröffentlichung vor Abschluss des Promotionsverfahrens nicht vornehmen werde.

Die von mir vorgelegte Dissertation ist von Prof. Dr. Jonathan C. Howard betreut worden.

Köln, im Feb 2008

## 11. Lebenslauf

Name: Yang Zhao  
Geburtsdatum: 26.10.1977.  
Geburtsort: Anqing, V.R.China  
Staatsangehörigkeit: Chinesisch  
Familienstand: Verheiratet

### Ausbildung

1983-1989 Anqing Gaoqi Grundschule, V.R.China

1989-1995 Anqing Nr.1 Gymnasiums, V.R.China

1995-2000 Bachelor of Medicine (Clinical Medicine)  
„Norman Bethune University of Medical Sciences“, V.R.China

2000-2003 Master of Medicine (Immunology)  
„Shanghai Second Medical University“, V.R.China

Okt. 2003 – März 2004 Rotationsperioden in den Laboren von Prof. Dr. Jonathan Howard,  
Prof. Dr. Diethard Tautz und Prof. Dr. Sigrun Korsching

ab April 2004 Promotionsstudiengang Biologie (Fachrichtung Genetik) am  
Institut für Genetik, Universität zu Köln,  
Abteilung von Prof. Dr. Jonathan C. Howard